miR-128: a Pleiotropic Regulator of Neuronal Translation

Inaugural-Disertation
to obtain the academic degree
Doctor rerum naturalium (Dr. rer. nat.)

submitted to the Department of Biology, Chemistry, and Pharmacy
of Freie Universität Berlin

by
ELEONORA FRANZONI
Berlin, 2014

Graduate Period from July 2009 to March 2014, under the supervision of Dr. F. Gregory Wulczyn at the Institute for Cell and Neurobiology, Charité Berlin.

1^{st} Reviewer: Dr. F. Gregory Wulczyn

2^{nd} Reviewer: Prof. Dr. Fritz G. Rathjen

Date of defence: 30.05.2014

Abstract

microRNAs are an evolutionarily conserved mechanism for controlling mRNA translation. The genomes of living organisms contain hundreds of microRNA genes, each with the ability to regulate specific pathways. The focus of my thesis was to study in detail one particular microRNA: miR-128. When I started my PhD the only information on miR-128 was that it is one of the most abundant microRNAs in the brain, that it is specifically expressed in the neuronal lineage and that it is dramatically upregulated during embryonic and postnatal brain development.

There are two genes for miR-128, each encoding distinct stem-loop precursors, pre-miR-128-1 and pre-miR-128-2, that generate identical mature microRNAs after processing. Using *in situ* hybridization and Northern blot analysis, we were able to confirm that the mature form of the microRNA increases substantially during development. Unexpectedly, we found that pre-miR-128-1 cannot be detected by either method. In clear contrast to this result, expression of the pre-miR-128-2 precursor remains constant and high from early embryonic stages to adulthood. Moreover, the *in situ* hybridizations for miR-128 and pre-miR-128-2 show that there is a differential localization of the mature and the precursor forms. All cells that express mature miR-128 also express pre-miR-128-2. However, there are structures in the CNS, such as cortical layer V, or the progenitor zones of the embryonic cortex, the Rostral Migratory Stream (RMS) and the adult subgranular zone of the dentate gyrus, that are pre-miR-128-2 positive and mature miR-128 negative. Together, these discrepancies are evidence for post-transcriptional regulation of miR-128. Mechanisms of post-transcriptional regulation of microRNA expression are still largely unexplored, and our data reveal a significant role for such mechanisms in the regulation of miR-128.

Because miR-128 expression increases both during neuronal maturation *in vitro* and during brain development *in vivo*, we asked which functions miR-128 performs in these processes and in the mature brain. Using primary cell culture, we showed that premature miR-128 gain of function in polarized neurons leads to growth of supernumerary axons. We tested several pathways involved in neuronal polarization or in the maintenance of axon dominance that might be altered under gain of function conditions. However, we were unable to suppress the multiple axons phenotype by manipulating classical regulators of neurite outgrowth such as Cdc42, Rac1 and RhoA, components of the polarity complex (Par6b), or the semaphorin pathway (Nrp2). We therefore decided to complement the *in vitro* studies with functional assessment of miR-128 functions *in vivo*. Guided by our expression analysis, we used *in utero* electroporation to manipulate miR-128 expression in progenitors for upper layer neurons. We assayed for effects on neuronal migration, dendritogenesis and spine morphology. We found

that neurons ectopically expressing pre-miR-128-2, but not pre-miR-128-1, do not migrate to the correct position in the upper layers of the cortex. The affected neurons maintain their identity as upper layer neurons even though they are scattered throughout the cortical layers and the white matter. We were able to rescue this migration impairment by coexpressing pre-miR-128-2 and Phf6. We showed that miR-128 is an important regulator of Phf6, a nuclear/nucleolar protein that is mutated in Börjeson-Forssman-Lehmann Syndrome, a developmental disorder associated with mental retardation and epilepsy. Pre-miR-128-2 gain-of-function also affected dendritogenesis and spine morphology. Neurons expressing pre-miR-128-2 show a less complex dendritic arbor and fewer and bigger dendritic spines.

In summary, my results indicate that miR-128 is a pleiotropic microRNA that regulates the expression of multiple genes, including the human disease gene Phf6, to influence axonal outgrowth, neuronal migration and structural connectivity during mouse brain development.

Zusammenfassung

MicroRNAs stellen einen evolutionär konservierten Mechanismus zur Kontrolle von mRNA Translation dar. Die Genome lebender Organismen besitzen hunderte verschiedener microRNA-Gene, die jeweils spezifische Signalwege regulieren können. Der Fokus dieser Arbeit lag auf der Untersuchung einer spezifischen microRNA: miR-128. Zu Beginn der Arbeit war lediglich bekannt, dass miR-128 eine der am häufigsten vertretenen miRNAs im Gehirn ist und ausschließlich in Neuronen exprimiert wird. Mit fortschreitender embryonaler und postnataler Entwicklung des Gehirns steigt die Expression von miR-128 deutlich an.

Es existieren zwei miR-128 Gene, die für jeweils zwei verschiedene miR-128 Vorläuferformen, miR-128-1 und miR-128-2, codieren. Beide Haarnadel- förmigen Vorläufer-microRNAs erzeugen nach ihrer Prozessierung die identische reife microRNA. Mittels *in situ* Hybridisierung sowie Northern Blot konnte der bereits beschriebene Anstieg an reifer miR-128 während der Entwicklung bestätigt werden. Überraschenderweise konnte jedoch mit beiden Methoden keine pre-miR-128-1 Expression gezeigt werden. Im Gegenteil hierzu konnte eine konstante und hohe Expression des miR-128-2 Vorläufers in frühen embryonalen Stadien bis hin zum adulten Tier nachgewiesen werden. Zudem zeigten *in situ* Hybridisierungen für miR-128 und pre-miR-128-2 eine unterschiedliche Lokalisierung von reifer und Vorläufer-Form. Alle Zellen, die die reife miR-128 Form exprimieren sind ebenfalls positiv für die Vorläufer-Form. In bestimmten Bereichen des zentralen Nervensystems, wie der Lamina fünf des Kortex, der Vorläufer-Zone des embryonalen Kortex, dem rostralen Migrationsstrom und der Subgranulärzone des Gyrus Dentatus, findet man jedoch Zellen, die positiv für die miR-128 Vorläufer-Form, jedoch negativ für die reife Form, sind. Diese Diskrepanz deutet auf eine post-transkriptionelle Regulation der miR-128 Expression hin. Mechanismen der post-trankriptionellen Regulation von miRNA Expression sind größtenteils unbekannt. Die hier vorgestellten Ergebnisse deuten auf eine wichtige Rolle solcher Mechanismen in der Regulation von miR-128 hin.

Aufgrund des starken Anstiegs der miR-128 Expression bei der neuronalen Differenzierung *in vitro* und während der Entwicklung des Gehirns sollte die Frage beantwortet werden, welche Rolle miR-128 in diesen Prozessen spielt. Mit Hilfe primärer Neuronenkulturen konnte gezeigt werden, dass ektopische miR-128 überexpression in bereits polarisierten Neuronen zur Ausbildung überzähliger Axone führt. Verschiedene Signalwege, wichtig für die neuronale Polarisierung sowie Erhaltung der Axon-Dominanz, wurden auf Veränderungen unter miR-128 überexpression untersucht. Durch Manipulation klassischer Regulatoren für die Ausbildung von Neuriten (Cdc42, Rac1, RhoA), Komponenten des Polarisierungskomplexes (Par6b) oder des Semaphorin Signalweges (Nrp2) konnte der „multiple-Axon-Phänotyp“ jedoch nicht unterdrückt werden. Aufgrund dessen wurden die durchgeführten *in vitro* Studien durch Expe-

rimente ergänzt, die die Funktion von miR-128 *in vivo* aufklären sollten.

Basierend auf der Expressionsanalyse wurde mit Hilfe von *in utero* Elektroporation die miR-128 Expression in Vorläuferzellen für Neurone der oberen Kortexschichten manipuliert. Die entstandenen Neurone wurden auf Effekte bei der Migration, der Ausbildung der Dendriten und auf ihre Spine Morphologie hin untersucht. Die Ergenbisse zeigten, dass Neurone die ektopisch pre-miR-128-2 überexprimieren, nicht bis zu ihrer korrekten Position in den oberen Schichten des Kortex wandern. Ektopische pre-miR-128-1 Expression zeigte hingegen keinen Effekt. Trotz der Tatsache, dass die betroffenen Neuronen über alle Kortexschichten und die weiße Substanz verteilt sind, behalten sie ihre Identität als Neurone der oberen Kortexschichten. Dieses Migrationsdefizit konnte durch Ko-Expression von pre-miR-128-2 zusammen mit Phf6 aufgehoben werden. Dies zeigt, dass miR-128 ein wichtiger Regulator von Phf6 ist. Phf6 ist ein nukleäres und nukleoläres Protein, welches im Börjeson-Forssman-Lehmann Syndrom, einer mit mentaler Retardierung und Epilepsie assoziierter Entwicklungsstörung, mutiert ist. miR-128 überexprimierende Neurone zeigten ebenfalls weniger komplexe Dendritenbäume sowie weniger und größere dendritische Spines.

Zusammenfassend deuten meine Ergebnisse darauf hin, dass es sich bei miR-128 um eine pleiotrope miRNA handelt, welche die Expression mehrerer Gene, eingeschlossen Phf6, steuert um Axon-Ausbildung, neuronale Migration und strukturelle Konnektivität während der Entwicklung des Mausgehirns zu beeinflussen.

Contents

List of Figures

List of Tables

List of Acronyms

AGO	Argounaute
AML	Acute Myeloid Leukemia
AMPAR	AMPA Receptor
aNCS	adult Neuronal Stem Cell
aPKC	Atypical Protein Kinase C
BDNF	Brain-Dereived Neurotrophic Factor
BFLS	Börjesom-Forssman-Lehmann Syndrome
BSA	Bovine Serum Albumin
Chrdl1	Chordin-Like 1
CNS	Central Nervous System
CP	Cortical Plate
Ctdsp	C-terminal Domain Phosphatase
D1 neuron	Dopamine-receptor 1 neuron
D2 neuron	Dopamine-receptor 2 neuron
DCX	Doublecortin
DGCR8	DiGeorge Syndrome Critical Region 8
DIG	Digoxigenine
FACS	Fluorescence-Activated Cell Sorter
FBS	Fetal Bovine Serum
FSC	Forward Scatter
GE	Ganglionic Eminence
GSK3β	Glycogen Synthase Kinase 3 β
HRP	Horseradish Peroxidase
IPC	Intermediate Progenitor Cell
ISH	*In Situ* Hybridization
IUE	*In Utero* Electroporation
IZ	Intermediate Zone
LNA	Locked Nucleic Acid
MBD1	Methylated-CpG Binding Protein
MG	Marginal Zone
MeOH	Methanol
miRISC	microRNA Mediated Silencing Complex

NBT/BCIP	Nitro blue tetrazolium chloride/ 5-Bromo-4-Chloro-3-indolyl phosphate
NCS	Neuronal Stem Cell
NMD	Non-sense Mediated Decay
NMDAR	NMDA Receptor
Nrp2	Neuropilin 2
nt	nucleotide
NT-3	Neurotrophin 3
NurD complex	Nucleosome Remodeling and Deacetylation complex
PABP	Polyadenylation Binding Protein
PCR	Polymerase Chain Reaction
Phf6	Plant Homeo Domain-like Finger Protein
PK	Proteinase K
PTBP1	Polypyrimidine Tract-Binding Protein 1
PTBP2	Polypyrimidine Tract-Binding Protein 2
RBP	RNA Binding Protein
qRT-PCR	Quantitative Real Time PCR
RE1	Repression Element 1
REST	RE1 Silencing Transcription Factor
RGC	Radial Glial Cell
RMS	Rostral Migratory Stream
RT	Room Temperature
SP	Subplate
SSC	Side Scatter
Sema 3A	semaphorin 3A
Sema 3E	semaphorin 3E
SGZ	Subgranular Zone
srGAP2	slit-robo GTPase Activating Protein
SVZ	Subventricular Zone
T-ALL	Lymphoblastic Leukaemia
TSA	Tyramide Amplification System
UTR	Untranslated region
VZ	Ventricular Zone

Chapter 1

Introduction

1.1 microRNAs Biogenesis, Regulation and Function

microRNAs are small non coding RNAs, discovered in *C. elegans* at the beginning of the 1990's (Lee et al., 1993). Only a decade later, in 2001, three back-to-back papers in Science showed that microRNAs are an evolutionarily conserved and widespread class of small regulatory RNAs (Lagos-Quintana et al., 2001; Lau et al., 2001; Lee and Ambros, 2001). Some of the microRNAs identified in these cloning papers were later shown to be present in the whole animal kingdom (let-7), others in vertebrates (miR-128); and others in primates or humans (miR-941) (Berezikov et al., 2006; Ibáñez-Ventoso et al., 2008; Hu et al., 2012; Somel et al., 2011). In the genome microRNAs can be located either in intronic or exonic regions of coding or non-coding genes, or in intergenic regions lacking other known genes. They can be present either singly, for example the intronic miR-128-1 and miR-128-2, or they can be clustered, for example the tandem pair of miR-212 and miR-132 or the miR-290 cluster containing 14 individual, but related microRNA genes (reviewed in Kim et al. 2009a). microRNAs are usually transcribed by RNA polymerase Polymerase II (Pol II) (Lee et al., 2004), but in rare cases also by RNA Polymerase III (Pol III) (Borchert et al., 2006; Monteys et al., 2010). The primary transcript (pri-microRNA) is then processed by the Microprocessor, which has two main components: the RNAse type III Drosha and DGCR8 (DiGeorge syndrome critical region 8). Drosha cleaves the pri-microRNA into the shorter (around 70 nucleotide -nt-) microRNA precursor (pre-microRNA), that has a characteristic stem-loop secondary structure. Pre-microRNAs are then actively exported from the nucleus to the cytoplasm. In the cytosol another RNAse type III protein, Dicer, in complex with auxiliary proteins (TRBP or PACT), "dices" the pre-microRNA by cleaving circa 22 nt from the free ends generated by Drosha. Initially doublestranded, one strand of the cleavage product is selected for loading into the miRISC complex (microRNA mediated silencing complex), and the so-called star form from the non-selected strand is generally degraded. The microRNA in the miRISC complex is bound to one of the Argonaute proteins (AGO). In mammals there are four different AGO proteins (1-4) that are thought to perform redundant functions in the microRNA pathway. However, only AGO2 retains the endonucleolytic enzymatic activity characteristic of the siRNA pathway, which allows the direct cleavage of the passenger strand(Hammond et al., 2001; Liu et al., 2004). GW182 proteins (in mammals TNRC6a-c) are another important

component of the miRISC (Figure 1.1). Comprehensive reviews on the processes of the microRNA biogenesis described above are: Kim et al. 2009a, Krol et al. 2010b, Siomi and Siomi 2010.

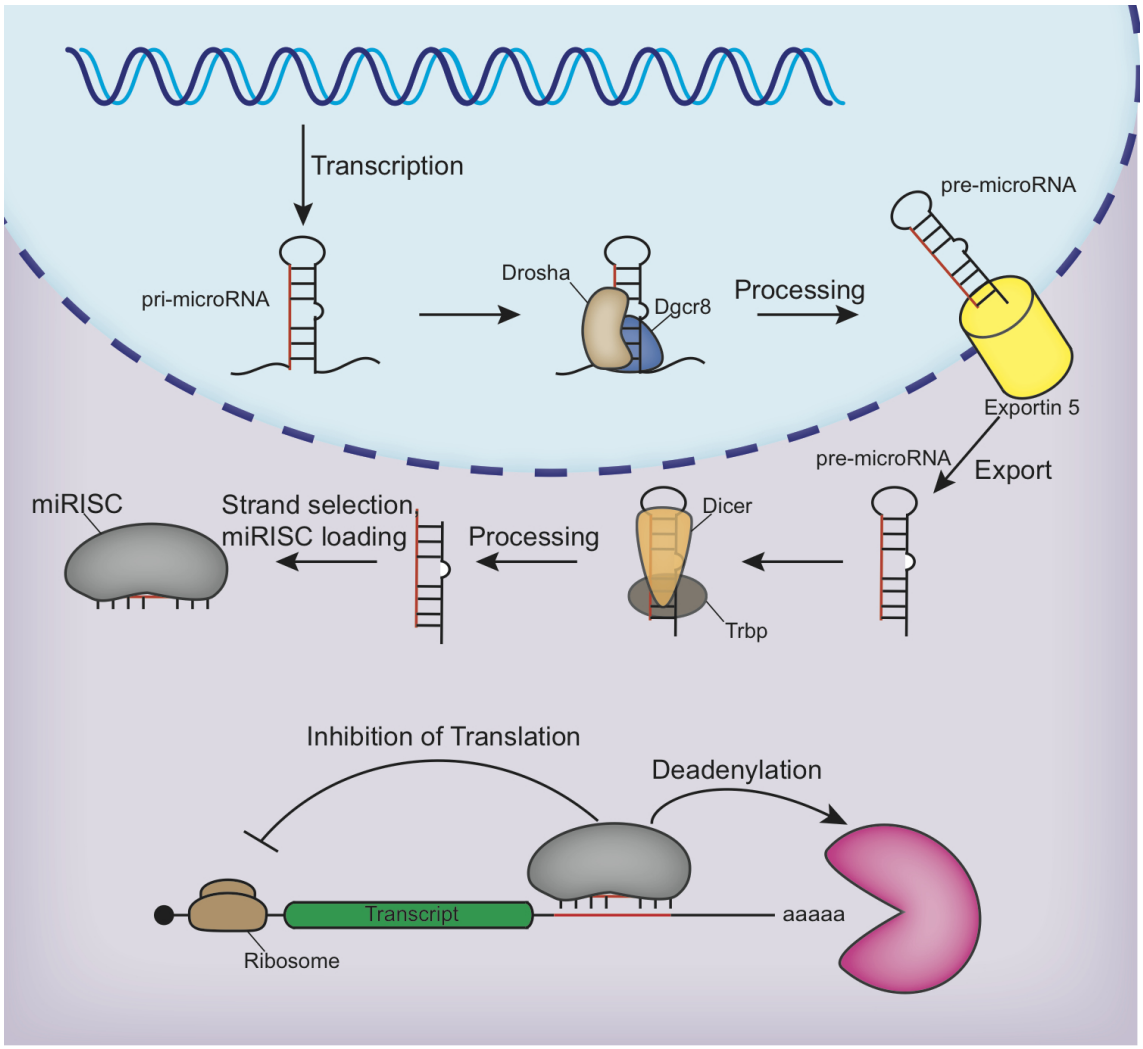

Figure 1.1: *microRNA Biogenesis Pathway.*

microRNA biogenesis is tightly regulated at both the pri-microRNA and pre-microRNA stages. Wulczyn et al. showed that in embryonic stem cells the primary transcript for the let-7 microRNA, pri-let-7, was constitutively present, whereas the mature 22 nt form was missing (Wulczyn et al., 2007). Several studies demonstrated that the key protein in the regulation of let-7 maturation is Lin28, an RNA binding protein specifically expressed in pluripotent stem cells. Lin28 can regulate processing of the let-7 pri-microRNA (Piskounova et al., 2011) or the let-7 pre-microRNA, preferentially mediated by the related Lin28B or Lin28A proteins, respectively. Lin28A can interfere directly with Dicer activity and/or can induce polyuridylation at the 3' end of pre-let-7, targeting it for degradation (Rybak et al., 2008; Heo et al., 2008). let-7 is not the only microRNA undergoing regulated processing. For example, pre-miR-138 is expressed in almost every cell type of a mouse embryo, but the miR-138 mature form is restricted to neuronal cells (Obernosterer et al. 2006, reviewed in Kim et al. 2009a, Siomi and Siomi 2010).

In animals microRNAs repress mRNA translation and/or target the mRNA for deadenylation and subsequent decay. It is still a matter of debate when and how microRNAs repress protein synthesis. The majority of studies indicate that the miRISC complex binds the 3' Untranslated Region (UTR) of an mRNA before translation initiation. In fact it seems likely that GW182 binds to the PABP (polyadenylation bindig protein), in the same region where PABP usually interacts with the one of the translation initiation factors. GW182 interaction with PABP impedes the formation of the circular mRNA structure that facilitates ribosome binding (Huntzinger et al., 2010). Other models support a direct role for Argonaute proteins in inhibiting the translational initiation complex, or even other steps such as translational elongation or peptide release. Models for microRNA mediated mRNA degradation have also been proposed.When microRNAs target a mRNA for degradation, the process is thought to take place in multiple stages. It is rare that AGO2 directly degrades mRNAs in animals., In fact, AGO2 slicer activity requires full complementarity between the microRNA and the target sequence, and such sites have apparently been subject to intense negative selection pressure in evolution. Normally when the miRISC binds to the 3'UTR of an mRNA this promotes deadenylation of the 3' end, followed by decapping of the 5' end and then degradion via 5'-3' decay (Wu et al., 2006; Behm-Ansmant et al., 2006; Eulalio et al., 2007). It is likely that all these processes take place in P-bodies. P-bodies are focal structures in the cytoplasm that are enriched for proteins involved in mRNA catabolism, translational repression and microRNA function. Interestingly, the formation of P-bodies is dependent on a functioning microRNA pathway, but microRNA-mediated silencing can occur when P-bodies are disrupted experimentally (Comprehensive reviews are: Huntzinger and Izaurralde 2011, Krol et al. 2010b, Filipowicz et al. 2008).

microRNAs biogenesis and functional mechanisms are well studied, however microRNA turnover is poorly understood. There are few studies dealing with this fundamental step. microRNA turnover can be extremely slow in liver and heart cells, with measured half lives of several days (van Rooij et al., 2007; Gatfield et al., 2009). At the other extreme are reports of turnover rates in the brain. After neuronal stimulation the half live of some microRNAs (miR-124, miR-128, miR-134, miR-138) is around one hour. Rapid microRNA metabolism might be related to the control of translation by neuronal activity, for example activity dependent degradation of a certain microRNA might induce translation of proteins necessary for memory formation (Krol et al. 2010a and reviewed in Krol et al. 2010b).

1.2 From Neuronal Stem Cells to Neuronal Spines

The structural complexity of the vertebrate neocortex is achieved in a construction process requiring several functionally distinct and temporally overlapping steps. After birth in the process of neurogenesis, neurons pass through a migration phase before undergoing morphological maturation. The wiring of neurons into circuits and ultimately networks creates the final architecture that allows us to interact with the outside world.

The cortex has two main intermingled neuronal types: principal cells and interneurons. These derive from different regions of the forming brain, respectively the ventricular zone (VZ) and the ganglionic eminences (GE). They migrate to their final position either radially from

the VZ or tangentially from the GE. Tangential migration is not a topic of this introduction but is reviewed in Marín et al. 2010.

The brain cortex comprises six layers, layer I or Marginal zone is the outermost and layer VI is the innermost one. Each layer houses a subtype of principal neuron, which projects to specific and distinct parts of the brain. For example, deep layer neurons (layer V and VI) have corticofugal (subcortical), and upper layer neurons (IV, III and II) have mainly corticocortical projections. Bear in mind, however, that within each cortical layer the principal neurons vary. How different neuronal types are generated is still a matter of debate, but it seems more and more evident that it requires a fine balance of different elements including progenitor pool diversification, cell autonomous processes and extrinsic signaling factors.

1.2.1 Embryonic Neurogenesis

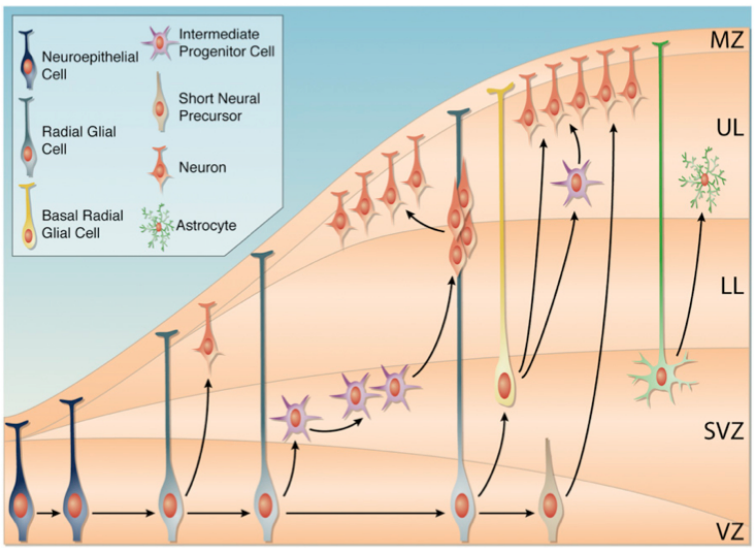

Figure 1.2: *Scheme of Neurogenesis and Migration.* Taken from Franco and Müller 2013.

Recent and exhaustive reviews on neurogenesis are Götz and Huttner 2005, Pinto and Götz 2007, Dehay and Kennedy 2007 and Franco and Müller 2013, the following paragraphs provide only a brief overview of the topic.

In the first stages of embryogenesis the neural tube has a single layer of neuroepithelial cells, that then give rise to a population of Radial Glial Cells (RGC). The cell bodies of RGCs are in the VZ and they extend processes to contact both the apical (ventricular zone) and the basal surface of the brain. They divide either symmetrically, in so-called proliferative divisions that generate two daughter cells equivalent to the mother; or asymmetrically, in so-called differentiative divisions, that generate one daughter cell equivalent to the mother and one more differentiated cell. One important factor for the asymmetric division of RGCs is the Glycogen Synthase Kinase 3 β (Gsk3β). High Gsk3β activity in a daughter cell leads to degradation of pro-proliferative proteins to generate either an Intermediate Progenitor Cells (IPC) or a neuron. If, on the contrary, Gsk3β activity remains low, the daughter cell retains the ability to proliferate (Kim et al., 2009b, 2011). RGCs parent only a minimal proportion of neurons (between 10 and 20%), they contribute mainly to the generation of IPCs. IPCs differ

from RGCs in their localization, they have their cell body in the SVZ; in their morphology, they are multipolar and do not reach either the apical or the basal surface; and in their marker expression, for example the IPC-specific transcription factor Tbr2. IPCs can undergo several symmetrical divisions to produce more IPCs and then undergo a final, symmetric neurogenic division. In recent years it has been discovered that there are more than one type of IPC, among others Basal progenitors and basal RGC (more abundant in primate brain).

Despite the increasing number of studies on cortical development and progenitor pools there is still debate on how the different neuronal types arise. There are mainly two different points of view: one in which an intrinsic genetic clock is the sole driving force behind the different waves of neurons and another in which extrinsic cues restrain the genetic programs, modulating and defining the fate of the nascent neurons.

The genetic clock model is the prevailing model in invertebrates. Doe and colleagues in a series of publications show that all the lineages of neurons in Drosophila descend from a single progenitor type in a perfectly timed, successive pattern (Pearson and Doe, 2003; Grosskortenhaus et al., 2005). Also in vertebrates there is evidence for the fact that neurons come from a single progenitor pool that differentiates in a time dependent manner. For example, heterochronic transplant in ferret cortex demonstrated that progenitors for lower layers neurons have the intrinsic potential to produce upper layer neurons, whereas upper layer progenitors are no longer able to produce lower layers neurons (McConnell and Kaznowski, 1991; Frantz and McConnell, 1996; Desai and McConnell, 2000). Other studies *in vitro* showed that cultured progenitors or murine and human pluripotent stem cells reproduce *in vitro* the pattern of progenitor waves seen *in vivo*, maintaining even the same timing (Shen et al., 2006; Gaspard et al., 2008; Espuny-Camacho et al., 2013).

Other studies challenge this view, postulating that there are several classes of predetermined progenitors that remain quiescent and require activation by extrinsic factors. For example, some of the genes characteristic for upper- or lower layer populationsare expressed in subpopulations of RGCs, such as Sox2 (Bani-Yaghoub et al., 2006) or in subpopulations of IPCs, such as Cux2, Satb2 or Svet1/Unc5D (Zimmer et al., 2004; Britanova et al., 2005; Tarabykin et al., 2001). In the first case, the Sox2 RGCs divide asymmetrically and produce deep layers neurons. The SVZ hosts IPCs and starts to expand only when upper layer neurons are generated. The story, nevertheless, is more complicated because cell autonomous cues also play a role in the final fate decision of a neuron. For example, the transcription factor Satb2 is necessary for the switch from subcallosally projecting neurons found in layer V to callosal projecting neurons typical of layer II by repressing the transcription factor Ctip2 (Britanova et al., 2008; Fishell and Hanashima, 2008).

The diversity of the neocortical progenitors, and their fundamental role in the generation of neocortical cell identities, has only been discovered in the past decade. Of particular interest is the relevance of these discoveries for brain evolution and the insight they have begun to provide on how the primate brain has attained its unique complexity (reviewed in LaMonica et al. 2012). Figure 1.2 show schematically the different progenitor types and the neuronal migration steps.

1.2.2 Adult Neurogenesis

Neurogenesis also occurs in the mammalian adult brain but only two established niches retain this ability: the subventricular zone (SVZ) of the lateral ventricle and the subgranular zone (SGZ) of the dentate gyrus in the hippocampus. The neuroblasts of the SVZ are the progenitor pool for the olfactory bulb granule neurons. There are three types of precursors in the SVZ: type B (GFAP positive progenitors), type C (transit amplifying cells) and type A (migrating neuroblasts). Type C and type A cells both express Doublecortin (DCX). Note that GFAP, usually considered to be an astrocyte marker is also expressed in adult progenitors. The neuroblasts migrate tangentially from the SVZ to the olfactory bulb in a path known as the Rostral Migratory Stream (RMS). There is evidence that the ependymal cells of the ventricular wall secrete factors necessary for the maintenance of a functional progenitor pool (Sawamoto et al., 2006; Ramírez-Castillejo et al., 2006; Zhao et al., 2008; Paez-Gonzalez et al., 2011). In the dentate gyrus of the hippocampus there are two different types of progenitors: type 1 and 2. Type 1 is most likely a quiescent progenitor cell with a radial process that spans the entire granular layer. Type 1 cells are distinguished by their expression of GFAP, Sox2 and Nestin. Type 2 progenitors are derived from type 1, they have short processes and are Sox2 and Nestin positive but GFAP negative. Type 2 progenitors generate DCX positive neuroblasts that then mature into glutamatergic dentate gyrus neurons. Hippocampal astrocytes play a similar role to ependymal cells by secreting factors required for maintenance of the stem cell population (reviewed in Zhao et al. 2008; Yao et al. 2012).

1.2.3 Radial Migration in Corticogenesis

Principal neurons, generated either from RGCs or IPCs, migrate to reach their final positioning in an inside out manner. In the first stages of cortical development the earliest born neurons form the preplate between the VZ and the Pia. The preplate, then splits into the marginal zone (or layer I), that hosts Cajal-Retzius cells, the source of Reelin; and the subplate, a structure present only during embryonic development that is important for the correct wiring of the neurons and functional maturation of the neocortex (reviewed Kanold and Luhmann 2010). Waves of neurons form the cortical plate starting from layer VI and finishing with layer II (for reviews Pinto and Götz 2007; Franco and Müller 2013). Correct execution of cortical lamination, starting from the innermost layer (VI) and finishing with the outermost one (II), is necessary for the functioning of the brain. Impaired lamination during corticogenesis leads to severe phenotypes such as lissencephalies or heterotopias. Probably the most famous example is the reeler mouse, discovered in 1951. Reeler mice lack Reelin, a protein secreted from Cajal-Retzius cells in the marginal zone (D'Arcangelo et al., 1995). Reelin is required for inside-out migration and in its absence lamination is reversed with the earliest born neurons forming the outermost layer and the last neurons the innermost layer (reviewed also in Tissir and Goffinet 2003). In reeler mice radial migration is affected due to the loss of Reelin, one of the best characterized secreted molecules necessary for brain morphogenesis. Other important mechanisms in which Reelin is involved will be further discussed below.

Radial migration can be divided into four stages: in the first phase neuroblasts move radially from VZ to SVZ, in the second neuroblasts stall for up to 24 h in the SVZ/IZ and

become multipolar. The third stage is optional, with some neuroblasts projecting toward the VZ a process used to translocate their nuclei back to the VZ. In stage 4 the neuroblasts, regardless of their initial localization, become bipolar and migrate radially into the cortical plate (Noctor et al., 2004). Bipolar neurons have a trailing process with axonal identity, and a leading process that remains in contact with the radial glia until the neuron reaches its final position. It is still unclear which signals force the projection neurons to have a single leading process, in contrast to the multipolar neurons migrating tangentially. It is likely that there are feedback signals from the pial surface that block the formation of scouting branches. The maintenance of a functional cytoskeleton seems the key to correct migration; the modification of one of its constituents or of an upstream signaling molecule necessary to modulate it, results in impaired migration either due to failure to enter the cortical plate or premature detachment of the migrating neuroblast from the radial glia. If the microtubule-stabilizing protein DCX is knocked down by RNAi, during embryogenesis, the multipolar neurons in SVZ/IZ (stage two) are no longer able to become bipolar and to reach the final position (Bai et al., 2003; LoTurco and Bai, 2006).

Secreted proteins are important for guiding migrating neuroblasts. Reelin, for example, in early stages of corticogenesis is necessary for RGC-guided locomotion by directing the end feet of the leading process into the cortical plate and facilitating their attachment to the pial surface (Jossin et al., 2004; Magdaleno et al., 2002; Zhou et al., 2008). Sema 3A, another chemoattractant for migrating neurons (Polleux et al., 2000), is indispensable for stabilizing the radial process. Downregulation of Sema 3A or one of its receptors impairs neuronal migration, most likely by interfering with the cytoplasmic signals that coordinate the motility of migrating neurons (Chen et al. 2008; reviewed in Zhou et al. 2008). To reach the correct end position the migrating neurons must remain in contact with the radial glia, this can also be mediated by gap junction adhesions. A disruption of the gap junction causes the neuron to modify its cytoskeleton, leading to protruding filipodia and branches and to premature termination of migration (Elias et al., 2007). Other cases of prematurely branching neurons in corticogenesis involve p35 and srGAP2. Loss of p35, an activator of CdK5 involved in actin cytoskeleton modification, leads to inverted cortical layering (Gupta et al., 2003). SrGAP2 (slit-robo GTPase activating protein) negatively regulates neuronal migration by inducing filipodia and branches in the leading process. srGAP2 is a complex protein in which the different domains serve distinct functions, nonetheless all converging on filopodial sprouting. In fact, the F-BAR domain of srGAP2 directly sculpts and deforms the plasma membrane. The GAP domain contributes by interacting with Rac1, increasing Cdc42 activity, and therefore leading to filipodia formation (Guerrier et al., 2009).

Another key component of radial migration related to the cytoskeleton involves the arrangement of microtubules. The centrosome, a microtubule organizing center, positions itself in front of the neurite that will become the leading process at the same time that the trailing process (destined to become the axon) sprouts from the rear of the cell. In multipolar migrating neurons, on the contrary, the centrosome locates initially in front of the neurite that will become the axon and then shifts position to the base of a new neurite that will become the leading process (Sakakibara et al. 2013b; Sakakibara et al. 2013a review).

When the neuron reaches its final destination the cytoskeleton stabilizes and the nucleus ceases to move. Once again Reelin is an important player, acting at least in two different and complementary ways. Interaction between Reelin and integrin-$\alpha1\beta3$ is a signal for the neuron to detach from the radial glia (Dulabon et al., 2000). By inducing phosphorylation of n-Cofilin Reelin also stabilizes the actin cytoskeleton (Chai et al. 2009, reviewed in Zhao and Frotscher 2010). Detailed reviews on this topic are Franco and Müller 2013; Solecki 2012; Cooper 2013; Heng et al. 2010.

1.2.4 Neuronal Polarization *in vitro*

The account of neuronal migration presented in the previous section has primarily come from *in vivo* investigations. These have been supplemented by *in vitro* studies attempting to model the composite steps of the process at the individual neuron level. In particular, researchers focused their attention on an *in vitro* model to understand the intrinsic neuronal changes during polarization. Primary cortical and hippocampal neuronal cultures are good models that can be easily manipulated and that recapitulate the stages a neuron undergoes from the multipolar stage in the SVZ/IZ to the polarization and finally to the complex structure of a mature and wired neuron (Polleux and Snider, 2010). Primary neuronal cultures are prepared from embryonic cortex or hippocampus. During the preparation they lose their natural polarity and become spherical. Once the cells attach to the culturing surface, they start to explore the environment by protruding and retracting lamellipodia and filipodia (stage 1). These protrusions develop into multiple, immature neurites that are initially equivalent (stage 2, DIV 1-2), until at a certain point one of them breaks the symmetry and elongates to form the axon (stage 3, DIV 2-4). The other neurites then begin to grow, adopting dendritic identity (stage 4, DIV 4-15). Once the dendritic arbor is complete, synapses form. All the stages described correspond approximately to specific events *in vivo* (Figure 1.3).

Many studies on neuronal polarization and maturation focused on the cytoskeletal dynamics. *In vitro* the centrosome takes up a position in front of the future axon and organizes the microtubules. If a cell has multiple centrosomes, it will also have multiple axons (de Anda et al., 2005; Sakakibara et al., 2013a). The centrosome position contributes to microtubule rearrangement as the neuron breaks symmetry (stage 3). In the nascent axon the cytoskeletal modification consists of the destabilization of actin components and the stabilization of microtubules. At the growing tip of the axon, the growth cone exerts a strong influence on the elongation of the axon. All the neurites possess a growth cone, but the one of the growing axon becomes dynamic, whereas the others remain quiescent. The growth cone is divided into several functional domains, including the wrist that forms the connection to the neurite shaft, the central domain (C-domain) that hosts the microtubules that enter the axon shaft and the peripheral domain (P-domain) that is enriched in actin filaments. Protrusion of actin filaments from the P-domain are an initial step in the creation of filipodia and lamellipodia (reviewed in Stiess and Bradke 2011; Lowery and Van Vactor 2009; Bradke and Dotti 1999; Hoogenraad and Bradke 2009).

There are several interlaced pathways that cooperate in axon formation, for example, the polarity complex, Gsk3β, Cdc42, DCX, Reelin, Smurf1 and 2 and semaphorins that I will now

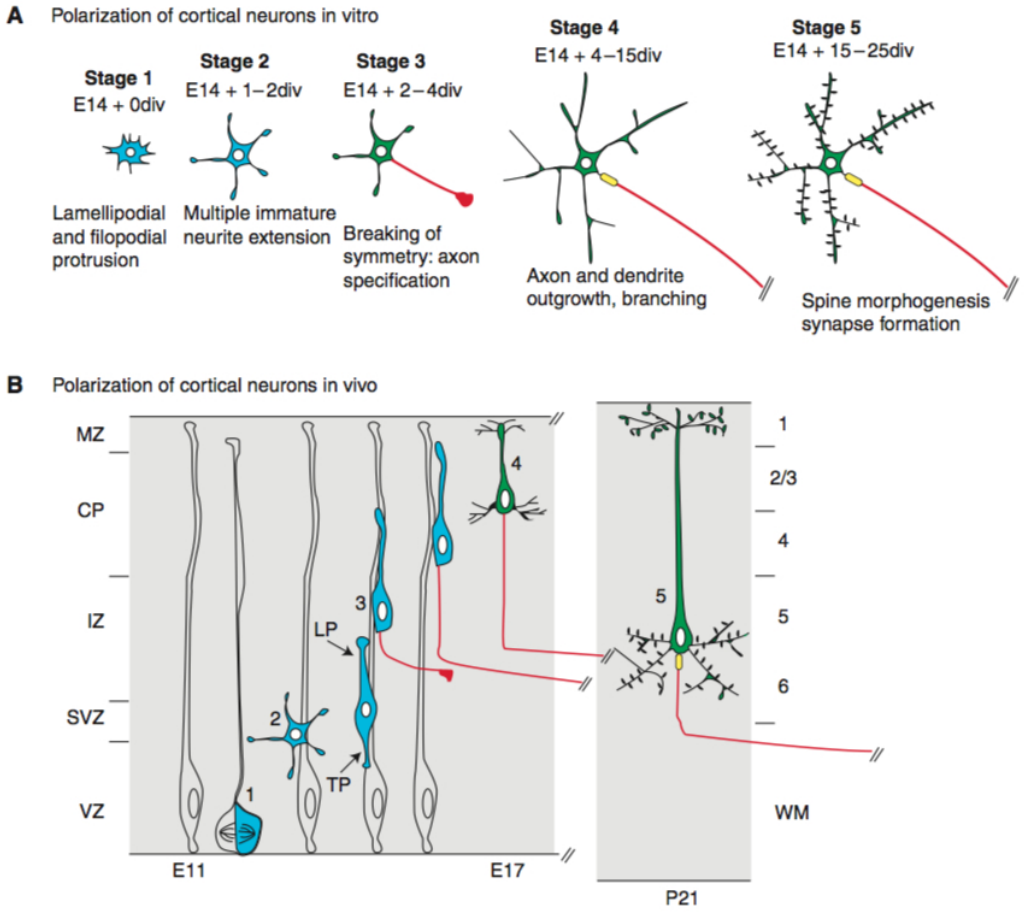

Figure 1.3: *Stages of Neuronal Polarization In Vitro* compared to neuronal maturation *in vivo*. Taken from Polleux and Snider 2010

discuss in turn. The receptor for the secreted protein Reelin is primarily located at the tip of the active growth cone, where it is able to inactivate Gsk3β (Beffert et al., 2002). Reelin signaling also activates the kinases Cdc42 and Rac1, key players in growth cone motility and the formation of filipodia and branches (Leemhuis et al., 2010; Leemhuis and Bock, 2011). Cdc42 and Rac1 activate the polarity complex, an assembly of the proteins Par3, Par6 and atypical protein kinase C (aPKC) that is restricted to the growing axon. Upon its activation the polarity complex phosphorylates and inhibits Gsk3β. Gsk3β inactivation is a key event in the process of axon formation, because active Gsk3β negatively regulates microtubule stability (Yoshimura et al. 2005, reviews Jiang et al. 2005; Schwamborn and Püschel 2004; Hoogenraad and Bradke 2009). The polarity complex also interacts with the HECT E3 ligases Smurf1 and Smurf2, both fundamental in breaking neurite symmetry. Smurf2 is shuttled to the growth cone by Par3, where it is required for the restriction of active Rap1b (RAS related protein 1b) to the nascent axon (Schwamborn et al., 2007a,b). The ubiquitination targets of Smurf1 change according to its phosphorylation state. In the future axon the Brain-derived neurotrophic factor (BDNF) pathway leads to Smurf1 phosphorylation and consequent recognition and targeting of RhoA, a growth inhibitory small GTPase. In minor neuritis, by contrast, the unphosphorylated form of Smurf1 targets the polarity complex protein Par6 (Cheng et al., 2011). BDNF receptors are generally located throughout the

neuronal periphery, but they can be transported to and stabilized at the distal part of the axon by Jip3, a protein required for the functional interaction of axonal cargos with Kinesin-1 (Huang et al., 2011). This allows differential activation of the BDNF pathway in the growing axon, and as I discussed before this is required for the polarization process. Jip3 interacts also with Gsk3β and DCX (a microtubule stabilizing protein) to restrain axon branching and to promote self avoidance (Bilimoria et al., 2010). Semaphorins and their receptors influence polarization and axonal or dendritic specification by modulating the ratio between cAMP and cGMP. In the absence of Semaphorin signaling in the growing axon cAMP levels are high, maintaining activity of the polarity complex and axon. In minor neurites, in contrast, Sema 3A and its receptors increase the level of cGMP, which activates a cascade of events that leads to dendrite identity. Even after polarization, alterations in the balance between cAMP and cGMP can modify the identity of the neurites (Shelly et al., 2007, 2010, 2011; Shelly and Poo, 2011; Nishiyama et al., 2011).

In summary, neurons are among the most polarized cells in the body. Polarity is the outcome of complex interactions between multiple, interrelated pathways. A fine-tuning of pathway components is necessary to have a single axon and multiple dendrites. If one of the proteins described above is not functional the balance between the pathways is disrupted and the result is a neuron that has either zero or multiple axons. Until now, however, zero or multiple axons phenotypes have not been described *in vivo*.

1.2.5 Dendritic Arborization and Spines Formation

During corticogenesis, when polarized neurons reach their final position in the cortex, they start to build their dendritic arbor. Dendrites and axons have different and complementary functions: dendrites receive inputs from other neurons and integrate the signals; axons fires the output of the received information. The cytoskeletal structure differs in the two compartments: in the axon the microtubules are all oriented with the plus (or growing) end at the tip; in the dendrites there is a mixture of orientations. Dendrites grow away from the soma, following external cues. They protrude filipodia, at the end of which there is a growth cone-like structure. If the environment is permissive, the filipodia mature into actual branches. Dendrites stop growing when they encounter repulsive signals, these limit dendritic growth and establish a so-called territory of competence, or dendritic space, for each neuron. The territory of competence is fundamental for the correct wiring of the neurons into their characteristic circuits; only correctly wired neurons undergo full maturation. Dendrites, however, are not static structures, they can remodel their cytoskeletal components by growing or retracting filipodia and spines in response to the inputs received from the neighboring cells, including synaptic activity (reviewed in Kulkarni and Firestein 2012; Puram and Bonni 2013).

The different steps of dendrite formation are synchronously regulated via intrinsic mechanisms, such as transcription factors and extracellular cues, such as guidance molecules, growth factors or neurotrophins. The principal neurons of each cortical layer differ from the principal neurons in the other layers in a cell intrinsic manner, such as the expression of layer-specific transcription factors. The differences might be established at the time of birth or be a consequence of the progenitor pool from which they came (see Section 1.2.3). The transcription

factors Cux 1 and Cux 2 are exclusively expressed in layer II/III, where they are necessary for the regulation of dendritic branching (Cubelos et al., 2010). Some universal cytoskeletal components, present in all neurons, can be regulated in distinct ways in different layers. NOMA-GAP, an inhibitor of Cdc42, is crucial for attaining a complex dendritic arbor in upper layers, but not in deep layers (Rosário et al., 2012; Simó and Cooper, 2012). Moreover, external cues have opposite effects on particular neuronal types. BDNF stimulates layer IV, inhibits layer VI and is neutral for layer V branching, whereas Neurotrophin 3 (NT-3) promotes layer VI but inhibits layer IV branching (reviewed in Simó and Cooper 2012; Kulkarni and Firestein 2012; Puram and Bonni 2013). The secreted factor Reelin promotes dendritic branching *in vitro*, due to the activation of the Serine/Threonine protein kinase mTOR (Jossin and Goffinet, 2007). mTOR forms two complexes termed mTORC1 and mTORC2 that are both involved in the development of the dendritic arbor (Urbanska et al., 2012). mTORC2, for example, enhances dendrite and spine formation by activating the Akt pathway and the downstream effector protein CALEB/NGC (Brandt et al., 2007).

The complex and ramified structure typical of mature neurons is therefore the result of both cell autonomous and extrinsic mechanisms. A well-built dendritic arbor is critical for neuronal function, allowing extensive interactions with neighboring cells. The interaction between two neurons occurs at the synapse, comprised of a presynaptic component that is part of the axon, and a postsynaptic component, the spine, that is part of the dendrite. Spines are structures protruding from the dendritic shaft. They begin as thin and headless filipodia that are highly motile and able to sample the environment and find a presynaptic target. If they find it, they mature into functional spines (reviewed in Hoogenraad and Akhmanova 2010; Yoshihara et al. 2009; Tada and Sheng 2006). These have a complex internal structure in which scaffolding proteins are bound to the actin cytoskeleton and anchor the receptors to the upper part of the spine, called the post-synaptic density. Spines have a characteristic morphology with a neck and a head, and their shape is modified according to their degree of maturation. They are classified according to their degree of maturation either as immature, with a long neck and small head, or mushroom shaped, or stubby with almost no neck and a large head. The head width is directly correlated with AMPA and NMDA receptor pools (reviewed in Hoogenraad and Akhmanova 2010; Yoshihara et al. 2009; Tada and Sheng 2006; Segal 2010; Hayashi and Majewska 2005.) AMPA and NMDA receptors (AMPAR and NMDAR) are glutamate receptors, responsible for the depolarization of the postsynaptic site. In particular, there is evidence that the head size of a spine correlates positively with the number of AMPA receptors. The higher the number of AMPA receptors the bigger the head. AMPAR are tetramer assemblies of four highly homologous subunits (Gria1-4). The assembled tetramer is shuttled in and out from the membrane in synchrony with the strength of the inputs received from the presynapse. In so-called silent synapses, for example, there are only NMDARs, which alone are not able to depolarize the membrane. When silent synapses receive strong stimuli a pool of AMPARs, stored next to the spine, is inserted into the membrane of the synapse and the spine becomes active (reviewed in Milstein and Nicoll 2008; Anggono and Huganir 2012; Huganir and Nicoll 2013; Yokoi et al. 2012; Kerchner and Nicoll 2008). AMPARs require either TARPs or chornichons as auxiliary proteins. Stargazin, also called Cacng2, is one

of the most studied auxiliary proteins for the AMPAR. Stargazin is able to bind both the receptor and PSD95, one of the proteins of the post-synaptic density, stabilizing the receptor tetramer in the plasma membrane (Chen et al., 2000). More detailed information on synaptic receptors, their functions and interaction with the cytoskeleton are reviewed in Anggono and Huganir 2012; Huganir and Nicoll 2013; Yokoi et al. 2012; Segal 2010.

1.2.6 Phf6

Phf6 (Plant Homeo Domain-like finger protein) is a protein encoded on the X chromosome, discovered a decade ago as the cause of Börjesom-Forssman-Lehmann syndrome (BFLS, OMIM #301900, Lower et al. 2002). Phf6 protein has 365 amino acids comprising two PHD zinc finger-like domains and 4 nuclear localization sequences (Lower et al., 2002). Patients with BFLS are obese, present with swelling of subcutaneous tissues, a narrow palpebral fissure and big earlobes. Moreover, they have moderate to severe mental retardation and epilepsy (Gécz et al., 2006). Phf6 somatic mutations are also linked to lymphoblastic leukaemia (T-ALL, Van Vlierberghe et al. 2010; Chao et al. 2010) and to acute myeloid leukemia (AML, Van Vlierberghe et al. 2011), therefore it is also considered to be a tumor suppressor gene.

Phf6 suppresses rRNA synthesis as a function of the cell cycle (Wang et al., 2013) and it is able to target chromatin remodelers to posttranscriptionally modify histones. Phf6 interacts with the NurD complex (nucleosome remodeling and deacetylation complex), that has both histone deacetylase and ATP-dependent chromatin remodeling activity (Todd and Picketts, 2012). A comprehensive study on the Phf6 expression pattern in murine brain shows that the protein is highly expressed in embryonic development with a slight reduction in adulthood (Voss et al., 2007). Depletion of Phf6 by shRNA treatment in *in utero* electroporation leads to a cell autonomous failure of migration, with the affected neurons unable to reach their final position, and instead stopping randomly in the cortex and in the white matter. The knockdown neurons also show hyperexcitability, similarly to the BFLS patients. Zhang et all demonstrate that Pfh6 associates with the transcription elongation complex PAF1 and regulates CALEB/NGC (Zhang et al., 2013). CALEB/NGC was already known for its positive regulation of dendritic arborization and spine formation (Brandt et al., 2007). Unfortunately, Zhang et al. did not comment on the dendritic arbor of Phf6 knockdown neurons.

1.3 microRNAs in the Brain: from Neuronal Stem Cells to Synapses

The gene regulatory function of microRNAs is fundamental for embryonic development. As such, targeted deletion of genes required for microRNA biogenesis, including DGCR8, Dicer or Ago2, is incompatible with life (Stark et al., 2008; Wang et al., 2007; Bernstein et al., 2003; Liu et al., 2004). There are also studies in which the proteins of the biogenesis machinery are conditionally depleted in particular cell types. Dicer ablation in neuronal progenitors results in a thinner cortex with disorganized layers and increased apoptosis, indicating that microRNAs are necessary for the expansion of neuronal progenitors and neuronal differentiation (McLoughlin et al. 2012, reviewed in Sun et al. 2013). Dicer removal from specific postmi-

totic neuronal subtypes results in increased apoptosis of the knockout neurons, underscoring the vital role of microRNAs (reviewed in Sun et al. 2013). Moreover, conditional deletion of DGCR8 or Dicer in the same cell types produces a more severe phenotype in Dicer knockout neurons, indicating that non-canonically processed, DGCR8 independent microRNAs are important for cellular viability and functionality (Babiarz et al., 2011).

In the brain, some microRNAs display either region-specific or neuronal subtype-specific expression patterns (Pichardo-Casas et al., 2012; He et al., 2012). For example, miR-128 expression is 4-fold higher in the cortex compared to the cerebellum but miR-195 and miR-197 are 10-fold higher in the cerebellum compared to the cortex (He et al., 2012). Similarly, some microRNAs are specifically expressed in particular subregions such as miR-206 in the cerebellum, miR-136 in the cortex, or miR-200 in the olfactory bulb (Pichardo-Casas et al., 2012). Different classes of neurons can express differential sets of microRNAs: miR-128 is expressed in CamKII but not in GAD2 neurons, and miR-187 is expressed with the opposite pattern (He et al., 2012). Another interesting fact is that microRNAs can be preferentially localized subcellularly within the neuron. Some microRNAs are enriched in dendrites, dendritic localization of miR-134 depends on a specific sequence in the loop that allows its shuttling to the dendrites before being processed (Bicker et al., 2013). There are also microRNAs that are enriched in synapses (miR-200 or miR-182) (Lugli et al., 2008), soma (miR-125a and let-7b) (Lugli et al., 2008); or nucleus (miR-92a and miR-25) (Khudayberdiev et al., 2013).

Along with these general studies on microRNA localization in brain regions and in neurons many studies have addressed specific microRNAs and their functions (Figure 1.4). Some microRNAs are necessary for stem cell maintenance (miR-17-92 cluster, miR-184, miR-134, miR-195), for stem cell differentiation and neuronal maturation (let-7a and b, miR-9, miR-26b, miR-124, miR-125b,), for dendritic branching (miR-124, miR-132, miR-134), or for synapse formation and functionality (miR-125, miR-134, miR-138, miR-188, miR-181a).

Several studies show that microRNAs are necessary to retain stemness features in embryonic and adult neural stem cells (NSC). miR-134 and the miR-17-92 cluster are positive regulators of embryonic stem cell survival. miR-134 regulates both the mRNA of Chordin-like 1 (Chrdl1), a proapoptotic protein, and of DCX, a microtubule associated protein that coordinates the radial migration of neurons. Therefore miR-134 expression in NSCs allows their survival, by blocking translation of the proapoptotic protein Chrdl1, and the maintenance of their stemness, by blocking translation of DCX (Gaughwin et al., 2011). The miR-17-92 cluster controls the expansion of NSCs and RGCs as well as the transition to IPCs (Bian et al., 2013). In particular, the cluster is responsible for the regulation of PTEN, which negatively controls RGCs production, and Tbr2, which positively governs IPCs generation. Likewise, there are microRNAs implicated in the maintenance of adult stem cells (aNSC). miR-184 and miR-195 are expressed in aNSCs and are important for the maintenance of aNCS stemness. In this context miR-184 regulates Numblike mRNA. Numblike is a protein involved in brain development, most likely as a negative inhibitor of Notch signaling (Liu et al., 2010). miR-195 regulates MBD1 (methylated-CpG binding protein) mRNA. MBD1 is expressed in neurons but not in NSCs and it is able to methylate DNA sequences to block DNA transcription. In particular, Liu and colleagues showed that MBD1 is able to repress transcription of miR-184

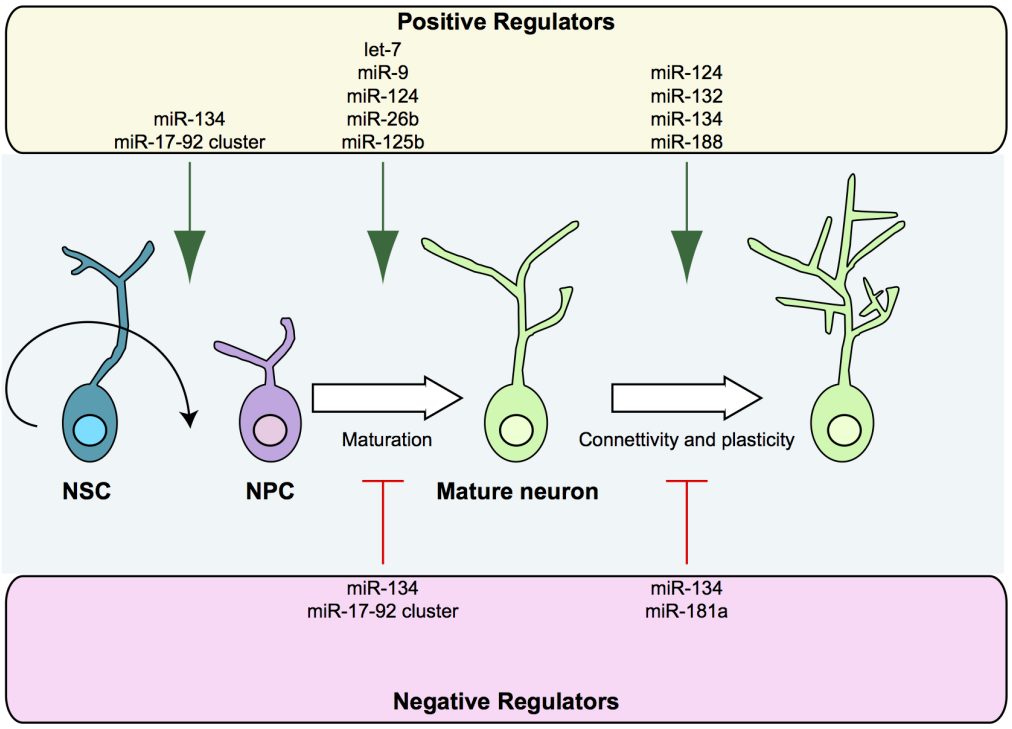

Figure 1.4: *microRNAs regulate different steps of neuronal life* from the maintenance of NSC to the formation of spines. Modified from McNeill and Van Vactor 2012.

and miR-195 (Liu et al., 2010, 2013). miR-195 and MBD1 form, therefore, a negative feedback loop, with miR-195 blocking MBD1 mRNA translation and MBD1 protein repressing miR-195 transcription.

On the other hand, there are microRNAs that positively regulate the transition from NSCs to postmitotic neurons. In fact, miR-9 and miR-124 are necessary and sufficient for the reprogramming of human fibroblasts into neurons. They promote the expression of neurogenic transcription factors such as NeuroD2, ASCL1, and MYTIL (Yoo et al., 2011; Xue et al., 2013). miR-9 and miR-124 are also implicated in embryonic neuronal differentiation. miR-9, for example, is able to regulate TLX, a factor important for transcriptional control in undifferentiated neuroepithelial cells (Zhao et al., 2009). miR-9 regulates neurogenesis also in the subpallium by inhibiting several transcription factors (Shibata et al., 2011). miR-124 regulates diverse mRNAs coding for stem cell specific proteins. Polypyrimidine Tract-Binding Protein 1 (PTBP1) is an RNA-binding protein able to repress nervous system specific alternative splicing. In non-neuronal cells PTBP1 represses the correct splicing of PTBP2, a closely related protein that is enriched in the nervous system. miR-124 is able to bind to the PTBP1 3'UTR, blocking its translation. This leads in turn to the productive splicing and consequently the expression of PTBP2 (Makeyev et al., 2007). Furthermore, miR-124 and miR-26b are both able to regulate Ctdsp (C-terminal domain phosphatase), proteins involved in global suppression of neuronal gene expression in non-neural cells. REST (RE1 silencing transcription factor) is able to bind to the RE1 (Repression Element 1) sequence present in the promoters of neuronal genes, blocking their transcription with different mechanisms. One of these involves the formation of a complex with three phosphatases (Ctdsp1, Ctdsp2, and

Ctdspl) that are able to dephosphorylate the C-terminus of RNA pol II, thereby inhibiting the expression of genes with the RE1 sequence. miR-124 binds to the 3'UTR of Ctdsp1 and miR-26b binds to the 3'UTR of Ctdsp2, blocking their translation and therefore allowing the transcription of neuronal genes. Ctdsp2 and miR-26b form a negative feedback loop, as miR-26b is a target for transcriptional suppression by the REST/Ctdsp2 complex (Visvanathan et al., 2007; Dill et al., 2012). In the adult SVZ miR-124 can be detected in transient amplifying cells (type C) where it is able to repress Sox9 expression, leading to neuronal maturation (Cheng et al., 2009; Åkerblom et al., 2012). Members of the let-7 family also participate in neuronal differentiation. let-7b represses Lin28, a stem cell RNA-binding protein, forming a negative feedback loop (Rybak et al., 2008). And let-7a, a microRNA required for neuronal differentiation, increases its activity due to TRIM32, a TRIM-NHL protein (Schwamborn et al., 2009). The last example regards miR-125b, a microRNA that promotes neuronal maturation by repressing Nestin mRNA translation. Nestin is an intermediate filament protein abundant in neural stem/ progenitor cells (Cui et al., 2012).

Comparatively little is known about the regulatory role of microRNAs in neuronal migration. miR-9 and miR-132 control, in a positive way, neuronal migration. They downregulate FoxP2, a transcription factor normally expressed in layer VI of the cortex. When FoxP2 is ectopically expressed neurons are unable to migrate radially and to grow a proper axon (Clovis et al., 2012). Therefore, downregulation of FoxP2 mRNA in migrating neurons is necessary for correct cortical lamination and axonal outgrowth.

More is known about the regulation of the dendritic arborization and branching by microRNAs. miR-124 and miR-132 have a positive effect on dendritic outgrowth and branching (Yoo et al., 2009; Franke et al., 2012; Vo et al., 2005; Pathania et al., 2012; Marler et al., 2014). miR-124 promotes neurite outgrowth (Yoo et al., 2009) and induces dendritic and axonal complexity by regulating the 3'UTR of RhoG. RhoG reduces dendritic ramification via Cdc42 and axonal ramification via Rac1/ELMO1DOCK1 (Franke et al., 2012). miR-132 is part of the miR-212/132 cluster, whose transcription is induced by BDNF-mediated phosphorylation of CREB. miR-132 modulates the expression of p250GAP, a GTPase activating protein that reduces dendritic growth by suppressing Rac1 (Vo et al., 2005). miR-132 regulation of p250GAP is also necessary in axons of retinal ganglion cells, where it promotes branching (Marler et al., 2014). Diametrically opposite roles have been assigned for miR-134, part of the miR-379-410 cluster, in two studies using different experimental paradigms. miR-134 was shown to promote dendritic branching of cultured hippocampal neurons (Fiore et al., 2009) but to inhibit dendritogenesis in layer V neurons *in vivo* (Christensen et al., 2010). The miR-134 precursor contains a sequence motif responsible for shuttling it into dendrites. The motif is recognized by DHX36, a member of the large DEAH-Box family of RNA helicases, for facilitated transport to the dendrite (Bicker et al., 2013). In the dendritic spine miR-134 is able to locally regulate the actin cytoskeleton in an activity dependent manner. In resting conditions miR-134 binds to the Limk1 3'UTR, impeding spine growth. The interaction is disrupted by BDNF stimulation. This enhances modification and growth of active spines, in line with the maturation of dendritic spines seen upon BDNF stimulation (Schratt et al., 2006). AMPAR and NMDAR expression can also be modulated by microRNAs: miR-181a regulates

the AMPAR subunit Gria2 (Saba et al., 2012) and miR-125 regulates the NMDAR subunit NR2A. Another microRNA, miR-188, is able to mediate an increase in the size of synapses. miR-188 downregulates the semaphorin receptor Nrp2. Semaphorins inhibit spine development and the formation of synaptic structure, therefore miR-188 may play a fundamental role in memory formation (Lee et al., 2012).

Roles for microRNA in the presynaptic compartment have also been described in the sensory neurons of the mollusc Aplysia. In this system miR-124 constrains serotonin-induced facilitation by downregulating CREB1 (Rajasethupathy et al., 2009).

From these examples, it can be seen that microRNA are necessary to control all the steps of brain development, from the maintenance of a functional NSC pool to the regulation of memory formation. Several microRNAs, such as miR-134, miR-124 or miR-132, have important roles in the regulation of diverse processes throughout the life span. However, this phenomenon is not surprising or unexpected, as microRNAs are predicted to modulate hundreds of genes and their targets can change in parallel to changes in the cellular transcriptome. One recurring feature of microRNA-mediated regulatory networks is the presence of negative feedback loops. For example, the loop consisting of the let-7 microRNA and its inhibitor, Lin28, is especially important for the fine-tuning of delicate mechanisms, such as neuronal differentiation. The ever increasing number of publications about microRNAs in the brain is only the tip of the iceberg. We still do not fully understand the general role of microRNAs and other non-coding RNAs in the nervous system.

1.4 miR-128, known functions

The focus of my research was to characterize the functions of one particular microRNA, miR-128, in the brain. When I started my PhD little was known about miR-128 function in neurons. In the last five years an increasing number of publications have shed light on the importance of miR-128 as a tumor suppressor microRNA and as a strategic regulator of memory extinction and neuronal homeostasis.

Most of the studies about miR-128 regard its association with cancers. miR-128 is downregulated in glioma, neuroblastoma, prostate cancer and in breast cancer (Ciafrè et al., 2005; Evangelisti et al., 2009; Papagiannakopoulos et al., 2012; Li et al., 2013). However miR-128 is upregulated in triple negative breast cancer, in acute lymphoblastic leukemia (ALL) and in monocytes of patients with sporadic Alzheimer Disease (Liu et al., 2014b; Zhu et al., 2012; Tiribuzi et al., 2014). Many studies have identified target genes for miR-128 in the context of these cancers.

miR-128 is a brain-enriched, neuron specific microRNA (Smirnova et al., 2005). Its expression in the embryonic cortex increases more than 20-fold between E12 and E16 (unpublished observation Wulczyn, Tarabykin, Chen), second only to miR-124 in the degree of upregulation. In human brain miR-128 is the second most highly expressed microRNA after the let-7 family (Shao et al., 2010). But a comprehensive understanding of the many roles miR-128 may play in brain development and in adult brain functions remains to be achieved.

miR-128 has two isoforms: pre-miR-128-1 and pre-miR-128-2. Their mature form is identical but they differ in the length of their precursor, 56 and 58 nucleotides, respectively, and

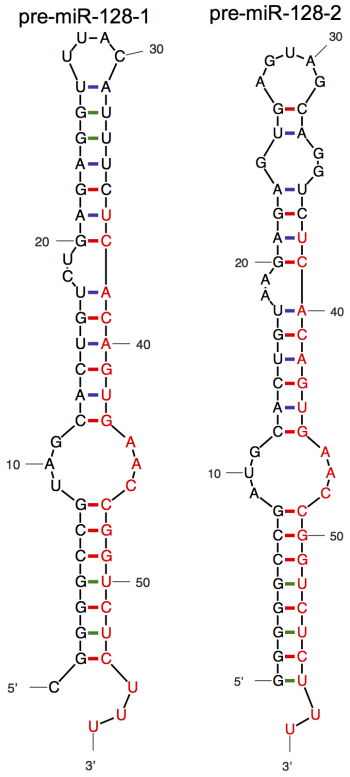

Figure 1.5: *pre-miR-128-1 and pre-miR-128-2* are shown in their secondary structure, miR-128 mature form is in red. Sequences taken from miRBase.

in their secondary structure (Figure 1.5). pre-miR-128-1 and pre-miR-128-2 are conserved among vertebrates and they are hosted in an intron of two highly homologous genes, R3hdm1 and R3hdm3 (better known as Arpp21), respectively.

Three recent publications show that miR-128 regulates non-sense mediated decay in the brain (Bruno et al., 2011), helps to extinguish fearful memories (Lin et al., 2011) and controls motor behavior and neuronal excitability (Tan et al., 2013). Non-sense mediated decay (NMD) is a quality control for mRNA that leads to the degradation of transcribed genes containing premature stop codons. Bruno et al. showed that miR-128 regulates the expression of Casc3 and Upf1, two important proteins for NMD. This study suggests that miR-128 might reinforce neuron-specific patterns of mRNA utilization, similar to the role of miR-124 in the control of neuron-specific alternative splicing (Makeyev et al., 2007). Lin et al. studied miR-128 functions in an experimental fear-extinction paradigm, demonstrating that miR-128 levels increase after fear conditioning and, to an even greater extent, after fear extinction. This is in line with a previous report showing increased miR-128 in the hippocampus after fear conditioning (Kye et al., 2011). With the help of lentiviral constructs overexpressing or blocking miR-128 functions in prefrontal cortex, Lin et al. could correlate miR-128 activity with the ability of mice to erase fearful memories. The authors screened for potential miR-128 targets using a published predictive algorithm and confirmed as bona fide targets several genes involved in neuronal plasticity (Creb1, Reelin, Arpp21). The upregulation of miR-128 during the fear extinction protocol leads to the downregulation of proteins important in synaptic

plasticity such as the miR-128 host gene Arpp21 (Lin et al., 2011). One of the Arpp21 splicing variants is involved in calcium signaling pathways in neurons expressing dopamin 1 (D1) receptor (Rakhilin, 2004). The last piece of evidence for miR-128 functions in the brain comes from the work of Tan et al.. They produced different conditional knockout mice lines for miR-128. In particular, they showed that pre-miR-128-1 contributes less than 20% to the total amount of the mature microRNA, whereas pre-miR-128-2 contributes the remaining 80%. Pre-miR-128-2 knockout animals suffer from severe epileptic seizures that cause the death of all the animals by the 5^{th} month of age. The authors tested the contribution of the two major classes of CamKII dopaminergic neurons to the phenotype. Dopamine-receptor 1 expressing neurons (D1 neurons) are known to increase locomotion, whereas Dopamin-receptor 2 expressing neurons (D2 neurons) are known to decrease locomotion. Only the ablation of miR-128 from D1 neurons resulted in the drastic and lethal seizure phenotype. Moreover, loss of miR-128 in D1 neurons increases calcium transients and therefore neuronal excitability. The increase in calcium transients might be related to the higher number of spines in the dendrites of D1 neurons of knockout mice. Overexpression of miR-128 in the same striatal neurons attenuates neuronal responsiveness, represses motor activity and alleviates motor abnormalities, a constellation similar to that observed in Parkinson's patients (Tan et al., 2013).

From these groundbreaking studies, miR-128 appears to be a microRNA with multiple functions, from the direct control of mRNA regulatory proteins in development to the modulation of input sensitivity and memory.

1.5 Goal of this Thesis

The major aims of my PhD thesis were to investigate the expression patterns and functions of miR-128 and its precursors, pre-miR-128-1 and pre-miR-128-2.

We wanted to follow miR-128, pre-miR-128-2 and pre-miR-128-1 expression during embryonic corticogenesis, with a particular interest in detecting differences between mature and precursor forms. For this purpose, we took advantage of *in situ* hybridization using double Digoxigenin labelled LNA probes, and Northern blots using radioactively labelled LNA probes.

We also wanted to identify the pathways that miR-128 regulates in neurons. We therefore used gain- and loss of function strategies *in vitro* and *in vivo*.

In vitro we worked with primary cortical and hippocampal neurons and we manipulated miR-128 concentration at two different stages. Knowing that miR-128 levels increase during neuronal maturation, we wanted to check what happens if the gain/loss of function was performed when the microRNA is expressed at low levels compared to later stages when the microRNA is more highly expressed.

In vivo we took advantage of the *in utero* electroporation technique, which allows the ectopic expression of a construct of interest in the proliferating progenitors of the ventricular zone. These experiments primarily targeted the developmental window when upper layer neurons are formed. Given that miR-128 expression increases during embryonic development and remains at high levels throughout adulthood we analyzed the electroporated brains at different stages. To check if miR-128 has an effect on neuronal migration we looked at newborn and at early postnatal animals. To check if miR-128 influences dendritic arborization and spine morphology and number we examined juvenile animals.

To gain insight into molecular pathways regulated by miR-128 we tested and confirmed several predicted mRNA targets for sensitivity to miR-128.

Chapter 2

Materials and Methods

2.1 Materials

Reagents

The special reagents used for experiments are listed in Table 2.1. Common chemicals are not listed.

Name	Cat. Number	Company
Agarose gel-DNA electrophoresis		
Agarose SeaKem®	50004	Lonza
100 bp-DNA-Ladder extended	T835.1	Roth
1 Kb DNA-Ladder	Y014.1	Roth
Avertin sedative		
2,2,2-tribromoethanol	T48402	Sigma
tert-Amyl Alcohol	A730-1	Fisher
cDNA synthesis		
Oligo(dT) primer	SO132	Thermo Scientific
RiboLock RNAse inhibitor	EO0381	Thermo Scientific
RevertAid™ Reverse Transcriptase	EP0733	Fermentas
dNTP Mix, 10 mM	R0192	Thermo Scientific
Cell Culture		
0.05% Trypsin-EDTA (1x)	25300-054	Gibco
2.5%Trypsin	15090-046	Gibco
2-Mercaptoethanol 50mM	31350-010	Gibco
GlutaMAX 100x	35050-038	Gibco
Penicillin-Streptomycin, Liquid	15140-122	Gibco
Foetal Bovine Serum GOLD	A15-151	PAA
DMEM (1x)	21969-035	Gibco
Neurobasal® medium (1X)	21103-049	Gibco
Neurobasal-A® medium (1x)	10888-022	Gibco
HBSS + calcium + magnesium	24020-117	Gibco

HBSS - calcium - magnesium	14170-120	Gibco
B-27® (50x)	17504-044	Gibco
Poly-L-Lysine	P1524	Sigma
Poy-L-Ornithine	P2533	Sigma
Laminin	L2020	Sigma
Lipofectamine® 2000	11668-019	Invitrogen
Opti-MEM® I 1x	31985-047	Gibco
Molecular Biology		
Phusion™ Hot Start DNA Polymerase	F-540L	NEB
GoTaq® DNA Polymerase	M3178	Promega
dATP 100 mM	272-050	Pharmacia Biotech
dCTP 100 mM	272-060	Pharmacia Biotech
dTTP 100 mM	272-080	Pharmacia Biotech
dGTP 100 mM	272-070	Pharmacia Biotech
NucleoBond Xtra Midi®	740410100	Macherey Nagel
QIAquick Gel Extraction Kit	28706	Qiagen
QIAquick Nucleotide Removal Kit	28306	Qiagen
QIAquick PCR Purification Kit	28106	Qiagen
RT^2 SYBR® Green qRT-PCR Mastermix	330529	Sabio sciences
Immunostaining and *In Situ* Hybridization		
Goat serum	G9023	Sigma
Albumine from bovine serum	A9647	Sigma
Blocking reagent	10057177103	Roche
DRAQ5 (5mM)	DR50200	Biostatus
OCT COMPOUND	3808610E	Leica
Gelatine	1.04078	Merck
EDC (N-(3-Dimethlylaminopropyl)-N'-ethlycarbodiimide hydrochloride)	39391	Sigma
Methylimidazole	N353.1	Roth
TSA™, Plus Cyanine 3 system	NEL744001KT	PerkinElmer
Fast Red Tablets	11496549001	Roche
NBT/BCIP Ready-to Use Tablets	11697471001	Roche
Western blot and Northern blot		
30% Acrylamide/Bis Solution 29:1	161-0156	BIO-RAD
TEMED	T-8133	Sigma
PageRuler™ Protein Ladder Plus	SM1811	Fermentas
Immobilon-P Transfer Membrane	IPVH00010	Millipore
Amersham Hyperfilm ECL	521572	GE Healthcare
Clarity Western ECL Substrate	170-5060	BIO-RAD
Protease Inhibitor Cocktail Set I	539131-10VL	Calbiochem
TRIzol® Reagent	15596-026	Invitrogen
40% Acrylamide/Bis Solution 19:1	161-0144	BIO-RAD

2x RNA Loading Dye	R0641	Thermo Scientific
RiboRuler Low Range RNA Ladder	SM1831	Thermo Scientific
Hybond-N+	RPN303B	GE Healthcare
T4 Polynucleotide Kinase	EK0031	Thermo Scientific

Table 2.1: Reagents

Living organisms

Organism	**Strain**	**Source**
Bacteria	*E. coli* XL10GOLD	Stratagene
Bacteria	*E. coli* TOP10	Invitrogen
Mouse	C57BL/6J	FEM (Charité)
Mouse	NMRI	Charles River

Table 2.2: Living Organisms Used in the Experiments

All experiments were conducted according to the European and German laws, following the Animal Welfare Act and the European legislation Directive 86/609/EEC, followed by Directive 2010/63/EU from 2010 on and updated in 2013. The number of sacrificed animals and their stress or discomfort was kept to the minimum.

Antibiotics

Antibiotic	**Stock Concentration**	**Work Concentration**
Ampicillin	100 mg/ml in H_2O	50-100 μg/ml
Kanamycin	12.5 mg/ml in H_2O	25 μg/ml

Table 2.3: Antibiotics

Plasmids

Plasmid	**Comment, source**
pWu	Based on pEGFP-C1
pCAGEN	Mammalian expression vector for expressing genes under the CAG promoter, Addgene
pK-myc-Par6B	Par6B expression construct, Addgene
pRS003	Expression construct with GFP protein
Vivid Colors™ pcDNA™ 6.2/N-EmGFP-GW/Topo®	Invitrogen

Table 2.4: Plasmids

Antibodies

Name	Species	Company	Cat Number	IF	WB
		Primary antibodies			
Ankyrin G	Mouse	NeuroMab	75-146	1:450	
Ankyrin G	Mouse	NeuroMab	73-146	1:450	
Ctip2	Rat	Abcam	18465	1:500	
DCX	Rabbit	Abcam	1:200		
FoxP2	Rabbit	Abcam	ab16046	1:200	
FMRP	Rabbit	Abcam	ab17722	1:300	
GAPDH	Mouse	Abcam	ab9484		1: 10000
GFP	Rabbit	Abcam	ab6556	1:1000	
GFP	Mouse	NeuroMab	75-132	1.500	
GFP	Chicken	Abcam	ab13970	1:500	
Gsk3β	Mouse	Abcam	ab93926		1:1000
Gsk3β Ser-9	Rabbit	Cell Signaling	9323		1:1000
Phf6	Rabbit	Novus Biological	NB100-68261		1:1500
Reelin	Mouse	Millipore	MAB5364	1:500	
RFP	Rabbit	Abcam	ab62341	1:150	
RFP	Rabbit	Clonetech	632496	1:150	
Satb2	rabbit			1:200	
Tau1	Mouse			1:200	
Tbr2	Chicken	Chemicon	AB2261	1:200	
Vinculin	Mouse	Sigma	V9131		1:10000
		Secondary antibodies			
Anti-rabbit A 568	Goat	Invitrogen	A11036	1:1000	
Anti-mouse IgM A 568	Goat	Invitrogen	A21043	1:1000	
Anti-rat A 568	Rabbit	Invitrogen	a21211	1:1000	
Anti-chicken A 568	Goat	Invitrogen	A11041	1:1000	
Anti-chicken FITC	Goat	Abcam	ab6873	1:500	
Anti-rabbit A 488	Donkey	Invitrogen	A21206	1:1000	
Anti-mouse A 488	Goat	Invitrogen	A11029	1:1000	
Anti-rat A 488	Rabbit	Invitrogen	A21210	1:1000	
Anti-rabbit A 647	Donkey	Invitrogen	A31573	1:1000	
HRP- Conjugated Anti-Rabbit	Donkey	Jackson Immunoresearch	711-035-152		1:5000
HRP- Conjugated Anti-Mouse	Donkey	Jackson Immunoresearch	715-035-150		1:5000

Table 2.5: Antibodies

LNA Probes from Exiqon

Probe	Sequence	Tm
hsa-miR-128	AAAGAGACCGGTTCACTGTGA	78°
miR-128-1 precursor	GTGAGAAATGTAAACCTCTCAG	70°
miR-128-2 precursor	GAGACCTGCTACTCACTCTC	70°
hsa-let-7b	AACCACACAACCTACTACCTCA	77°
hsa-miR-124	GGCATTCACCGCGTGCCTTA	80°
hsa-miR-125-5p	TCACCAGGTTAAAGGGTCTCAGGGA	79°
Scramble-miR	GTGTAACACGTCTATACGCCCA	78°

Table 2.6: LNA Probes

Primers

Primer	Sequence	Purpose
Reelin For	TGAAGCCGTCCGTCTGTCCCTGG	Sensor Assay
ReelinRev	GCGGCCGCTGCTGGTGTTGGCTCCACCT	Sensor Assay
Plk2 2 For	TGACTCGAGCGAGCGGACCTCATGGGACT	Sensor Assay
Plk2 2 Rev	GCGGCCGCACAAGGAATGCACTTTTCCAACCACA	Sensor Assay
Adora2b For	TGACTCGAGCCTAGGCTCTGGCCTTTTGGAGA	Sensor Assay
Adora2b Rev	GCGGCCGCTCTGAGTTGCTGCCCCAGGA	Sensor Assay
DCX For	TGACTCGAGACCATGTGCTTAGGGCTGTGGT	Sensor Assay
DCX Rev	GCGGCCGCTGGCATGCATGGCTTTCACCT	Sensor Assay
Creb 1 For	TGACTCGAGTGTTACGGTGGAGAATGGACTGG	Sensor Assay
Creb 1 Rev	GCGGCCGCAGCCTCCACTGTCCTCATATTTGTC	Sensor Assay
Jip3 For	CATGTCTCGAGAGAGGGATGAAGCAGGGTTT	Sensor Assay
Jip3 Rev	ACTTGGAATTCCGTCACACTCATGTGGGAAC	Sensor Assay
Cdc42 For	CATGTCTCGAGGCCCTGCACCTACCCACATGC	Sensor Assay
Cdc42 Rev	ACTTGGAATTCATGACTGACAGGGGCAAAAG	Sensor Assay
Gsk3β For	CATGTCTCGAGGGCGTGTGATGTCAGGTATG	Sensor Assay
Gsk3β Rev	ACTTGGAATTCTTCAATCCACCTTGCTTTCC	Sensor Assay
Nedd4 For	CATGTCTCGAGATGTGTACGGCAGGATGTGA	Sensor Assay
Nedd4 Rev	ACTTGGGATCCCTCGCTTTCCTGTCCTTCTG	Sensor Assay
Par6b For	CATGTCTCGAGCGCAGTTGTCTTCCCTTACC	Sensor Assay
Par6b Rev	ACTTGGGATCCCAACAGCACAGCATCTGGTT	Sensor Assay
srGAP2 For	CATGTCTCGAGGGGCACCCCTTGGTCCTTTGG	Sensor Assay
srGAP2 Rev	ACTTGGAATTCAGGGAGGTGACGTACAGCGG	Sensor Assay
Nrp2 For	TGAGCTCACCCTCAGATGGTCTC	Sensor Assay
Nrp2 Rev	ACAAATCATATAAACACAGTCTGACAT	Sensor Assay
Sema 3A For	TGACACGTCCGCTGACTTAGTGT	Sensor Assay

Sema 3A Rev	AGCCACCGCATCACTTGTAT	Sensor Assay
Sema 3E For	TGAGGCTGAGGAACCTAGGATGGA	Sensor Assay
Sema 3E Rev	TGTAGCGAGGCAGTTTGTGT	Sensor Assay
Gria1 For	TGAAAAGCCACCCTGAGTGATAC	Sensor Assay
Gria1 Rev	ATGGGTCCACAGTGATTTAA	Sensor Assay
Cacng2 For	TGACACGGGGAGACCTTCCATAC	Sensor Assay
Cacng2 Rev	CAGAAAGATGGTGGGGCCTT	Sensor Assay
Gria3 For	TGAAGCCTGGAATTACAGCCCAC	Sensor Assay
Gria3 Rev	TTGACTACCGCCAAACTCCC	Sensor Assay
Phf6 cDNA For	AAGGTCTCGAGATCATGTCAAGCTCAATTGA	Expression Construct
Phf6 cDNA Rev	AAGGTGAATTCAAGTGGAAAAGAAGCACAGGA	Expression Construct
Nrp2 cDNA For	AAGGTGCTAGCATGGATATGTTTCCTCTTACC	Expression Construct
Nrp2 cDNA Rev	AAGGTCTCGAGAGACACAATCGGTCATGCCT	Expression Construct
Phf6 RT PCR For	GTGAGCCCCACTGCATTTCT	mRNA quantification
Phf6 RTPCR Rev	CGCTGTCTCGTAGACCCTTTT	mRNA quantification

Table 2.7: Primers

Microscopes

Microscope	Software	Purpose
Olympus BX51	MagnaFire (Olympus)	Epifluorescent Imaging
Olympus BX60	AxioVision (Zeiss)	Bright Field Imaging
Olympus IX81	Cell Sense Dimension	Z-stacks electroporated neurons
Leica SL	LCS software	Confocal Imaging

Table 2.8: Microscopes

Software

Software	Purpuse
Microsoft Office 2011 for Mac	Writing, tables and analysis
Prism 5.0 for Mac	Statistical analysis
FlowJo vX for Mac	Analysis of FACS experiment
Fiji (ImageJ)	Analysis of images
Adobe Illustrator CS4	Figures and Poster preparation
Adobe Photoshop CS4	Image preparation
Papers2 from Mekentosj	Scientific papers organizer
Ensembl genome browser	gene analysis
BLAST	DNA sequences analysis
NCBI database	genes, nucleotides and litterature screaning
Primer BLAST	Primers design

Table 2.9: Software

Cell Culture Media

Cell line	Medium
HEK 293T, N2A	DMEM 1x, 10% FBS, 1% P/S, 1% Glutamax
Primary Cortical Neuron	Neurobasal® medium (1X), 1% Glutamax, 1% P/S, 2% B-27® (50x), 25 μM Beta-mercaptoethanol
Primary Hippocampal Neuron	Neurobasal® A medium (1X), 1% Glutamax, 1% P/S, 2% B-27® (50x), 25 μM Beta-mercaptoethanol

Table 2.10: Cell Culture Media

Buffers

Buffer	Reagents
	Solution
PBS 10x (1L) pH 7.4	80g NaCl, 0.2g KCl , 14.4g $Na_2HPO_4 \bullet 2\ H_2O$, 0.2g KH_2PO_4
TBS 10 x pH 7.4	0.5 M Tris Base, 1.5 M NaCl
TBE 10x (1L) Northern blot	1 M Tris Base, 1 M Boric Acid, 25 mM EDTA
TBE 10x (1L)	0.45 M Tris Base, 0.45 M Boric Acid, 10 mM EDTA
SSC 20x (1L) pH 7.0	3 M NaCl, 300 mM Sodium Citrate
SSPE 20x (1L) pH 7.4	3 M NaCl, 0.2 M $NaHPO_4$, 7.4g EDTA
	In Situ Hybrydization
Proteinase K (20μg/ml)	2 mg PK in 1xPBS
Methylimidazole solution pH 8.0 (160 ml)	0.13 M 1-Methylimidazole (1.6 ml), 300 mM NaCl, milli-Q
EDC Solution pH 8.0	10 ml Methylimidazole solution, 0.16 M EDC (176 μl), 95 μ HCl
Acetylation solution	197 ml H_2O, 2.7 ml Triethaonlamine, 350 μl HCl, 500 μl Acetic Anhydride
Hybridization buffer	50% Formamide, 5x SSC, 0.1 mg/ml yeast tRNA, 0.5 mg/ml Salmon sperm, 0.1 mg/ml heparin, 0.1% Tween, 10% Dextran Sulphate, 5x Denhardt's solution
After hybridization buffer (150 ml)	50% Formamide, 1xSSC, 0.1% Tween
1xTBST	1xTBS, 0.1% Tween
ISH Blocking solution	0.5% Blocking Reagent Roche, 10% Goat Serum, 1xTBST
Detection Buffer (NBT/BCIP) pH 9.5	0.1 M Tris Base, 0.1 M NaCl

	Staining
Blocking Buffer	3% BSA, 0.25% Triton-X, 1xPBS
Cresylviolet	1.5% Cresylviolet, Acetate buffer ovn, filter day after
Acetate Buffer	980 ml H_2O, 10 ml Sodium Acetate 1M, 10 ml Acetic Acid 1 M
Potassium Sulfide	50% Potassium (di)sulfide in H_2O
Differentiation Buffer	500 μl H_2O, 700 μ Acetic Acid
	Norther Blot
Polyacrylamide-Urea Gel, 12% (80 ml)	38.4 g Urea, 18.2 ml H_2O, 8 ml 10xTBE, 24 ml 40% Acrylamide/Bis 19:1, 400 μl APS, 40 μl TMED
Hybridization Buffer	250 mM Na_2HPO_4 (pH 7.2), 7% SDS, 1 mM EDTA, 1% BSA
Washing Buffer 1	2xSSPE, 0.1% SDS
Washing Buffer 2	0.5xSSPE, 0.1% SDS
Stripping Buffer	0.1% SDS, 0.1xSSC
	Western Blot
TNN Lysis Buffer	50 mM Tris pH 7.4, 150 mM NaCl, 0.5% NP-40, 5 mM EDTA
Bäuerle Lysis Buffer	1% NP-40, 20 mM Hepes pH 7.9, 350 mM NaCl, 1 mM $MgCl_2$, 0.5 mM EDTA, 0.5 mM EGTA, 50 mM NaFl, 20% Glycerol, 1 mM DTT
4x Laemli Buffer	200 mM DTT, 100 mM Tris pH 6.8, 20% Glycerol, 4% SDS, 0.2% Bromphenol Blue
Stacking Gel (5 ml)	3.4 ml H_2O, 0.83 ml 30% Acrylamide, 0.63 ml 1.0 M Tris (pH 6.8), 0.05 ml 10% SDS, 0.05 ml 10% APS, 0.005 ml TEMED
Separation Gel 10% (15 ml)	5.9 ml H_2O, 5 ml 30% Acrylamide, 3.8 ml 1.0 M Tris (pH 8.8), 0.15 ml 10% SDS, 0.15 ml 10% APS, 0.006 ml TEMED
Electrophoresis Buffer 10x	0.25 M Tris Base, 1.92 M Glycine, 1% SDS
Blotting Buffer 10x	0.25 M Tris Base, 1.5 M Glycine
PBST 1x	1xPBS, 0.2% Tween 20
Blocking Buffer	5% skim milk Powder, 1xPBST
Blocking Buffer 2	3% BSA, 1xPBST
Stripping Buffer pH 2.5	0.2 M Glycine, 0.05% Tween20, 0.1% SDS

Table 2.11: Buffers

2.2 Methods

2.2.1 RNA Isolation

Total RNA was isolated from cultured cells and from tissues using TRIzol® Reagent according to manufacturer's instructions and stored at -80°C.

2.2.2 cDNA Synthesis

The RNA (1pg up to 5 μg) was mixed with 1 μl dNTPs (10 mM), 1 μl oligodT and milli-Q for a final volume of 12.5 μl. Then 4 μl of 5x RT Buffer, 0.5 μl Thermo S. Riboblock RNAse Inhibitor, 1 μl RevertAid Premium Reverse Transcriptase were added to the RNA mixture, incubated 30 minutes at 50°C and then 5 minutes at 85°C.

2.2.3 Molecular Cloning

Polymerase Chain Reaction

Polymerase Chain Reaction (PCR) was carried out in 0.2 ml tubes. The reaction was prepared in a final volume of 50 μl as in Table 2.12.

5x Phusion or GoTaq Buffer	10	μl
dNTP mix (20 μM)	1	μl
Primer for (10 μM)	2.5	μl
Primer rev(10 μM)	2.5	μl
Template(100-500 ng DNA)	x	μl
milli-Q	x	μl
Total volume	50	μl

Table 2.12: PCR mix

The cycling conditions used are in Table 2.13 and in Table 2.14.

The PCR product was either directly purified using the PCR Purification kit (Qiagen) or run on a 1,5% Agarose gel and then the fragment of interest was extracted with the Gel Purification kit (Qiagen).

Restriction Digest

Usually it is necessary to prepare plasmids and PCR products for the subsequent steps of molecular cloning. Enzymatic digestion is used to produce compatible ends in the DNA

Temperature	Time	Cycles number
95°C	2 min	1
95°C	30 sec	
42-65°C	1 min	25-35
72°C	1 min/kbp	
72°C	5 min	1

Table 2.13: PCR Cycling condition for GoTaq® DNA Polymerase

Temperature	Time	Cycles number
98°C	30 sec	1
98°C	10 sec	
60-72°C	30 sec	25-35
72°C	1 min/kbp	
72°C	5 min	1

Table 2.14: PCR Cycling condition for Phusion™ Hot Start DNA Polymerase

fragments that will be ligated. The enzyme used for restriction digest were all purchased by NEB and were used according to manufacturer's instructions.

DNA analysis

10x DNA Loading buffer was added to the restriction digest or to the PCR products. The mixture was run on an Agarose gel (1 to 1.5% Agarose in 1x TBE buffer) at 100 V for the time necessary to the fragments to separate according to their size. A proper ladder control for the detection of the fragments size was run next to the samples. Once the fragments were separated the ones of interest were cut out from the gel and extracted using the Gel extraction kit (Qiagen).

Ligation

The linearized plasmid and the cut fragment were ligated using T4 DNA ligase (NEB). The ligation of plasmid and insert was done using a ratio plasmid:insert 1:3, with the vector concentration between 50 and 400 ng total. The reaction was prepared in a final volume of 20 μl adding to the vector and the insert 0.5 μl of T4 DNA Ligase, 2 μl of T4 DNA Ligase buffer and milli-Q. The ligation was incubated 2 hours at room temperature or overnight at 16°C.

Transformation

The competent cells used were either *E. coli* XL10Gold or *E. coli* TOP10. The competent cells were thawed on ice. 5 μl of ligation product were added to 50 μl of competent cells, and incubated on ice for 30 minutes. The mixture of cells and DNA was heat shocked at 42°C for 30 seconds and then cooled on ice for 5 minutes. 950 μl of SOC medium were added to the cells/DNA mixture. The bacteria were incubated, shaking, for 1 hour at 37°C and then they were plated on pre-warmed selection agar plate and incubated overnight at 37°C.

Mini and Midi prep

5 to 10 colonies of the transformed ligation were picked, inoculated in 3 ml of LB medium containing the selective antibiotic and let grow overnight in a shaker at 37°C. Mini prep was then performed. 2 ml of the overnight culture were collected in a 2 ml Eppendorf tube and centrifuged at 6000 g for 5 minutes. The pellet was resuspended with 200 μl of RES buffer (NucleoBond Xtra Midi®), the cells were lysated with 300 μl of Lys buffer (NucleoBond Xtra Midi®), and incubated 5 minutes at RT. Neu buffer (NucleoBond Xtra Midi®) was added (350 μl) and the tube was centrifuged at maximum speed for 5 minutes. The supernatant was collected in a new Eppendorf tube containing 1 ml of 100% Ethanol and centrifuged at maximum speed for 20 minutes. The precipitated DNA pellet was visible and the supernatant was discarded. 200 μl of 70% Ethanol were added and the tube was centrifuged at maximum speed for 5 minute. The supernatant was discarded, the pellet let dry at RT for 10 minutes and then resuspended in milli-Q. DNA concentration was measured using a Nanophotometer 1374 (IMPLEN). The resulted plasmids were tested using restriction digest. Correct plasmid

needed in big quantities were grown in 100 ml of LB medium with selective antibiotic in a 37°C shaker. The plasmid was then isolated using NucleoBond Xtra Midi® from Macherey and Nagel according to manufacturer's instructions.

Bacteria Glycerol Stock

To preserve the plasmid routinely used 200 μl of Glycerol were added to 800 μl of bacterial culture, vortexed briefly and then conserved at -80°C.

2.2.4 TargetScan Predictive Algorithm

To find possible targets for miR-128, the predictive algorithm TargetScan has been used. With TargetScan it is possible to find targets for a particular microRNA/microRNA family and to find the putative microRNAs binding sites in the 3'UTR of genes of interest. The algorithm is based on the strength of the paring between the microRNA seed and the sequence in the 3' UTR, and on the evolutionary conservation of the 3' UTR sequence.

2.2.5 Quantitative real-time PCR

mRNA relative quantification was performed using quantitative real-time PCR. This procedure allows the relative and absolute quantification of the mRNA of interest during the polymerase chain reaction. The quantification is possible thanks to the intercalation into the double strand DNA of a specific fluorophore, in our case RT^2 SYBR® Green qRT-PCR Mastermix

RT^2 SYBR® Green qRT-PCR Mastermix

RT^2 SYBR® Green qRT-PCR Mastermix reagent was used to asses the expression of mRNA transcript. Primers for the qRT-PCR were designed to span at least one intron, in order to avoid amplification of genomic DNA and to produce an amplicon of size ranging between 80 and 200 nt. Efficiency of the primers was tested using cDNA of cells known to expressed the gene of interest, measuring 5 serial dilution (1:5) and analyzed using the StepOne Software. The qRT-PCR product was run on a 1,5% Agarose gel to check if the amplicon size was correct. qRT-PCR was performed on 1 μl of 1:3 diluted cDNA using RT^2 SYBR® Green from Sabio Sciences. Master mix was prepared as in Table 2.15

RT^2 SYBR® Green qPCR Mastermix	10	μl
Primer for (10 μM)	0.4	μl
Primer rev (10 μM)	0.4	μl
milli-Q	8.2	μl
Total volume	19	μl

Table 2.15: qRT-PCR SYBR® Green Master mix

Master mix was added to the well of the 96-well optic plate and subsequently the cDNA was added. Each sample was analyzed in triplicate to minimize pipetting errors. The 96-well plate was covered with an optical adhesive film, centrifuged at 1500 g for 1 minute. The PCR was then run in StepOne Plus (Applied Biosystems) real-time machine.

qRT-PCR Analysis

During the PCR the software measures in real-time the Threshold Cycles (C_T), a logarithmic value that is defined as the number of cycles required for the fluorescent signal to cross a threshold, normally the background level. C_T are inversely proportional to the nucleic acid in the sample: the higher is the C_T the lower is the presence of the mRNA of interest. Before exporting the raw C_T from the software the automatic threshold for the C_T was corrected, moving the threshold in the middle of the linear region of the amplification plot. Once the threshold was corrected the values could be analyzed. The C_T value of the target gene (T) was normalized to an internal control (C), in the case of the thesis GAPDH for neuronal culture and Oaz1 for brains, using the formula (2.1).

$$C_T(T) - C_T(C) = \Delta C_T(T) \tag{2.1}$$

The ΔC_T(T) values obtained was further normalized to a reference sample (R) (as in the formula (2.2)).

$$\Delta C_T(T) - \Delta C_T(R) = \Delta\Delta C_T(T) \tag{2.2}$$

The logarithmic values was then converted to a linear value (2.3) and the data were compared.

$$2^{-\Delta\Delta C_T(T)} \tag{2.3}$$

2.2.6 Cell Culture HEK 293T and N2A cells

HEK 293T, Human Embryonic Kidney cells, and N2A, Mouse Neuroblastoma cells were grown at 37°C with 5% CO_2 and 95% humidity. Every 2 or 3 days they were split and plated 1:10 in fresh medium.

2.2.7 Primary neuronal culture

Cortical and hippocampal neurons were prepared from mouse E16.5 embryos. Primary cortical neurons were used either for single cell study or for biochemistry, hippocampal neurons only for single cell study. Neurons for single cell study were seeded in 24-well plates on 12 mm glass coverslips, neurons for biochemistry were seeded in 6-well plate. In both cases the plate or the coverslips were coated with Poly-L-Lysin or Poly-L-Ornithin overnight at 37°C and washed 3 times with sterile distilled water before use. Coated and washed plates can be frozen and used when needed.

Baking of the Glass Coverslips

Purchased coverslips have to be washed before being ready to use for cell culture. The dirt and the fat on their surface have to be removed, neurons are sensitive and will not survive in contact with it. During all the washing steps the coverslips were gently shaken.

- Place the coverslips in a Beaker filled with 70% Ethanol and gently shake them overnight.

- Wash the coverslips with distilled water 3 times for 1 hour
- Wash the coverslips in 100% Ethanol 2 times for 90 minutes.
- Wash the coverslips in 70% Ethanol for 15 minutes and then store them in 100% Ethanol.
- Carefully remove all the Ethanol and then bake the coverslips at 200° for 6 hours. Remember to cover the Beaker with aluminum foil before backing, the coverplips must be completely sterile.

Primary cortical and hippocampal preparation

Before starting the neuronal prep, fill with HBSS +/+ one 10 cm Petri dish, one 15 ml Falcon tube and a 2 ml Eppendorf tube. HBSS +/+ should be cold. Isolation step of the cortex and hippocampus is done on ice and in an open hood.

- Collect the embryos in the 10 cm Petri dish, previously filled with HBSS +/+.
- The best results are obtained if cortex and hippocampi are isolated from one embryo at a time, keeping the rest of the tissues on ice. For each embryo cut with a scalpel the upper part of the head. The cut must be horizontal and should start in the middle of the eyes.
- Remove with 2 sharp tweezers the skin and the forming skull. Scoop out the brain from the rest of the head.
- Separate the two hemisphere cutting with the tweezers along the midline.
- Work with one hemisphere at a time. Peel off the meninges, starting form the bottom outside part of the cortex and ending at the hippocampus. Meninges can be recognized because they contain blood vessel. If the meninges are correctly pinched they can be peel off in one piece without breaking.
- Work with the inside part of the hemisphere facing upward. Striatum and hippocampus can be recognized because they have a slightly darker color compared to the cortex. remove the striatum using the tweezers. Then carefully cut the hippocampus (has a banana shape). Collect the hippocampus and the cortex in the 2 ml Eppendorf tube and in the 15 ml Falcon tube, respectively. Proceed as described for all the embryos.

The next steps must be performed in a cell culture hood. All the steps of the preparation are common for cortical and hippocampal neurons. The amount of medium for the washes and the amount of enzymes needed are different for cortical and hippocampal neurons and they are listed in Table 2.16.

- Wash the tissue with HBSS -/- for three times. Take care of let the tissue sink to the bottom of the tube before starting the following wash. It is important to remove all the previous HBSS +/+ because it contains Mg^{2+} and Ca^{2+} that will block Trypsin enzymatic digestion.

- After the last wash remove part of the medium and add Trypsin 2.5%.
- Incubate in a water bath at 37°C for 20-30 minutes, taking care of inverting the tubes every 10 minutes. Trypsin is an harsh treatment for neurons, the enzymatic digestion should be kept as short as possible. When it is time to proceed with the next wash can be estimated by looking at the tissue when the tube is inverted: if the pieces are all sticking together then continue with the next step.
- Add FBS to block the Trypsin activity.
- Wash three times with HBSS +/+. At this point, in particular for hippocampal tissue, the washing step must be as careful as possible, the tissue is sticky and can be pipetted up easily. After the last washing step remove almost all the medium.
- Add the DNAse I and wait 30 seconds.
- Wash three times with Neurobasal medium. After the last wash leave some of the medium in the tube.
- Resuspend the tissue for about 8 times and then add a little more Neurobasal medium and resuspend until when there is no tissue left and the medium is milky.
- Centrifuge the tubes at 150 g for 5 minutes.
- Remove the medium and keep the pellet.
- Resuspend the pellet with freshly prepared and warm medium.
- Count the neurons is a Neubauer chamber. Trypan blue is not necessary, healthy neurons are spherical and iridescent. A good concentration of neurons for single neuron resolution in cytochemistry is 50000 cell per well in 24-well plate and 10^6 in 6-well plate for biochemistry.
- Let the neurons attach to the plate in a 37°C, 5% CO_2 incubator for a minimum of 4 hours and then change the medium completely.

Neurons are sensitive to environmental changes. To maintain them in culture for weeks, the medium should be refreshed once per week removing half of the old medium and adding the same quantity of fresh one.

2.2.8 Cell Transfection

Transfection was used both in cell lines and in primary cortical or hippocampal neurons. The reagent used is Lipofectamine 2000 but the protocols are slightly different.

Cell line transfection

The transfection in cell lines was performed according to the manufacturer's instructions for the reverse transfection, using the minimum amount of Lipofectamine 2000 suggested. The cells were usually used 48 hours post-transfection.

Volumes	Cortex	Hippocampus
Medium for all the washes	7 ml	1 ml
Medium left before Trypsin treatment	3.5 ml	200 μl
Trypsin 2.5%	500 μl	25 μl
FBS	2 ml	100 μl
DNAse I	100 μl	10 μl
Medium for the first reuspension	2 ml	200 μl
Medium for the second resuspension	6 ml	1 ml
Medium to resuspend the pellet	10 ml	1 ml

Table 2.16: Volume to use for primary cortical and hippocampal neuronal prep

Primary cortical and hippocampal culture

Neuronal transfection was performed with Lipofectamine 2000 in the 24-well plate. The DNA/Lipofectamine 2000 mixture was prepared according to manufacturer's instructions. In the incubation time of DNA/Lipofectamine for the formation of liposomes, the medium of the neurons was change with 250 μl of medium without antibiotic . The condition medium was conserved in a Falcon tube. At the condition medium was added the same quantity of fresh medium and kept in the cell incubator. The DNA/lipofectamine 2000 mixture was added to the neurons and incubated 30 minutes at 37°C. The DNA/lipofectamine medium was removed, and the conditioned medium was added. The neurons were used 48 hours post-transfection.

A list of the plasmids and the concentration used for the experiments in the thesis is in Appendix Table 6.

2.2.9 Flow Cytometry

FACS (Fluorescence-Activated Cell Sorter) analysis was used to asses if miR-128 regulates 3'UTR of putative target genes. In FACS analysis the cells are analyzed one cell at a time, passing through a laser beam in a continue flow. Cells scattered some laser light and can emit fluorescence if excited by the correct wave length. Flow cytometer measures several parameters for each cell:

- Cell diameter of the cell, the low angle Forward scatter (FSC).
- Granularity of the cell, the orthogonal or Side Scatter (SSC).
- Fluorescence emitted from the cells.

Cell preparation

Cells were analyzed 48 hours after transfection. They were washed one time with sterile 1x PBS, trypsinized (0.05% Trypsin/EDTA). Trypsin reaction was blocked using 1x PBS,2% FBS, cells were collected in 1.5 ml Eppendorf tube, centrifuged at 4°C for 5 minutes and then

resuspended in 800 μl of 1x PBS, 2% FBS, and transferred in tube appropriate for the FACS machine.

FACS analysis

Prior analysis the cells were gated for the living population using Mock transfected cells (the transfection mixture does not contain DNA). Gates for dsRed and GFP were set using cells transfected only with dsRes or GFP constructs. Cells can emit autofluorescence when excited by a laser, the gating step for dsRed and GFP is necessary to measure only the fluorescence coming from the plasmid transfected in the cells. The FACS analysis was performed in two different ways:

1. Recording the living population and sorting for transfected and untransfected cells only during the analysis of the collected data.

2. Recording only the dsRed transfected cells, gated from the living population.

Analysis of collected data

The analysis using FlowJo software was different according to the method used for collecting the data.

1. Living population was gated from the mock transfected cells (in graph on the X-axis is the SSC and on the y-axis the FSC). The following steps were necessary to eliminate the autofluorescence from the data to analyze.

   - The red cells were gated from the cells transfected only with GFP. In the graph the x-axis showed SSC and the y-axis showed the red fluorophore (in FlowJo is called PEA). Green transfected cells were at the bottom of the graph and the gate was drawn above the green cells, taking care that the red population was under 1%
   - From the population defined in the previous step, the green cells were gated. This was done from the red subpopulation of cells transfected only with dsRed. In the graph the x-axis remained the SSC and the y-axis was changed to Alexa 488. The gating was done in the same way as for the red cells. The resulting population of cells is the GFP positive of red positive cells, in easier words the population of cells that has been cotransfected.

   The analysis of the GFP fluorescence intensity was performed calculating the geometric mean for the Alexa 488 fluorophore.

2. The living population was gated from the mock transfected cells, the x-axis of the graph showed the SSC and the y-axis of the graph showed the FSC. Because the collected data were already sorted for the red transfected cells, the only step before the analysis was to gate the green population of cells. From the living population of red transfected cells the GFP positive cells were gated. The y-axis showed the Alexa 488 fluorophore. The red transfected cells were at the bottom of the graph and the green population was

gated above it. Once the GFP positive cells were gated the Geometric Mean for the Alexa 488 fluorophore could be calculated.

The gated data were exported into an Excel file for further analysis. To be able to compare the data they were normalized to the dsRed control transfection. In Table 2.17 the cell lines, the miR-128 expression method and the GFP backbone can be visualized.

Cell line	miR-128 Expression	GFP backbone	Genes tested	Figure
HEK 293T	Ambion miR-128 synthetic	Vivid Colors™ pcDNA™ 6.2/N-EmGFP-GW/Topo®	Reelin, Adora 2b, Dcx, Plk2, Creb1	3.7
N2A	Ambion miR-128 synthetic	pWu	Gsk 3β, Par6b, SrGAP2, Jip3, Nedd4, Cdc42	3.8
HEK 293T	plasmids	Vivid Colors™ pcDNA™ 6.2/N-EmGFP-GW/Topo®	Sema3A, Sema3E, Nrp2, Phf6	3.9
HEK 293T	plasmids	Vivid Colors™ pcDNA™ 6.2/N-EmGFP-GW/Topo®	Gria1, Gria3, Cacng2	3.10

Table 2.17: List of the conditions used for the different Sensor Assay performed.

2.2.10 Western Blot

Protein for Western Blot analysis were isolated either from cells (HEK 293T, N2A) 48 hours after transfection or from primary cortical neurons at DIV 1, 2, 5, 7, 12, 15, 21.

Protein isolation

Protein isolation was done on ice, with cold medium. Cells were washed one time with 1xPBS. Then 500 μl of 1xPBS were added to the cells that were collected in a 1.5 ml Eppendorf tube using a cell scraper. The tubes were centrifuged (4°C) for 5 minutes at 6000 rpm. The supernatant was discarded. At this point the pellet of neurons was snap frozen in liquid nitrogen and stored at -80°C, the protein for all the stages analyzed were isolated in one time, avoiding differences in the procedure. The protein pellet was resuspended in lysis buffer (TNN or Bäuerle Buffer) using 1 ml syringe. The amount of buffer used was dependent on the pellet dimension. The resuspended pellet was then incubated for 15 minutes on ice and centrifuged (4°C) at maximum speed for 15 minutes. The supernatant was collected in a new tube and the protein concentration measured.

Measurement of protein concentration

To measure the protein concentration of the sample we used the Bradford Protein Assay. 1 μl of protein was pipetted at the bottom of the cuvette used for measuring protein concentration. The protein was then resuspended in 180μl of milli-Q. Only at the end 20μl of Bradford reagent

were added to the mixture and mixed well. The standard curve , necessary to measured accurately the protein concentration, consisted of BSA (initial concentration 2 mg/ml) at different dilutions: 0 mg/ml, 0.125 mg/ml, 0.25 mg/ml, 0.5 mg/ml, 1 mg/ml and 1.5 mg/ml. The protein concentration was measured in the Nanophotometer 1374 (IMPLEN) using a wavelength of 595 nm. For each experiment 10 to 20 μg of protein were used. Protein were denatured using 4x Loading Buffer and boiled at 95° for 3 minutes and cooled on ice.

Run of the Electrophoresis gel

SDS Polyacylamid gel electrophoresis (SDS-PAGE) was performed to separate and analyze the protein. The gel had a 5% stacking and a 10% separation gel. The samples were run at 70 V for 20 minutes and then at 130 V for the appropriate time needed to see a visible separation, normally around 90 minutes. Pageruler Plus Prestained protein ladder (Fermentas) was used to visualize the correct size of the proteins.

Western blot

The protein were transferred on Immobilion-P Transfer Membrane using wet Western Blot technique. The membrane was activated for 30 seconds in MeOH and then soaked in blotting buffer. The sponges and Whatman paper were prewet. The cassette was assemble, starting from the black side, with sponge, Whatman paper, gel, membrane, Whatman paper, sponge. Bubble were removed rolling carefully a tube on top of the sandwich. Transfer was performed in a chamber, cooled using an ice block, for 75 minutes at 90 V. Once the transfer was completed the sandwich was disassembled, the membrane was wet in MeOH and let dry for 30 minutes. The membrane was reactivated in MeOH, washed 1 minutes in PBST and then stained with Ponceau S solution to check if the transfer was successful. The membrane was washed in PBST and blocked for at least 1 hour using 5% skim milk powder dissolved in PBST. The blocking solution in which the primary antibodies were dissolved was prepared in PBST either with 5% skim milk powder or 3% BSA. Primary antibody dilution was according to manufacturer's instructions. The membrane was incubated overnight with the primary antibody at 4°C. After 4 washes (1, 5, 10, 15 minutes each step) in PBST the membrane was incubated with HRP conjugated secondary antibody for 1 hour at room temperature. The membrane was then washed 4 times (1, 5, 10, 15 minutes each step) and then protein of interest was visualized using ECL solution (1:1, Solution 1: solution 2). HRP dependent signal was detected either using films or with a CCD camera.

When necessary the protein signal was quantified using Fiji software.

2.2.11 Northern Blot

Northern Blot analysis was performed to visualize miR-128, pre-miR-128-1 and pre-miR-128-2. The specificity of the LNA probes was confirmed on HEK 293T transfected with pre-miR-128-1 or pre-miR-128-2 expression constructs (see Appendix .1). The sequences of the probes are in Table 2.6 and in Figure 2.1. The 12% acrylamide denaturing gel was pre-run in 0.5xTBE at 300 V for 30 minutes. For each probe 20 μg of RNA were mixed with 10μl of 2x Loading

Dye solution (Fermentas), then boiled at 80°C for 3 minutes and cooled on ice. Probes were run on the denaturing (Urea) gel at 250 V for 3.5 hours. The gel was then incubated with Ethidium bromide dissolved in 0.5xTBE for 5 minutes, exposed to UV light to check the RNA integrity and to visualize the loading. The RNA was then transferred to Hybon-N^+ nylon membrane (Amersham Bioscience) by wet blotting at 20 V overnight. The membrane was baked 1 hour at 80°C and then cross-linked with UV light (120 mjoules/cm^2). 20 μM of LNA probe were radioactively labeled with 60 μCi [γ-^{32}P] ATP using T_4 Polynucleotide Kinase (Fermentas), in a final volume of 10 μl. The reaction was incubated at 37°C for 30 minutes and then purified using the Nucleotide purification kit according to manufacturer's protocol. The radioactivity of the probe was measured with a scintillator and the 100 μl probe were added to 5 ml of Hybridization Buffer. The membrane was pre-hybridized with Hybridization Buffer at 45°C for 30 minutes and then incubated at 45°C with the probe overnight. The membrane was washed twice in 2xSSPE, 01% SDS and twice with 0.5xSSPE, 01% SDS at 45° for 10 minutes each step. The membrane was sealed in a plastic bag and exposed to audio radiographic films at -80°C. The membrane was stripped by boiling 10 minutes in 0.1xSSC, 0.1% SDS, and reprobed.

2.2.12 Immunohistochemistry and Immunocytochemistry

Cell Fixation

Cultured cells or neurons were washed 1 time in 1xPBS and then fixed in 4% PFA for 20 minutes. For AnkG antibody the fixation was done with 1% or 2% PFA for 30 minutes. AnkG antibody is sensitive to fixative, if the neurons or the tissue are fixed with 4% PFA the staining does not work. After the incubation in 4% PFA the cells were washed once in 1xPBS, they were stored in the fridge in 1xPBS, 0.001% Sodium Azide.

Tissue Fixation and Animal Perfusion

Brains isolated from embryos and from animals till P6 were fixed in 4% PFA overnight at 4°C. From P7 onwards perfusion was performed. Animals were anesthetized with a lethal dose of Avertin injected intra-peritoneally. When they were deeply asleep (irresponsive to the toe-pinch test), the ribcage was open, the diaphragm cut and the heart exposed. A butterfly needle, connected to two syringes containing 1xPBS or 4% PFA, was inserted in the left ventricle, a small quantity of 1xPBS was injected to increase the pressure in the heart and a small cut was done in the right atrium. 1xPBS was injected slowly into the heart, all the blood was washed out from the body. When from the right atrium was flowing out only 1xPBS, the liquid injected could be switched from 1xPBS to 4%PFA. In between 5 to 10 ml of 4% PFA were injected in the animals. Then the brains were isolated, incubated overnight in 4%PFA at 4°C. The 4%PFA was then removed and the brains stored in 1xPBS, 0.001% Sodium azide before processing for Immunohistochemistry.

Brain Embedding in 4% Agarose and Vibratome sectioning

Brains for himmunohistochemistry were cut using either vibratome or cryostat. Vibratome sections can be thicker than cryosections, this is an advantage, for example, if you want to visualize the complete dendritic arbor of a neuron. The disadvantage is that the sections cannot be stored for long periods. Cryosections are usually thin sections, around 10 μm, they can be stored at -20°C or -80°C for months without damaging them.

The brains cut at the vibratome were embedded in 4% Agarose in 1xPBS one hour before cutting. The brains embedded in Agarose cannot be stored.

Once the 4% Agarose was solidified, the sample was ready to be cut. The surplus agarose around the brain was trimmed away, the brain was glued, with superglue, to the metal disc of the vibratome. When the glue was dried the disc with the brain was immersed in 1xPBS and the sections were cut using a new blade. The thickness changed according to the experiments; for analysis of P0 *In Utero* electroplated brain the thickness was 60 μm, for P7 *In Utero* electroplated brains was 70 μm, for P21 *In Utero* electroplated brains was 100 μm. Sections were collected in 24-well plate filled with 1xPBS, 0.001% Sodium Azide, in each well only 4 or 5 sections were placed. The section can be stored up to 3 months in the fridge, but they become fragile, difficult to move, stain and mount. The brain slices were stained floating.

Brain embedding in gelatine and Cryosectioning

Brains for cryosection were embedded in advance and then stored at -20°C or -80°C. The brains were placed in 0.12M TPO_4, 10% sucrose solution during the day and, once sunken, transferred in 0.12M TPO_4, 20% sucrose and kept overnight at 4°C. They were then transferred in 0.24M TPO_4, 20% sucrose, 7.5% gelatine solution and incubated for around 4 hours or till when they sunk. The brains were then transferred in a mold containing 0.24M TPO_4, 20% sucrose, 7.5% gelatine and were let solidify 1 hour at 4°C. The excess of gelatine was trimmed and the brains were frozen in 2-methylbutan cooled to -50°C with dry ice.

Before cryosectioning the brains were stored at -20°C for about 1 hour. The temperature in the cryostat for cutting gelatin embedded brains was set to -30°C for the chamber and -25°C for the object. The slices were melted on the coverslips, let them dry for 1 hour a room temperature and the stored at -20°C or -80°C. Before staining the frozen slices were let at room temperature to thaw, and then profiled with a DAKO pen. Usually sections were post-fixed with 4% PFA 10 minutes at room temperature and then washed 3 times 5 minutes in 1xPBS.

Immunostaining

The blocking solution (1xPBS, 0.25% TritonX, 3% BSA) was common for immunosytochemistry and immonohistochemistry (both vibratome and cryo- sections). The samples were incubated with blocking solution at least for 1 hour at room temperature. The the first antibody was diluted according to manifacturer's instructions and recapitulated in Table 2.5. The thick vibratome sections were incubated with the first antibody overnight at room temperature, the cryosections and the cultured neurons were incubated overnight at 4°C. First

antibody on neurons in rare cases was incubated 5 hours at room temperature. All the samples were washed in 1xPBS 3 times for 5-10 minutes and incubated in the dark with secondary antibody, conjugated to fluorophore, 1 hour at room temperature. If nuclear sating was necessary DAPI or DRAQ5 were added to the secondary antibody. The samples were washed 3 times for 5 minutes and then mounted using an anti-fading reagent, either bought or self-made (DABCO). Slices must be kept in a cold and dark place to preserve the fluorophores.

2.2.13 *In Situ* Hybridization

microRNAs expression can be visualized in tissue using in *In Situ* Hybridization (ISH). We purchased customized LNA probes (Exiqon) for the detection of mature miR-128, pre-miR-128-1 and pre-miR-128-2, the probes are Digoxigenine (DIG) labeled at both ends; the sequences are in Table 2.6 and in Figure 2.1. ISH was performed according to two publishes

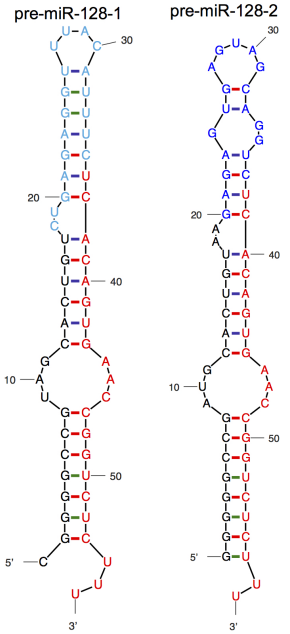

Figure 2.1: ISH probes for miR-128 mature form in red, pre-miR-128-1 in light blue, pre-miR-128-2 in blue. miR-128 mature form probe recognizes also the mature sequence in both precursor forms.

protocols:

1. Pena et al. 2009: this protocol is useful to test new ISH probes, there is a additional fixation step that enable the linkage of the 5' end of the microRNA to the protein of the matrix. This step, however, impedes costaining with antibodies.

2. Silahtaroglu et al. 2007: this protocol is good for costaining with antibodies.

ISH using EDC fixation step (Pena et al. 2009)

This protocol was used on cryosections stored at -80°C. All the steps were done in RNAse free condition using milli-Q water and RNAse free buffers, baked bottles and glass cuvettes.

- Thaw the cryosections for 30 minutes at room temperature. Profile the slices with a DAKO pen.
- Incubate the slices 10 minutes in 4%PFA and then wash 2 times for 5 minutes in 1xPBS.
- Incubate slices in Proteinase K (PK) solution (PK 20μg/ml final concentration in 1xPBS) for 2-5 minutes. PK treatment allows the permeabilization of the tissue, it is, however, a strong treatment and it can lead to tissue disruption. Therefore the incubation time has to be tested according to the sample. If the PK treatment is too harsh the tissue will have holes.
- Wash 5 minutes in 1xTBS, 0.2% glycine and 2 times 5 minutes in 1xTBS. The switch from PBS to TBS is to facilitate the next fixation step.
- Wash the slices 2 times for 10 minutes in Methylimidazole solution and then incubate the slices in an humid chamber with 500 μl each of EDC fixation solution for 2 hours. EDC is extremely toxic.
- Wash the slides 5 minutes in 1xTBS, 0.2% glycine and 2 times 5 minutes in 1xTBS.
- Incubate the slices 30 minutes in the acetylation solution. This step is necessary to decrease background.
- Wash the slices 2 times for 5 minutes in 1xTBS.
- Pre-hybridize the slices for 2 hours with 500μl of hybridization solutions in an hybridization chamber. The solution to wet the Whatman paper in the hybridization chamber is 1xSSC, 50% Formamide. The hybridization chamber can be stored closed, to avoid drying and reused several times.
- Dissolve the probe (5 μM) in 100 μl hybridization solution, boil it for 5 minutes at 80°C, spin it down and cool it on ice.
- Pipet the hybridzation probe on the slices and cover with Nescofilm. Incubate overnight at the correct hybridization temperature. The hybridization temperature depends on the probe. The purchased LNA probe have indicated in the data sheet the optimal hybridization temperature. Note that Nescofilm works better than Parafilm in ISH, because it does not melt with high temperature.

From this step onwards it is not necessary to work in RNAse free conditions

- Remove Nescofilm, if it is necessary to ease the procedure immerge the slices in 5xSSC.
- Wash the slices in the after hybridization buffer 2 times for 30 minutes. These washing steps must be done at hybridization temperature.
- Wash the slices in 0.2xSSC for 15 minutes and one time in 1xTBST for 15 minutes.
- Incubate the slices in 200 μl blocking solution for 1 hour and then incubate with anti-DIG antibody overnight at 4°C.

ISH with Antibody staining (Silahtaroglu et al. 2007)

This protocol was used to visualize together microRNAs and proteins of interest. It was used on cryosections stored at -80°C. All the steps were done in RNAse free condition using milli-Q water and RNAse free buffers, baked bottles and glass cuvettes.

- Thaw slices for 10 minutes at room temperature and for other 10 minutes at 50°C. Profile the slices with DAKO pen.
- Fix the tissue with 4% PFA for ten minutes at room temperature.
- Wash the slides in 1xPBS 3 times for 2 minutes.
- Incubate the slices in the acetylation buffer for 10 minutes at room temperature.
- Wash the slides in 1xPBS 3 times for 2 minutes.
- Add to the slices 100 μl of hybridization buffer, cover with Nescofilm and pre-hybridize for 30 minutes at hybridization temperature. The pre-hybridization and hybridization steps must be done in an hybridization chamber, the solution to moist the chamber air is 1xSSC, 50% Formamide. The hybridization chamber can be stored closed, to avoid drying and reused several times.
- Dilute 5 μM of probe in 100 μl of hybridization buffer, boil it at 85° for 5 minutes, and cool on ice.
- Add the probe to the slices and hybridize for 4 hours at the proper hybridization temperature. The temperature is probe dependent and for the LNA probes purchased from Exiqon is written in the data sheet and in the Table 2.6.

From this step onwards it is not necessary to work in RNAse free conditions

- Wash the slides in 0.1xSSC 3 times for 10 minutes at 4-8° above hybridization temperature, and one time with 5xSSC at room temperature.
- Equilibrate the slices in 1xTBS, washing 3 times for 3 minutes.
- Incubate the slices in 200 μl blocking solution for 1 hour and then incubate with anti-DIG antibody overnight and the chosen antibody for costaining at 4°C.
- Wash the slides in 1xTBS 3 times for 5 minutes.
- Incubate the slices with the appropriate secondary antibody to visualize the protein/proteins of interest.

Visualization of the microRNAs: Detection methods

The visualization of the microRNAs was done using three different methods: Tyramide Signal Amplification (TSA) system, Nitro blue tetrazolium chloride/ 5-Bromo-4-Chloro-3-indolyl phosphate (NBT/BCIP), Fast red. The TSA system is designed to amplify the signal of the

first antibody. To work it requires an Horseradish peroxidase (HRP) conjugated antibody, in ISH the anti-DIG antibody-POD is conjugated with HRP. NBT/BCIP and fast red, instead, are substrate for the alkaline phosphatase enzyme conjugated to the anti-DIG antibody-AP. The difference between TSA kit and the enzymatic reaction of NBT/BCIP or fast red is that in the first case the signal is highly amplified and cannot be used as a measure of visual quantification of the expression. NBT/BCIP and fast red are both enzymatic reactions that creates a precipitate, but the signal is not amplified and the differences in expression can be visually appreciated. TSA system was used in the visualization of the microRNAs in neuronal culture (Figure 3.12), NBT/BCIP was used in the visualization of the microRNA in chromogenic ISH (Figures 3.2, 3.4, 3.3), Fast red (fluorescent) was used to colocalize microRNAs and proteins of interest (Figures 3.5, 3.6)

TSA system (TSA kit from Perkin Elmer was used)

- Before incubation with the first antibody the endogenous activity of the HRP has to be quenched. Incubate the slides 10 minutes in a 3% H_2O_2 solution and afterwards wash them with 1xTBS 3 times for 5 minutes.
- Incubate with the antibody anti-DIG-POD overnight at 4°C.
- Wash in 1xTBS 3 times for 5 minutes, shake the slides while washing.
- (If there is a costaining for protein of interest this is the moment for staining with the secondary antibody)
- Dilute the fluorophore (Cy3 worked always nicely, Fluorescein was too weak) 1:50 in 1xAmplification diluend.
- Apply 100 μl of this solution to the slices, let develop the solution at room temperature for 7 minutes in the dark. Note that TSA amplification can give high background, a long developing time is not recommended.
- Wash in 1xTBS 3 times for 5 minutes and then mount the slides using an anti-fading reagent.

Fast Red Fast Red tables from Roche were used in the experiments.

- After the washes to remove the excess of the first antibody proceed with the detection of the secondary antibody if necessary.
- Wash in 1xTBS 3 times for 5 minutes.
- Equilibrate the slides with 0.1M Tris-HCl pH 8.2 for 5 minutes and in the meantime dissolve the Fast Red tablet in 2 ml of 0.1M Tris-HCl pH 8.2.
- incubate the slides with the staining solution for a maximum of 10 hours. The substrate precipitation can be checked under the microscope. Fast Red is visible also in bright field.
- Wash the slides in 1xTBS 3 times for 5 minutes and then mount them using an anti-fading reagent.

NBT/BCIP NBT/BCIP tablets from Roche were used in the experiments.

- After the washes to remove the excess of the first antibody, proceed with the detection of the microRNA
- Equilibrate the slides in Detection Buffer for 5 minutes and in the meantime dissolve the NBT/BCIP tablet (Roche) in milli-Q.
- Develop the reaction for a maximum of 16 hours, if necessary apply fresh NBT/BCIP solution. The precipitation of the reagent can be checked under the microscope to decide when to stop the reaction.
- Wash in 1xTBS 3 times for 5 minutes and then mount. In this case it is not necessary an anti-fading mounting medium.

2.2.14 Nissl Staining

Nissl staining is a nucleic acid staining methods, used to visualize brain lamination. Nissl staining was used to compare the microRNAs ISH with cortical layering at different embryonic stages and in the adult brain.

- Thaw cryosections in water.
- Incubate the slices in Potassium Sulfide for 15 minutes.
- Wash 2 times in water.
- Incubate the slices in Cresyl violet solution for 20-30 minutes.
- Wash in Acetate buffer twice for 1 minute.
- Wash in Differentiation Buffer for 10 to 30 seconds.
- Rinse in water and the proceed with the Ethanol row.
- Wash 2 minutes in 70% Ethanol and then 2 times for 2 minutes in 100% Ethanol.
- If you need to repeat the staining or to lower the background repeat the steps backwards.
- Incubate 2 times for 10 minutes in Xylol.

Note that if the staining is not satisfactory, either too weak or too strong, it can be modified following the steps backwards. For this reason, during the staining, it is better to use single cuvettes for each passage.

2.2.15 *In utero* Electroporation and Brain Analysis

In Utero Electroporation (IUE) is a technique that allows to manipulate neurons *in vivo*. DNA constructs are injected into the ventricles of the embryos, still in the uterus, and up taken by neuronal progenitors after an electric pulse. The embryos are then let develop until the moment of analysis, that can be either at embryonic or at postnatal stages. There are several published protocols for this technique a representative one is Saito 2006. We used *In Utero* electroporation to target mainly upper layer neurons progenitors, injecting the DNA at

E15.5. We assessed neuronal migration at E18.5 (Figure 3.17), P0 and P7 (Figure 3.19 and 3.18); neuronal and spine morphology at P21 and P15 (Figure 3.22, 3.23, 3.24 and 3.25). In case neuronal migration has to be assessed while neurons are still moving to reach the correct position, the animals should be electroporated and sacrificed at the same time. Some hours difference can affect the results.

In Utero electroporation experiments

The *In Utero* electroporation experiment should last no longer than 40 minutes, the longer the mother is under anesthesia the unlikelier it is to have a good number of healthy pups. The surgery has to be done in the most sterile way as possible, the instruments should be cleaned with 70% Ethanol or sterilized for few seconds in the germinator. The electrodes for injection are pulled to have a thin point suitable to penetrate the skull without damaging it.

- Prepare the DNA to inject at the desired concentration, diluting it with endotoxin-free water and adding 1 μl of Fast Green. Pre-warm the *In Utero* electroporation buffer (1xPBS, 10% P/S sterile solution), pull the electrodes and fill one of them with the DNA to inject.
- Anesthetize the mouse with isofluoran in an anesthetizing chamber. Only when the mouse is completely asleep the surgery can begin.
- Place the mouse on the surgery table with the back on the surface of the table and the nose into the anesthesia tube. The mouse must be under anesthesia for the whole time of the surgery.
- Inject 150 μl of Tamgesic (a morphin analogue) intraperitoneally.
- Disinfect the mouse fur. Cut the fur in the center of the belly, roughly where the uterus is. The smaller the cut the faster will be to suture it. The cut dimension is, however, related to the embryos size. Cut the skin underneath and extract the embryos using tweezers with end rings.
- Wet the embryos with warm IUE buffer and cut the tip of the electrode using fine tweezers under a microscope. Test the DNA ejection from the electrode: the DNA solution should drip out from the tip of the capillary.
- Holding gently the embryo, inject the DNA into the ventricle. Insert the needle next to the brain midline and fill the ventricle with the DNA solution.
- The plus end of the electrodes is placed in the position where the DNA should be up taken from progenitors. Apply current to the embryo's head. The current injected is standard for all embryonic stages: 35 mV and 6 pulses.
- Wet the embryo's head with IUE buffer and proceed in the same way for all the embryos.
- Wet the embryos with IUE buffer before placing them back into the mother's womb.

- Suture the peritoneum, the stitches must be quite close to each other. Then staple the fur.
- Let the mother awake from the anesthesia on the warm pad of the surgery table, and wet her eyes with artificial tears.

Analysis of neuronal migration (E18.5 and P7)

Neuronal migration was assessed at different time points: E18.5, P0 and P7. The analysis was nonetheless the same for all the stages. The brains were cut using vibratome, the slices were stained and then imaged. The imaging was done using the confocal microscope Leica SL. If only migration had to be assessed the pinhole was opened to visualize more neurons. The images were taken at 200 Hz, with the 10x objective. The nuclear staining was imaged, because it was necessary to help the positioning of the grid used to divide the cortical plate into sections. For each brain at least 3 different slices were imaged. A grid was applied on the images of the electroplated sections. The grid is composed of 10 boxes, connected to each other, when the grid is stretched or shortened the ratio between the boxes is maintained. The first 6 boxes of the grid were used to divide the cortical layers. The upper box of the grid was for the marginal zone. The marginal zone can be damaged during the cutting or the mounting of the slices, therefore the end of the first box was placed at the beginning of the second layer of the cortex. The end of the sixth box was placed at the border between sixth layer and white matter. If necessary more than one grid was used to divide the electroporated area. The analysis of the prepared images was done blind. The images were analyzed with Fiji software using the Cell counter plugin. The analysis of the raw data was done in Excel. The counted slices were grouped per brain. At least 3 slices per brain were counted and at least 3 independent brains were analyzed. The statistic was done using Graphpad Prims 5.0 analyzing the data with two-way Anova. The averaged number of neurons for each brain was inserted in the Prism table. Prism 5.0 plotted the average of each box per condition.

Analysis of neuronal migration: morphology at P0

For the analysis of neuronal morphology brains were electroplated with either pre-miR-128-2 or dsRed control in the same mother. In this way the detected differences were due to the intrinsic properties of the constructs injected and not to the time of injection or analysis. The brains were cut using a vibratome, the slices were stained and mounted. The imaging was done using a confocal microscope (Leica SL), taking z-stack (step 2 μm) with 40x objective. One overview image of electroplated construct and nuclear staining was also taken with 10x objective. The overview image was used to define the deep layers of the cortical plate. The images were coded so that the subsequent analysis steps were done blind. The upper layer neurons, still migrating to their final position, and located in the deep layers, were reconstructed with Fiji sotware using the plugin Simple Neurite Tracer. In the reconstructed neurons all the protrusion coming from the leading process or from the soma (a part the leading process and the axon) were measured in Fiji. The default measure in Fiji is in pixel, so the pixel number was converted into μm, using as a conversion scale the scalebar of the images. To decide if

a protrusion was a filopodia or a branch a cutoff of 5 μm was used, as suggested by Julien Courchet (Polleux lab, personal communication). The number of branches and filopodia was count in at least three slices per brain and then averaged. The average number of filopodia and branches was inserted in Prism 5.0 and there it was averaged per condition. The result was plotted using box and whisker plotting methods.

Analysis of neuronal morphology: dendritic tree reconstruction and Sholl analysis

Neuronal reconstruction was done on electroporated neurons in layer II/III in P21 animals and electroporated neurons in all layers in P15 animals. P21 neurons were imaged using an inverted epifluorescence microscope (Olympus IX81) taking stacks every 1 μm. P15 neurons were imaged using the confocal microscope Leica SL taking stacks every 1 μm. The stacks were reconstructed with Fiji software using the plugin Simple Neurite Tracer. The reconstruction file is a stack and was Z-projected to visualize the dendritic arbor. Sholl analysis was performed only on P21 neurons using the Sholl analysis plugin in Fiji software and working with the stacks of the reconstructed neurons. The concentric circles increased the radius with a step of 5 μm, the last concentric circle was not set. The number of intersection was then analyzed using Prism 5.0.

Analysis of spine morphology

Spine images were taken with a confocal microscope (Leica SL) using 200 Hz, a line step of 2 and a magnification of x63x4. The step of the stack was 0.2 μm. The spine morphology was analyzed in the same region for each neuron: the upper branch of the apical dendrite. It is important to be consistent with the region chosen for imaging. Working with the z-stack for each spine the following parameters were measured: spine length, neck length, head width, and when visible neck width. The default measure in Fiji software is done in pixel, the conversion in micrometer was done in Excel, using the scalebar to convert pixel and micrometer. The number of spines per 100 μm was also counted

Chapter 3

Results

microRNAs, small non coding RNA, target hundreds of genes leading to translational repression and/or to mRNA degradation. There are mainly two ways in which one can chase the targets of the microRNA of interest: one is to use the predictive algorithm, choose the favorite candidates according to particular criteria (grouping the candidates in families, picking the highest scores genes etc). The other is to overexpress or knockdown the chosen microRNA, looking at the resulting phenotype and then searching for the downregulated mRNAs. This thesis presents both approaches the first in Section 3.2 and the second in Sections 3.3.1, 3.3.3 and 3.3.4.

3.1 Characterization of miR-128 Expression

Previous studies have shown that miR-128 is a brain-enriched miRNA that is specifically expressed in neurons as opposed to other cell types in the CNS. To date, however, the developmental expression pattern of miR-128 has not been studied in detail. In addition, there is little information available concerning the regulation of miRNA expression in development in general, and for miR-128 in particular. It was therefore of interest to compare expression patterns between the mature 22 nucleotide (nt) miR-128 molecule and the two precursor molecules that can generate miR-128: pre-miR-128-1 and pre-miR-128-2. For these experiments I took advantage of locked nucleotide analog (LNA) probes specific for each of the three molecules and used them to compare their expression at selected developmental stages by Northern blot and *in situ* hybridization.

3.1.1 pre-miR-128-2 Precedes miR-128 Expression

Our group had already showed that miR-128 expression increases during embryonic Central Nervous System (CNS) development, what we had not checked so far was the comparison between the active 22 nt form (miR-128) and the two precursor forms, pre-miR-128-1 and pre-miR-128-2. We isolated total RNA from different embryonic stages, early postnatal stages and adult brain and used them to prepare Northern blots. Using a probe specific for miR-128, we observed strong induction of the 22 nt mature miRNA between embryonic day 12.5 and 18.5 (E12.5- E18.5) with high level expression continuing at postnatal day 3 (P3) and adult (Figure

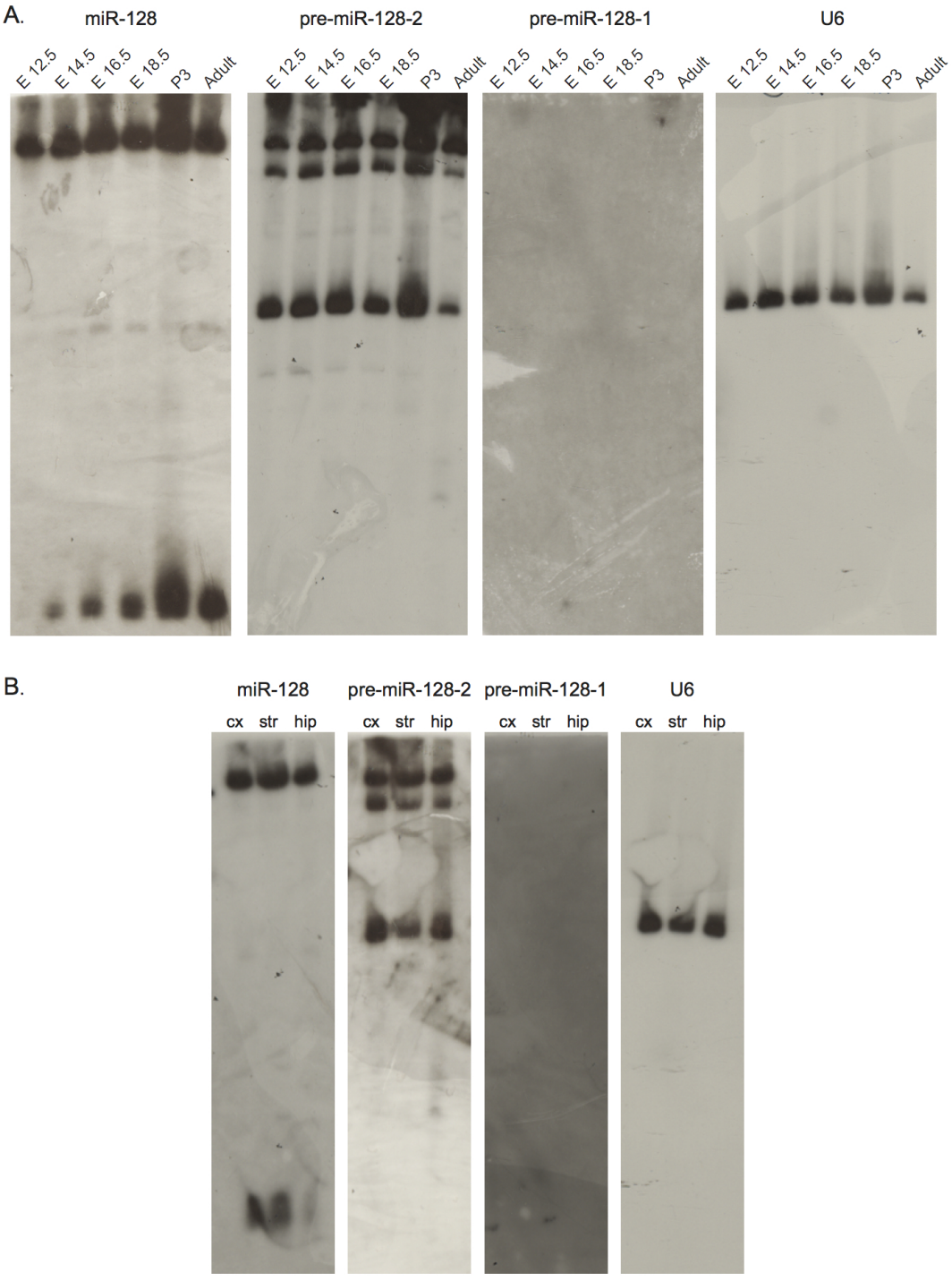

Figure 3.1: *Contrasting expression of pre-miR-128-2 and miR-128.* Northern blot analysis of miR-128, pre-miR-128-1 and pre-miR-128-2 in forebrain. In Panel **A** miR-128 (first blot from the left), pre-miR-128-2 (second blot from the left) and pre-miR-128-1 (third blot from the left) expression are analyzed at different embryonic stages (E12.5-E18.5), early postnatal stages (P3) and in adult brain as indicated. In Panel **B** the expression of miR-128 (first blot from the left), pre-miR-128-2 (second blot from the left) and pre-miR-128-1 (third blot from the left) are analyzed in different regions of E18.5 mouse brain. The regions considered are cortex (cx), striatum (str) and hippocampus (hip), as indicated. In both Panel **A** and **B** U6 RNA is used as a loading control (last blot from the left). Positive controls for the probes, including pre-miR-128-1 are shown in Figure 2, Appendix page ii.

3.1 A), confirming our earlier published reports (Smirnova et al., 2005). In addition to the mature form, this probe should also recognize both the primary transcripts (unresolved at the top of the polyacrylamide gel used for small RNA analysis) and the two precursors, predicted to migrate at approximately 70 and 75 nt. A single band presumably representing one of the precursors was visible in each lane. Interestingly, we found that in contrast to the mature form, pre-miR-128-2 was already detected at maximum levels at E12.5 and remained constant throughout embryonic development and postnatal stages (Figure 3.1 A). Most surprisingly, pre-miR-128-1 could not be detected at any stage (Figure 3.1 A). These observations showed that pre-miR-128-2 expression does not correlate with the mature form temporally, indicating that there is a strong component of post-transcriptional regulation underlying the increase in miR-128 levels during development. Moreover, pre-miR-128-1 and pre-miR-128-2 did not contribute equally to miR-128 expression, in fact it seemed that pre-miR-128-2 was responsible for most of the mature form.

We next compared expression of the three RNAs in different brain regions at E18.5. miR-128 was found in the cortex, in the striatum and to a lesser extent in the hippocampus. In contrast, pre-miR-128-2 was present at approximately equal levels in all samples (Figure 3.1 B). As in the previous experiment, pre-miR-128-1 was not detected in any region. These data indicated that pre-miR-128-2 may be subject to differential processing in particular regions, in this case the hippocampus, in addition to the evidence for temporal regulation shown in Figure 3.1 A.

3.1.2 *In situ* Hybridization Reveals Differences in the Developmental Expression of the Precursor and Mature Forms of miR-128

Despite a number of studies describing miR-128 function in the nervous system, there has not yet been an exhaustive description of its expression pattern. We used *in situ* hybridization to compare regional, temporal and cellular localization of miR-128, pre-miR-128-1 and pre-miR-128-2. For all experiments the results of Nissl staining are also shown to provide a structural comparison. At the earliest embryonic stage tested (E12.5, Figure 3.2 A), staining for miR-128 was negative. In contrast, pre-miR-128-2 was readily detected in the ventricular and subventricular zones. This result is consistent with the Northern blot experiment shown in Figure 3.1 A. Focusing on the cortex, at later stages (E14.5-E18.5), miR-128 staining was preferentially found in the cortical plate (Figure 3.2 B, C, D). At higher magnification a gradient in the expression is apparent with stronger staining in the deeper layers compared to the upper layers, for example at E16.5 (Figure 3.2 C). This gradient then disappeared at early postnatal stages (P3, Figure 3.2 E). pre-miR-128-2, on the contrary, was present in the cortical plate as well as in the ventricular, subventricular and intermediate zones at all embryonic stages tested (Figure 3.2 B, C, D). The difference in expression between pre-miR-128-2 and miR-128 in the ventricular zone is confirmed in the highest magnification views at E14.5 and E18.5 (Figure 3.2 B and D, magnification) and in the intermediate zone at E16.5 (Figure 3.2 C, magnification).

The adult brain deserves more detailed comment (Figure 3.2 F and Figure 3.3). First of all, in the overviews the intracellular staining of adult neurons appears to be specific for the

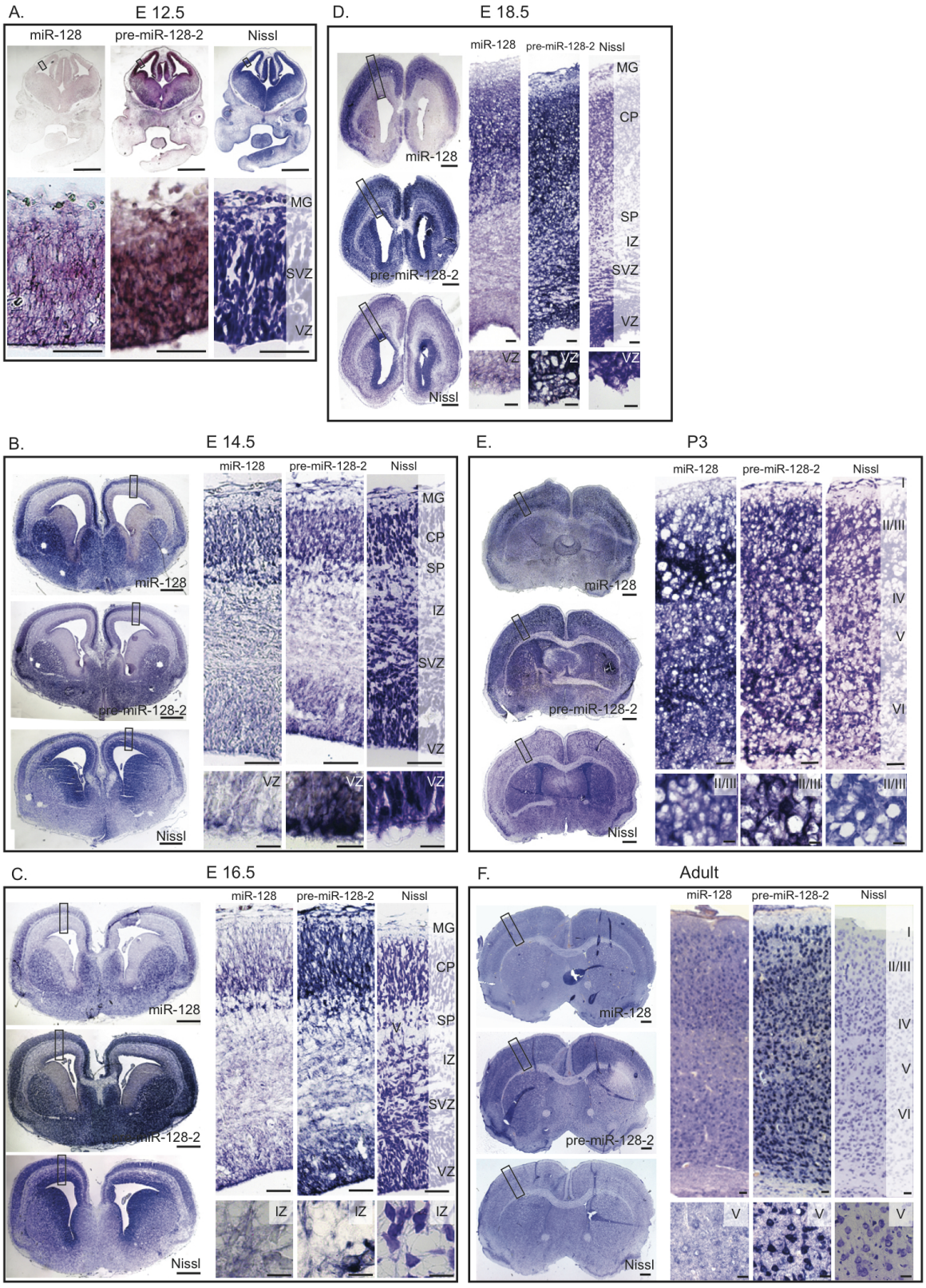

Figure 3.2: *miR-128 and pre-miR-128-2 in embryonic, new born and adult brain.* Mouse Brains at several embryonic stages (E12.5 Panel **A**, E14.5 Panel **B**, E16.5 Panel **C**, E 18.5 Panel **D**), early postnatal stages (P3 Panel **E**) and adult brain (Panel **F**) were hybridized using LNA probes against miR-128 and pre-miR-128-2, as indicated. In all stages analyzed Nissl staining was used to allow structural comparison. For each panel the overview of the brain is on the left side (scalebar 500 μm), a representative view of cortical staining, as marked on the overview, is on the right side (scalebar: 50 μm) and a magnification of selected regions of interest from the cortex is below the cortical section (scalebar 10 μm). MG: marginal zone, CP: cortical plate, SP: sub plate, IZ: intermediate zone, SVZ: sub ventricular zone, VZ: ventricular zone.

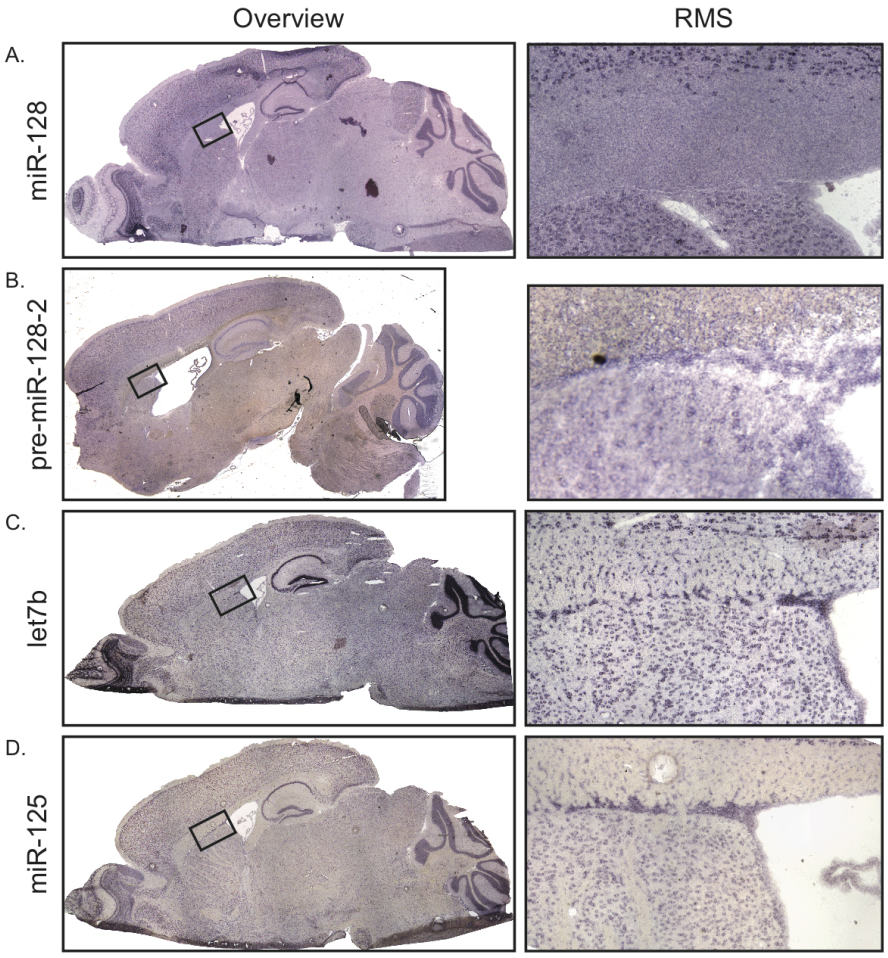

Figure 3.3: *pre-miR-128-2 but not miR-128 is expressed in migrating neuroblasts of the RMS.* Sagittal section of adult brain were hybridized with miR-128 (Panel **A**), pre-miR-128-2 (Panel **B**), let-7b (Panel **C**) or miR-125 (Panel **D**) probes to visualize the migrating neuroblasts of the RMS. An overview of the section is presented on the left, with the region corresponding to the RMS marked. A magnification of the ventricular zone and of the RMS is on the right side of each panel.

soma with little staining of the dendritic arbors. However, in embryonic neurons staining of precursor and mature forms was apparent throughout the cell, including the soma and all neurites. But in the case of pre-miR-128-2 staining clearly extended into the proximal apical and basal dendrites, as can be appreciated by comparison to the Nissl staining (Figure 3.2 F, magnification). Most likely the sensitivity is not sufficient to detect the miRNA in the finely ramified dendritic arbors of mature neurons. We also noticed differences in the expression pattern of miR-128 and pre-miR-128-2. The distribution of precursor staining in the cortical layers was almost indistinguishable from the Nissl staining. Staining with miR-128 was less uniform with much weaker expression in layer V (3.2 F, magnification). The differential staining in layer V is also visible in sagittal sections of the adult brain (Figure 3.3). In this case we compared miR-128 and pre-miR128-2 with let-7b and miR-125. let-7b and miR-125 showed a wider distribution across the brain regions compared to either miR-128 or pre-miR-128-2, for example in the hindbrain. We also noticed that pre-miR-128-2, let-7b and mir-125 were present in the migrating neuroblasts of the RMS (Figure 3.3 B, C, D magnification), whereas miR-128 was absent (Figure 3.3 A magnification).

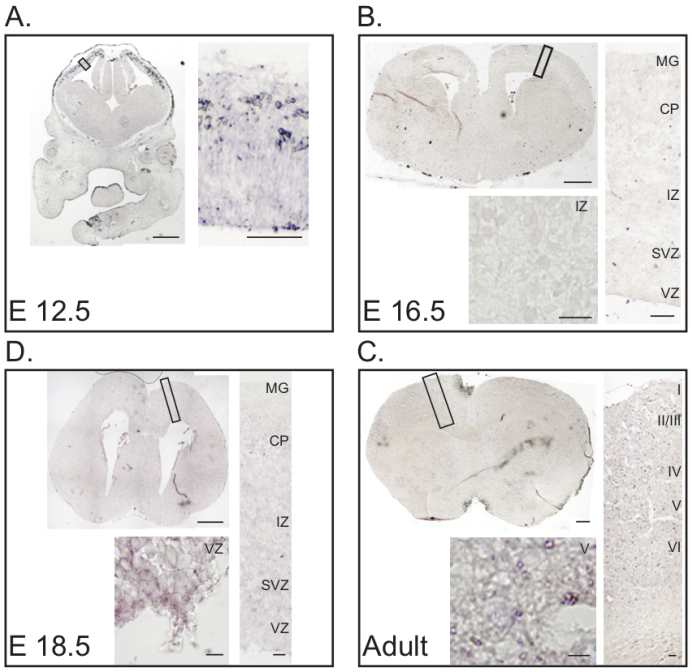

Figure 3.4: *pre-miR-128-1 expression in embryonic and adult brains.* Mouse brains at several embryonic stages (E12.5 Panel **A**, E16.5 Panel B, E18.5 Panel **C**) and adult brain (Panel **D**) were hybridized with an LNA probe specific for pre-miR-128-1. For each panel the overview of the brain is on the left (scalebar 500 μm), representative views of cortical staining are on the right (scalebar: 50 μm) and a magnification of a selected region of interest is below the overview of the brain (scalebar 10 μm). MG: marginal zone, CP: cortical plate, SP: sub plate, IZ: intermediate zone, SVZ: sub ventricular zone, VZ: ventricular zone.

As shown in Northern blots, we were unable to detect the presence of pre-miR-128-1 (Figure 3.4) at any of the stages analyzed. We believe this is not due to failure of the probe, as demonstrated by the ability of this probe to specifically detect pre-miR-128-1 in transfected cells (see Appendix .1).

To better characterize cell populations expressing either pre-miR-128-2 or miR-128, we performed fluorescent *in situ* hybridization to visualize the microRNAs combined with antibody staining for well-established progenitor markers. We analyzed the progenitor zones and cortical plate at E16.5, and the two adult neurogenic niches (rostral migratory stream (RMS), and hippocampal dentate gyrus).

For embryonic stage E16.5 we used Tbr2 as a marker for basal progenitors and as a positive control we also hybridized for miR-124, a microRNA necessary in the transition from neuronal progenitors to committed neurons (see Section 1.3). miR-128 (Figure 3.5 A) expression was restricted to the cortical plate (CP) and once again the deeper layer showed a stronger staining. This is particularly apparent in comparison to pre-miR-128-2 (Figure 3.5 B) and miR-124 (Figure 3.5 C) where the cortical plate showed a uniform expression pattern. In the subventricular zone (SVZ) miR-128 was almost completely absent from Tbr2 positive cells (Figure 3.5 A magnification). Pre-miR-128-2, in contrast, was expressed throughout the cortical plate from the subventricular zone to the marginal zone without interruption. Tbr2 basal progenitors in the subventricular zone were strongly pre-miR-128-2 positive. The expression pattern of miR-124 was distinct from either miR-128 or pre-miR-128-2 (Figure 3.5 C). miR-124 positive cells were present in the intermediate and to a lesser extent in

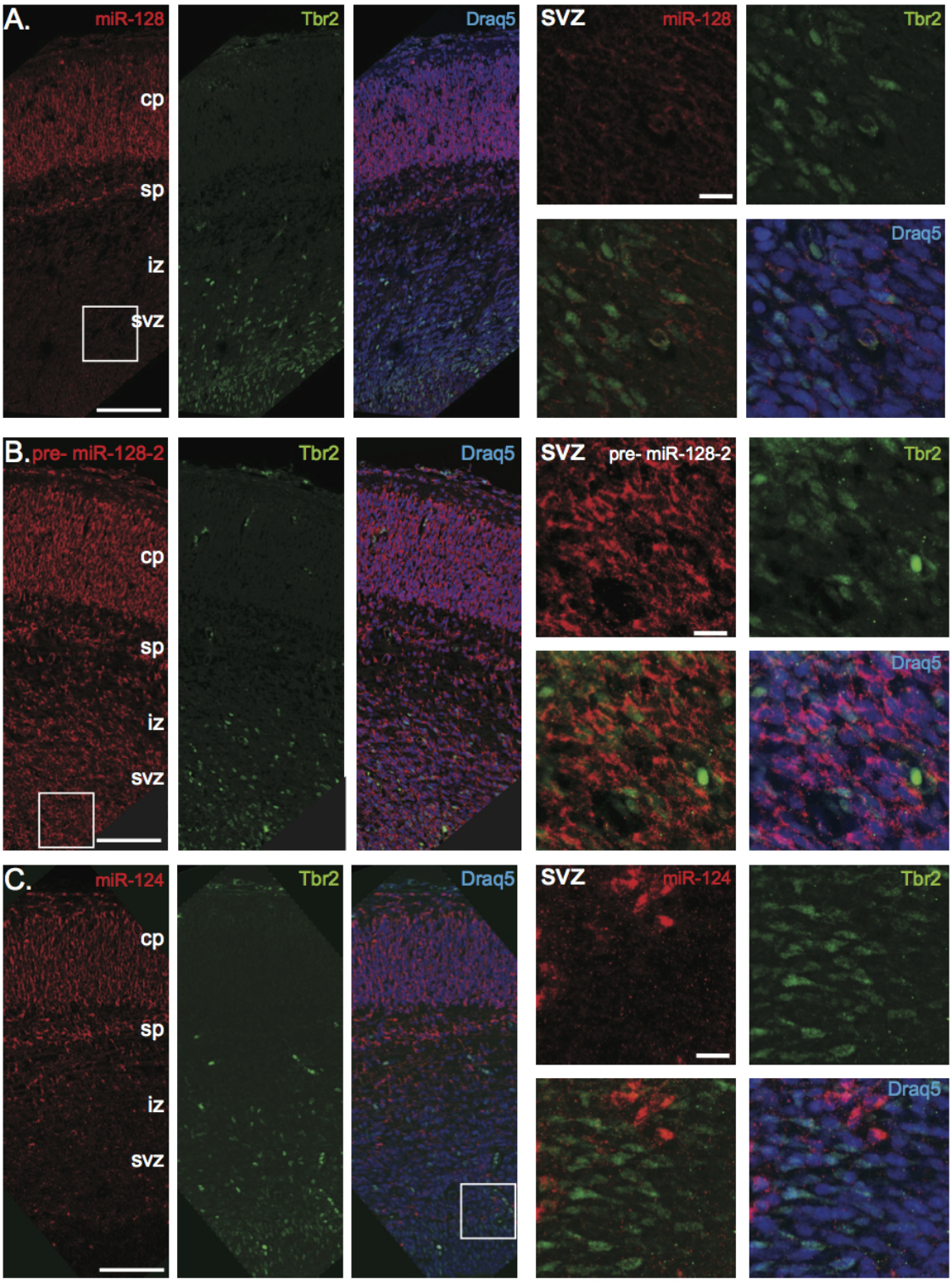

Figure 3.5: *miR-128 is expressed only in the cortical plate. In situ* hybridization showing miR-128 (Panel **A**), pre-miR-128-2 (Panel **B**) and miR-124 expression (Panel **C**) in E16.5 brain in red. The population of basal progenitors is visualized by immunostaining for the transcription factor Tbr2. The left side of each panel presents a view of the cortex from the SVZ to the cortical plate, as indicated. For each panel the third image presents merged channels of the first two images (miRNA plus Tbr2) together with the nuclear dye Draq5 rendered in blue (scalebar 100 μm). The right side of each panel are four images showing a region of the SVZ (as marked by a white box on the right) at higher magnification (scalebar 10μ). In clockwise order, the images depict staining for the indicated miRNA probe (in red), Tbr2 (in green), merged view plus Draq5 rendered in blue, and merged view without Draq5. CP: cortical plate, SP: sub plate, IZ: intermediate zone, SVZ: sub ventricular zone.

the subventricular zone. miR-124 positive cells intermingled with Tbr2 positive cells in the subventricular zone, but were not stained for Tbr2, suggesting that these cells are in the multipolar migration phase (Stage 3).

With these results, we demonstrated, for the first time, that miR-128 was exclusively postmitotic, whereas its precursor was already present in progenitors, in this case basal progenitors.

Neurogenesis is no longer considered to be prerogative of embryonic brains, and in fact, take also places in adulthood although to a much lesser extent. There are two neurogenic niches: one located at the lateral ventricular wall that gives rise to migrating neuroblasts forming the RMS; and the other the dentate gyrus of the hippocampus (for more details see Section 1.2.2). We wanted to confirm that miR-128 was also absent from progenitors in adult neurogenic niches. As a marker we used Doublecortin (DCX), which is expressed by migrating neuroblasts and hippocampal progenitors. In the RMS the DCX^+ migrating neuroblasts, do not show any miR-128 staining (Figure 3.6 A left panel). The overview showed that miR-128 positive cells were only present outside the stream. At higher magnifications it was evident that the DCX expressing cells did not express miR-128, whereas the neighboring neurons did. On the other hand, DCX^+ neuroblasts in the RMS were costained for pre-miR-128-2. At higher magnification it was clear that all DCX^+ neuroblasts costained for pre-miR-128-2 (Figure 3.6 A right panel).

The situation in the dentate gyrus of the hippocampus was similar, despite the more complex maturation process than the RMS. To better monitor the maturation state of the DCX positive cells we costained for NeuN, a postmitotic neuronal marker. In the maturation process progenitors are initially $DCX^+/NeuN^-$ before becoming $DCX^+/NeuN^+$ (see Section 1.2.2). For comparison, we also hybridized for let-7b, a miRNA known to be expressed in progenitors (see Section 1.3). miR-128 was absent from $DCX^+/NeuN^-$ progenitors and $DCX^+/NeuN^+$ newborn neurons (Figure 3.6 B and C arrow head). On the other hand, $DCX^+/NeuN^+$ cells were positive for pre-miR-128-2 or let-7b. The cellular resolution makes it difficult to determine with certainty if $DCX^+/NeuN^-$ are also costained (3.6 B and C empty arrow head).

In conclusion our results indicated that miR-128 was purely postmitotic both at embryonic stages and in adult brain, contrasting with a previous publication (see Sections 1.4 and 4.3). We could also show, however, that pre-miR-128-2 was present in progenitors at all stages and contexts tested. This mismatch in expression between mature and precursor forms, never shown before for miR-128, opens a new perspective for the regulation of microRNA processing (see Section 4.2).

3.2 miR-128 Target Genes

In this section I present the *in vitro* validation of several mRNA candidates as miR-128 targets. The experiments have been conducted throughout all my graduate period, therefore the conditions, such as cell lines, miR-128 overexpression and FACS analysis methods have evolved, as detailed in the Materials and Methods (Table 2.17).

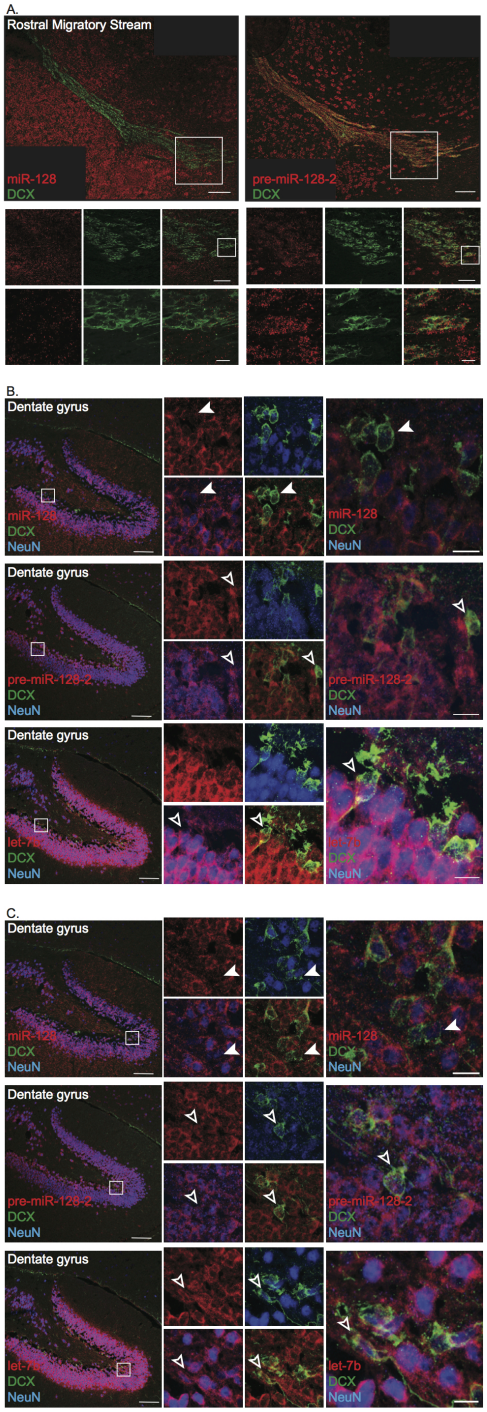

Figure 3.6: *pre-miR-128-2, but not miR-128, is expressed in DCX positive progenitors. In situ* hybridization of sagittal sections of adult brain showing the RMS (Panel **A**) and two different regions of the Dentate Gyrus (Panels **B** and **C**). Panel **A** compares ISH results for miR-128 (left side) and pre-miR-128-2 (right side). The overview of the RMS is in the upper part of the panel (scalebar 100μm), two magnifications of the regions in the white boxes are below the overview (scalebars: 50 μm for the middle images and 10 μm for the lower images). For each magnification, three images are shown with the results for RNA staining (miR-128 or pre-miR-128-2) in red on the left, DCX staining in the middle in green and a merged view of red and green channels on the right. Panels **B** and **C** show ISH for miR-128 (upper images), pre-miR-128-2 (middle images) and let-7b (lower images) as indicated in the overviews on the left in a merged view with DCX staining in green and NeuN rendered in blue. DCX antibody is used to visualize progenitors, and NeuN is used as a neuronal marker (scalebar 100 μm). Note **B** and **C** use the same overview with the position of higher magnification views indicated by a white box. In clockwise order, four higher magnification images depict staining for the indicated miRNA probe (in red), a merged view of DCX (green) and NeuN (rendered in blue), a merged view of the miRNA probe (red) and NeuN (rendered in blue) and a merged view the miRNA probe (red) and of DCX (green) Arrow heads indicate cells positive for DCX but not for the microRNA hybridized, and empty arrow heads indicate cells double-positive for DCX and the microRNA hybridized. Highest magnification images of these individual cells are presented on the right (scalebar: 10 μm).

3.2.1 Genes Involved in Brain Development

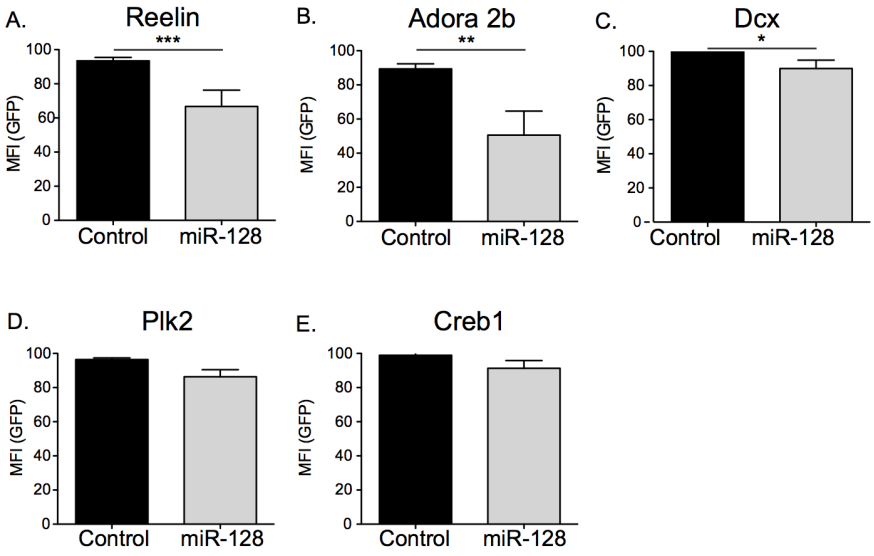

Figure 3.7: *Sensor assay for genes involved in brain development.* Sensor assay to test if miR-128 regulates the 3'UTR of Reelin (Panel **A**), Adora 2b (Panel **B**), DCX (Panel **C**), Plk2 (Panel **D**), Creb1 (Panel **E**). The experiments were done in HEK 293T cells using a scramble synthetic microRNA as a control or synthetic miR-128, as indicated. GFP expression is rendered as % mean fluorescence intensity (MFI) relative to control, set at 100%. The error bars represent standard deviation of at least three independent experiments with $* \ p < 0.05$, $** \ p < 0.01$ and $*** \ p < 0.001$.

At the beginning of my PhD there was not yet any functional analysis of miR-128. We therefore decided to use an *in vitro* assay to assess some of the most interesting and high scoring predicted targets of miR-128 with known functions in the early stages of neuronal maturation (Figure 3.7 C, D, E) and migration (Figure 3.7 A, B). We found that miR-128 regulated several of the tested 3'UTRs, such as Reelin (Figure 3.7 A), an extracellular matrix glycoprotein necessary for neuronal migration at early embryonic stages and important in Long Term Potentiation in the adult hippocampus; Adora2b (Figure 3.7 B), a G protein coupled receptor involved in axon pathfinding; and Doublecortin (Figure 3.7 C), a microtubule-associated protein expressed in neuronal progenitors. On the other hand miR-128 did not regulate the 3'UTR of Polo-like kinase 2 gene (Plk2, Figure 3.7 D), a serum- inducible kinase important in cell division, or the transcription factor Creb1 (Figure 3.7 E). Together these data suggested that miR-128 is important in the regulation of genes involved specifically in brain development (Reelin and DCX).

3.2.2 Genes Involved in Neuronal Polarization

During the course of the thesis, we discovered that miR-128 overexpression in cultured neurons gives rise to multiple axons (Figure 3.11) We were puzzled by the strong and stage dependent phenotype so we decided to test a set of genes connected either with neuronal polarization (Gsk3β, Par6b, srGAP2) or with axon outgrowth and branching (Nedd4, Jip3, srGAP2). We used Cdc42 as a negative control (Figure 3.8 F) that plays important roles in polarization and interacts with Gsk3β and Par6 but is not a predicted target. Gsk3β and the polarization complex, consisting of Par6b, Par3 and aPKC, work together to determine which of the neu-

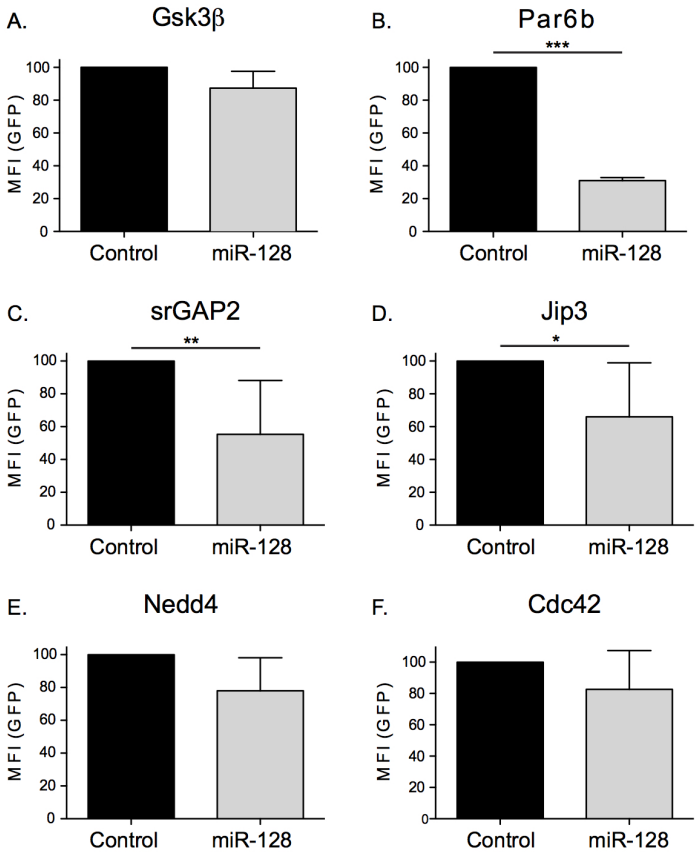

Figure 3.8: *Sensor assay for genes involved in neuronal polarization.* Sensor assay to test if miR-128 regulates the 3'UTR of Gsk3β (Panel **A**), Par6b (Panel **B**), srGAP2 (Panel **C**), Jip3 (Panel **D**), Nedd4 (Panel **E**) and the negative control Cdc42 (Panel **F**). The experiments were done in N2A cells using a scramble synthetic microRNA as a control or synthetic miR-128, as indicated. GFP expression is rendered as % mean fluorescence intensity (MFI) relative to control, set at 100%. The error bars represent standard deviation of at least three independent experiments with $* \ p < 0.05$, $** \ p < 0.01$ and $*** \ p < 0.001$.

rites in a polarizing neuron will become the axon. The polarization complex phosphorylates and inactivates the constitutively active Gsk3β. This process defines the axonal fate of the neurite in which it happens. Surprisingly we found that, in the assay, miR-128 regulated Par6b (Figure 3.8 B), but not Gsk3β itself (Figure 3.8 A). miR-128 also, appeared to regulate the 3'UTR of srGAP2 (Figure 3.8 C), a protein involved in the early stages of neuron migration and growth cone formation; and Jip3 (Figure 3.8 D), a protein that is involved in axonal transport and axonal branching; whereas it did not regulate the 3'UTR of Nedd4 (Figure 3.8 E), an ubiquitin ligase involved in axon branching.

Taken together these data identified candidate genes important for axon functionality and cell polarization that are regulated by miR-128.

3.2.3 Genes Involved in Semaphorin Pathway and Phf6

In the process of understanding the mechanisms behind the multiple axons (Section 3.3.1) and migration phenotypes (Section 1.2.3) we ended up testing several hypotheses, one of these involves semaphorins and their receptors. It has been shown that they are involved in axon specification *in vitro* and in neuronal migration *in vivo*. We tested Semaphorin 3E (Sema 3E, Figure 3.9 B) and the receptor Neuropilin 2 (Nrp2, Figure 3.9 C) using Sema 3A (Figure

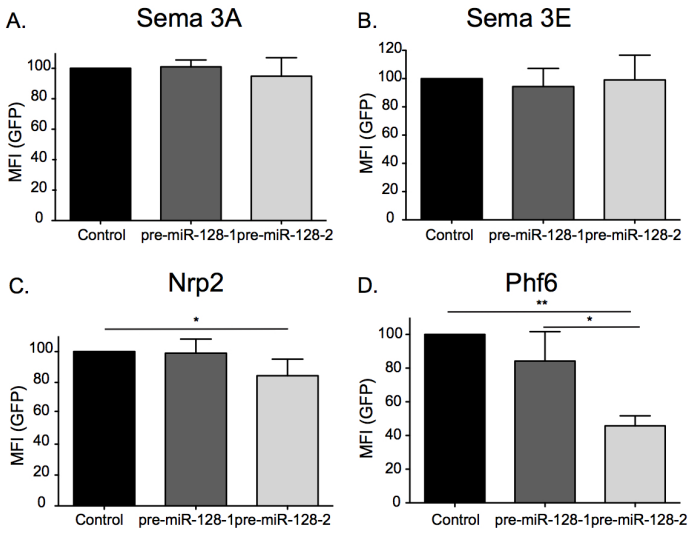

Figure 3.9: *Sensor assay for genes involved in the semaphorin pathway and Phf6.* Sensor assay to test if miR-128 regulates the 3'UTR of Sema 3A (Panel **A**, as negative control), Sema 3E (Panel **B**), Nrp2 (Panel **C**), Phf6 (Panel **D**). The experiments were done in HEK 293T cells using the intronic dsRed vector without insert as negative control, or the vector expressing pre-miR-128-1 or pre-miR-128-2, as indicated. GFP expression is rendered as % mean fluorescence intensity (MFI) relative to control, set at 100%. The error bars represent standard deviation of at least three independent experiments with $* \; p < 0.05$, $** \; p < 0.01$.

3.9 A) as a negative control. Moreover in this assay we used both miR-128 precursor forms: pre-miR-128-1 and pre-miR-128-2, given the difference in their ability to influence neuronal migration when overexpressed *in utero* (Figure 3.18). We wanted to see if their differential activity in migration is a consequence of their differential activity in target gene regulation. We could show that Nrp2 was mildly regulated by pre-miR-128-2 but not pre-miR-128-1 (Figure 3.9 C) and that Sema 3E was not regulated at all (Figure 3.9 B). This suggests that miR-128 does not play a key role in the regulation of semaphorin pathway (see Sections 3.3.2 and 3.3.3).

In parallel we tested Phf6 (PHD finger protein 6), a high-ranking target shown to have a function in neuronal migration (see Section 1.2.6). pre-miR-128-2 strongly donwregulated the Phf6 3'UTR (Figure 3.9 D), whereas pre-miR-128-1 had almost no effect. This result makes Phf6 a good candidate to explain the migration phenotype (Figures 3.18, 3.21).

It should be noted that both pre-miR-128-1 and pre-miR-128-2 are functional in this assay when using highly sensitive artificial sensor constructs containing perfectly complementary binding site arrays (Appendix Figure 3, page iii). The difference in activity seen with natural 3'UTRs is therefore most likely due to less efficient processing of pre-miR-128-1 compared to pre-miR-128-2.

3.2.4 Genes Involved in Neuronal Communication

miR-128 expression is high in adult brains and increases as embryonic neurons mature in culture (Figure 3.1 and 3.21 D). Therefore we analyzed the morphology of P21 neurons after *in utero* electroporation at E15.5. We found that dendritic spine size and number is affected (Figure 3.25). Among the predicted targets there are several genes for ion channels. Most surprising for us was that two of the four AMPA receptor subunits (Gria1 and Gria3) and Cacng2 (better known as Stargazin), a Tarp protein necessary for shuttling the AMPA receptor

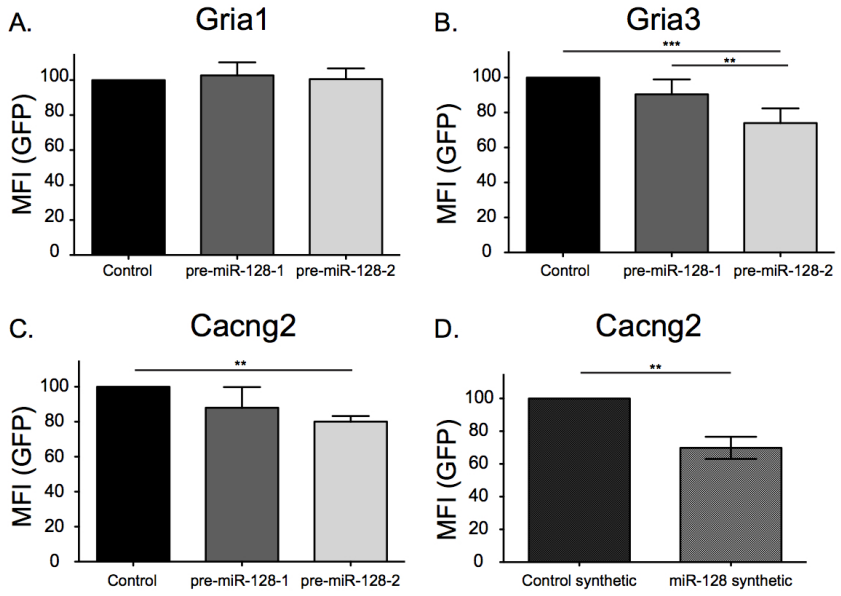

Figure 3.10: *Sensor assay for genes involved in neuronal communication.* Sensor assay to test if miR-128 regulates the 3'UTR of Gria1 (Panel **A**), Gria3 (Panel B), Cacng2 (Panels **C** and **D**). The experiments were done in HEK 293T cells using miR-128 expression constructs or vector without insert for the Panel **A**, **B** and **C** and synthetic miR-128 vs. synthetic control in Panel **D**. GFP expression is rendered as % mean fluorescence intensity (MFI) relative to control, set at 100%. The error bars represent standard deviation of at least three independent experiments with $* \ p < 0.05$, $** \ p < 0.01$ and $*** \ p < 0.001$.

from the soma to the spine, were among them. The 3'UTRs of Gria3 (Figure 3.10 B) and Cacng2 (Figure 3.10 C and D), but not Gria1 (Figure 3.10 A), were regulated by pre-miR-128-2 but not pre-miR-128-1. For Cacng2 we compared miR-128 overexpression by two different methods: one plasmid-based (Figure 3.10 C) and the other employing a synthetic precursor (Figure 3.10 D). As expected, the effect is stronger when we used the synthetic microRNA (Appendix Figure 3, page iii) but was also observed with the plasmid vector. These results validate candidates for future experiments to test the regulation of AMPA receptors by miR-128 *in vivo* and the possible relevance for the dendritic spine phenotype.

3.3 miR-128 Manipulation *in vitro* and *in vivo*

To study miR-128 functions we decided to perform gain and loss of function experiments *in vitro* and *in vivo* with the goal of understanding its functions at the single cell and organ levels.

3.3.1 miR-128 Gain of Function Leads to Multiple Axons *in vitro*

We manipulated miR-128 expression by transfecting primary cortical and hippocampal neurons with either overexpression and knockdown (so-called sponge) plasmid constructs or synthetic miR-128 mimics and antisense inhibitors. We chose two different time points: DIV 2, when the microRNA is barely detectable (Figure 3.21 F) and the neurons are undergoing the polarization process (see Section 1.2.4), and DIV 5 when miR-128 expression is increasing and the polarized neurons are actively elongating axon and dendrites. To visualize axonal structure we used Tau1, an axon-specific microtubule binding protein and Ankyrin G (AnkG),

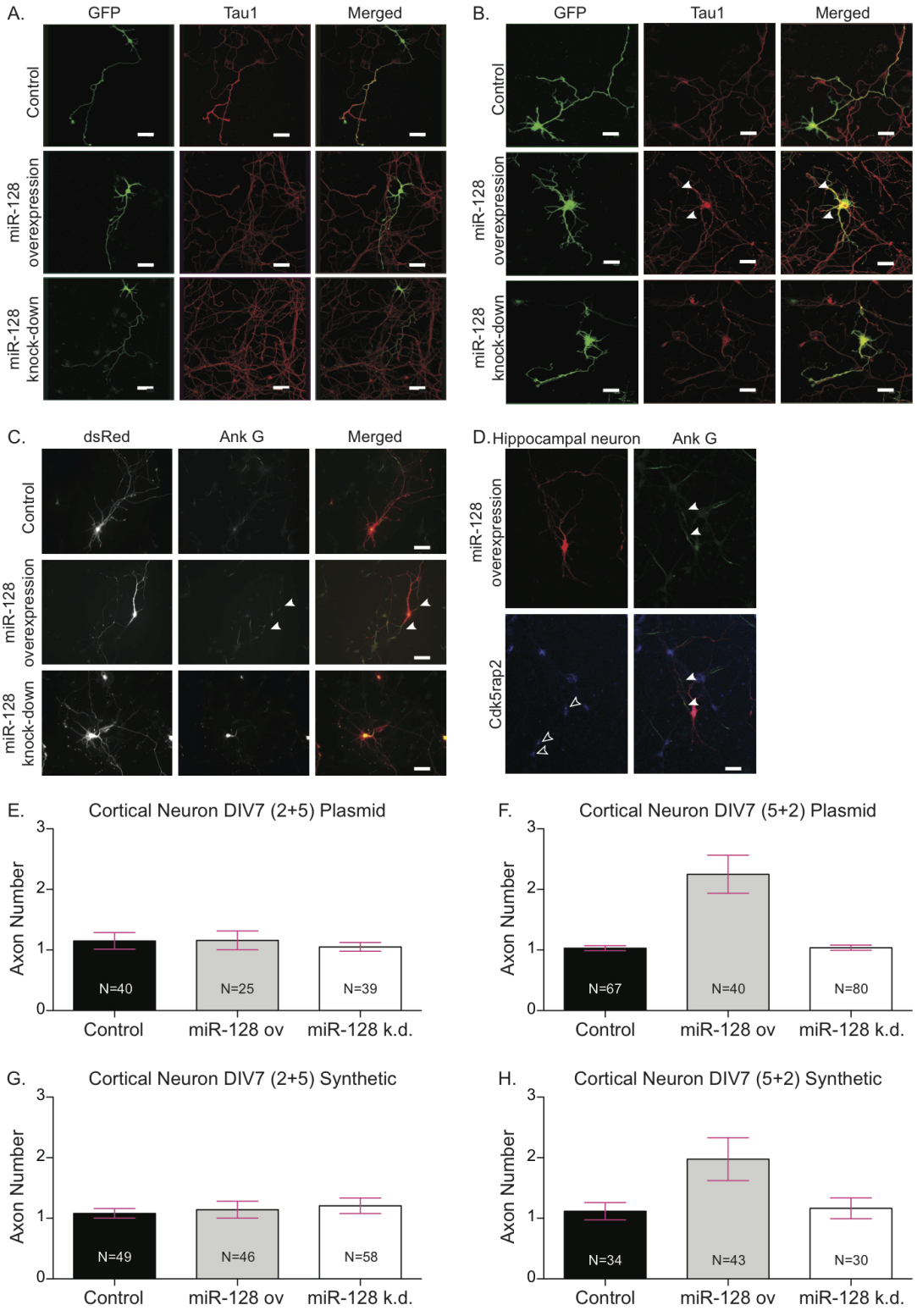

Figure 3.11: *miR-128 Gain of Function Leads to Multiple Axons in vitro.* miR-128 expression is manipulated in primary cortical culture (Panels **A**, **B**, **E**, **F**, **G** and **H**) or primary hippocampal culture (Panels **C** and **D**) using either gain/loss of function constructs (Panels **A**, **C**, **D**, **E** and **F**) or synthetic mimic and antagomiR (Panels **B**, **G** and **H**). miR-128 expression is manipulated either at DIV 2 (Panels **A**, **E** and **G**) or at DIV 5 (Panels **B**, **C**, **D**, **F** and **H**). All the neurons are analyzed at DIV 7. Neurons are stained for axonal markers Tau1 (Panels **A** and **B**) or AnkG (Panels **C** and **D**). Cdk5rap2 (blue staining in Panel **D**) is used to visualize centrosomes. Arrow heads indicate the multiple axons, empty arrow heads indicate the centrosomes. Quantification of the axon number is in panels **E, F, G** and **H**. Scalebar: 10 μm. The error bars represent the 95% confidence intervals. We analyzed at least three independent experiments.

a structural protein present in the axon initial segment. The axon initial segment is the specialized site for action potential initiation. Only axons with an initial segment are functional, therefore AnkG serves as a functional marker to complement the structural marker Tau1.

When we manipulated miR-128 expression at DIV 2 we could not detect any difference between control, overexpression and knockdown (Figure 3.11 A, E and G), either using vector or synthetic transfection. However, when the manipulation was done at a later time point (DIV 5), we could see that the miR-128 expressing neurons had multiple axons regardless of the overexpression method (plasmid or synthetic microRNA Figure 3.11 F and H) or the axonal marker (arrow heads in figure 3.11 B and C). The microRNA knockdown did not produce any evident difference in axon number (panel B and C). Differences in dendrite formation were also observed but have not been quantified. In miR-128 gain of function the dendrites looked shorter and less ramified; whereas in miR-128 loss of function neurons the dendritic arbor looked more mature and complex compared to control. However, under these transfection conditions Sholl analysis was not reliable because of the the high degree of overlap and difficulty in assigning dendrites to individual neurons.

To better characterize the multiple axons phenotype we asked if it could be due to the presence of multiple centrosomes. It has been shown that the centrosome is a marker for axon specification and that the centrosome is positioned at the base of the neurite destined to form the axon. If for an unknown reason the centrosome is duplicated, there would be an axon in front of each centrosome (see Section 1.2.4). As a centrosomal marker we used Cdk5rap2 in DIV 7 hippocampal neurons expressing miR-128 (Figure 3.11 D). We found that neurons presenting multiple axons (Figure 3.11 D arrow head) had only one centrosome (Figure 3.11 D empty arrow heads).

Summarizing, we discovered that expressing miR-128 at early *in vitro* stages (DIV 2) did not cause a detectable morphological phenotype. The early stages, until DIV 4, can be compared to the precursor stage of cortical development *in vivo*. It is therefore possible that the inhibitory mechanisms responsible for the lack of miR-128 processing we observe *in vivo* interfere with miR-128 activity *in vitro*. If so, these mechanisms must also act on the synthetic miR-128 mimic, which is unexpected but cannot be ruled out until more is known about the processes involved. Another possibility is that although miR-128 silenced the polarity genes Par6b and Nrp2 in the sensor assay, ectopic miR-128 does not sufficiently affect the network of polarity pathway genes to produce a phenotype. Nevertheless, manipulation of miR-128 levels at later stages (DIV 5), comparable to a committed neuron in cortical development *in vivo*, led to a multiple axons phenotype. This suggests that miR-128 most probably was not involved in the polarization process per se, but did interfere with the maintenance of the polarized state. Although the presence of a single axon is a defining feature of neurons, the molecular control of axon dominance is poorly understood.

3.3.2 Intracellular and Axonal Localization of miR-128 and pre-miR-128-2

It has been shown that miR-128 is evenly distributed between the soma and synaptosomes (Lugli et al., 2008; Pichardo-Casas et al., 2012). In gain of function experiments in neuronal culture we observed a multiple axons phenotype (Figure 3.11). Therefore we wanted to

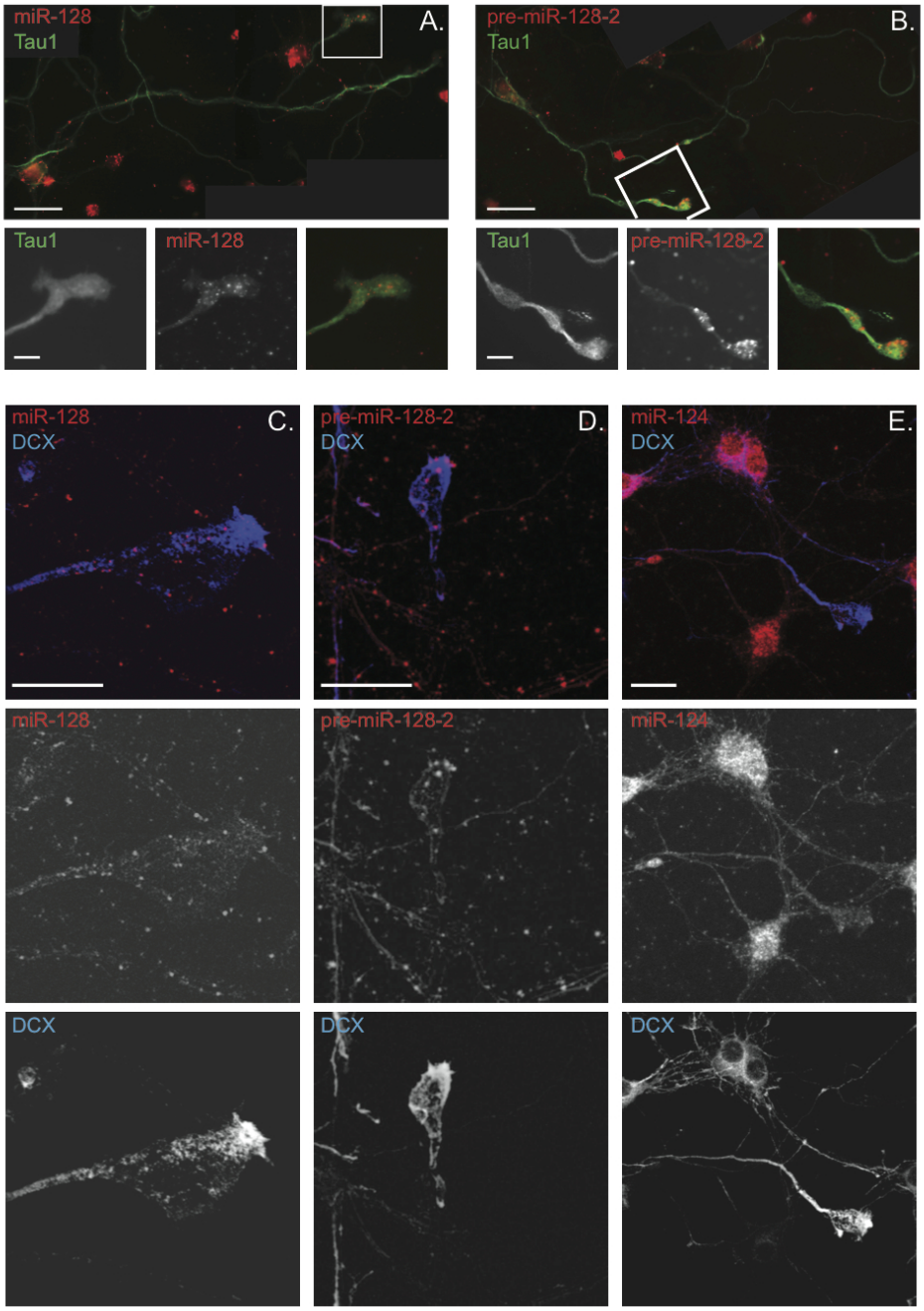

Figure 3.12: *Intracellular and axonal localization of miR-128 and pre-miR-128-2.* miR-128 (Panel **A**) and pre-miR-128-2 (Panel **B**) are present in soma, dendrites and axon as shown in the overview of DIV 7 cortical neurons. microRNA hybridization is depicted in red, Tau1 counterstaining in green, as indicated. Magnifications of Panel **A** and **B** (below the overview) show the localization of miR-128 and pre-miR128-2 in the axon and growth cone. Images from right to left show Tau1, the indicated microRNA, and a merged view of Tau1 (green) and the RNA (red). Panels **C**, **D** and **E** present a magnification of the growth cone, visualized by DCX staining, in blu in the top image and in white in the lower image. The microRNAs are presented in red in the top image and in white in the middle image, as indicated. miR-124 (Panel **E**) is used as a positive control. The scalebar is 10 μm.

see if miR-128 and pre-miR-128-2 were present in growing axons. We performed *in situ* hybridization on cultured neurons at DIV 7 using Tau1 and DCX to visualize the axon and the growth cone, respectively. For the purpose of comparison we also hybridized for miR-124. Both miR-128 (Figure 3.12 A) and pre-miR-128-2 (Figure 3.12 B), were detected in soma, dendrites and Tau1 positive axons. The microRNA and the precursor were located along the

Protein	Effect of upregulated activity	Effect of downregulated activity
Cdc42	V12: unpolarized	N17: no effect
Rac1	V12: increases length of minor neurites or unpolarized	N17: reduces length of minor processes or unpolarized
RhoA	V14: inhibits outgrowth	N19: enhances outgrowth

Table 3.1: Effect on polarizing neurons of constitutively active and dominant negative constructs for Cdc42, Rac1 and RhoA. Table modified from Arimura and Kaibuchi 2007.

entire length of the axon and also in the growth cone (Figure 3.12 A and B magnification). We used DCX to better visualize the growth cone. Doublecortin is located along the axon in an uneven manner (Figure 3.12 E) and in the growth cone is mainly at the tip (Figure 3.12 C, D, E lower picture). miR-128 was detected throughout the axon shaft and in the central domain of the growth cone (Figure 3.12 C middle picture). pre-miR-128-2 staining, in comparison, was less prominent in the axon and preferentially localized to the peripheral domain of the growth cone (Figure 3.12 D). miR-124 was evenly expressed along the length of the axon and to a lesser extent in the growth cone (Figure 3.12 E).

These observations led us to conclude that miR-128 and pre-miR-128-2 are shuttled to the axon, where miR-128 is likely to regulate axonal proteins. The presence of microRNAs in the axon is indirect evidence for local protein synthesis, a matter still highly debated (Jung et al., 2012). The results also showed that the microRNA and its precursor had a differential subcellular localization.

miR-128 and Actin Cytoskeleton Regulation

miR-128 gain of function at DIV 5 after neuronal polarization showed a multiple axons phenotype. Hence, we thought that miR-128 might be involved in the maintenance of neuronal polarity but not in the actual polarization process. We decided to test if miR-128 regulates stabilization of the actin cytoskeleton. We cotransfected in cultured hippocampal neurons, morphologically more uniform compared to cultured cortical neurons, miR-128 gain or loss of function plasmids and constitutively active or inactive proteins important for cytoskeletal remodelling. In particular we took advantage of constitutively active Cdc42 V12, Rac1 V12, RhoA V14 and dominant negative Cdc42 N17, Rac1 N17 and RhoA N19 (see Table 3.1, construct gift of Dr. Marta Rosario). We analyzed 3 independent experiments and we were unable to draw any conclusion. In fact, the effect of the constitutively active and dominant negative constructs overcame the miR-128 gain and loss of function constructs expression (data not shown). We therefore repeated the experiments using synthetic miR-128 (Ambion) and miR-128 antagomiR (Exiqon), whose effects are stronger than plasmids. In our control situation, when we expressed or knocked down the microRNA we obtained a substantial increase in neurons showing multiple axons in miR-128 gain of function and a substantial percentage of unpolarized neurons in miR-128 loss of function (Figure3.13 A). When we cotransfected the cells with Cdc42 N17, which should have no effect on neuronal polarity (Arimura and Kaibuchi 2007 review), we noticed an increase in the percentage of neurons with no axon in control transfections, a rescued axon number in miR-128 expressing neurons and an increase in multiple axons in miR-128 knockdown neurons (Figure 3.13 B). Overexpression of Cdc42

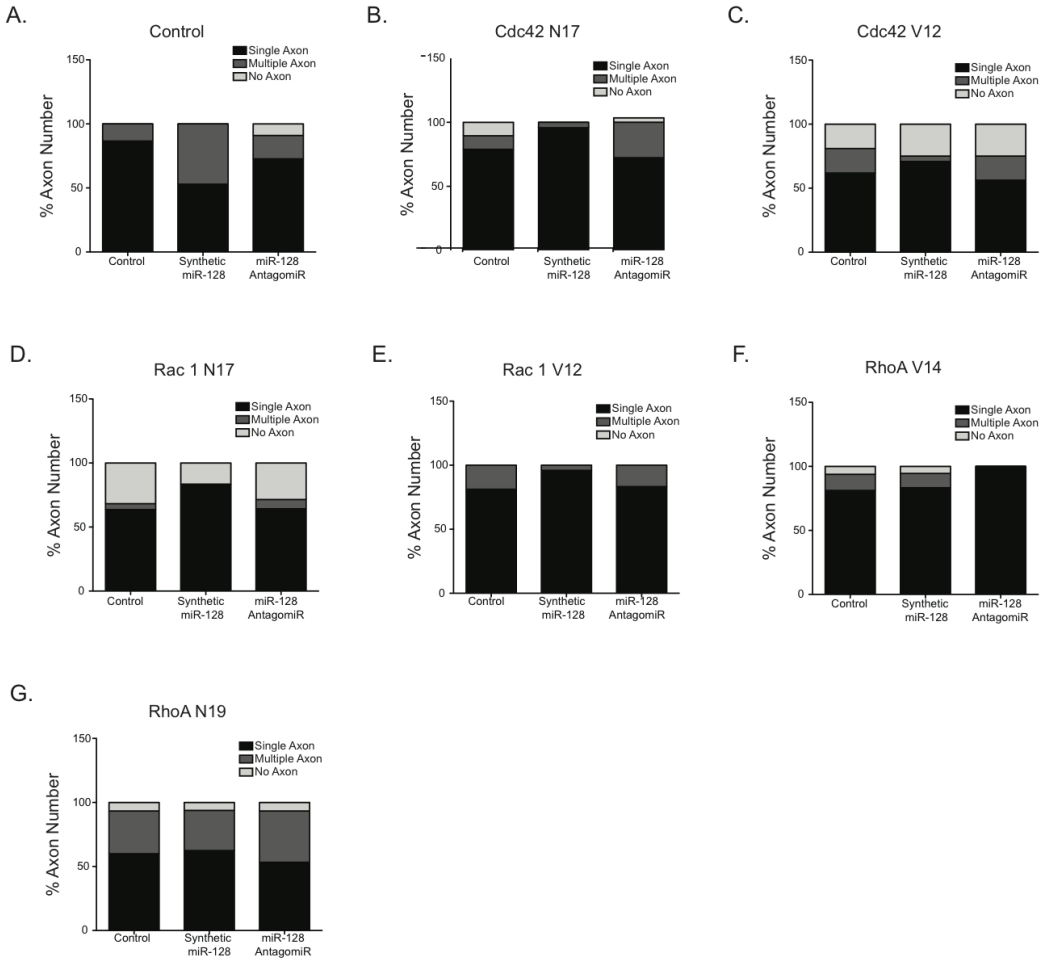

Figure 3.13: *miR-128 and actin cytoskeleton regulation.* Transfected neurons were scored for single, multiple or no axon and their relative percentage plotted for each transfection condition. The expression constructs for the mutant versions of the cytoskeleton regulators Cdc42, Rac1 and RhoA (as indicated above each Panel) encode either for constitutively active (Panels **C, E, F**) or dominant negative (Panels **B, D** and **G**) proteins. Panel **A** show gain/loss of miR-128 function in the absence of co-transfection as baseline. For gain of miR-128 function neurons were transfected with synthetic miR-128, miR-128 loss of function neurons were transfected with the miR-128 antagomiR. The experiments are performed in primary hippocampal neurons.

V12 normally leads to unpolarized neurons. We observed that this was the case in the co-transfection with control, overexpression or knockdown of miR-128. (Figure 3.13 C). In this case it seemed that the effects of miR-128 gain and loss of function have been overridden by Cdc42. Both Rac1 V12 and Rac1 N17 constructs, when overexpressed, lead to a failure of neuronal polarization. We observed this effect of Rac1 N17 on neurons cotransfected with either synthetic precursor or antagomiR (Figure 3.13 D): both conditions and the control had a substantial fraction of unpolarized neurons. Cotransfection of miR-128 gain and loss of function with Rac1 V12 led to a rescue of the multiple axons phenotype in the gain of function neurons, and to multiple axons in loss of function and control neurons (Figure 3.13 E). It has been shown that Rac1 V12 increases the length of minor neurites when transfected in polarizing neurons. We were manipulating Rac1 in already polarized neurons, so constitutively active Rac1 might be responsible for the formation of supernumerary axons. Overexpression

of constitutively active RhoA in polarizing neurons inhibits neurite outgrowth, whereas dominant negative RhoA enhances outgrowth. In our experiments we observed that cotransfection of RhoA V14 and miR-128 overexpression or control resulted in a similar pattern with only a small percentage of cells with supernumerary axons (Figure 3.13 F). In the cotransfection of miR-128 gain or loss of function and dominant negative RhoA, we observed that there was no difference between these conditions or the control. In each case the multiple axons fraction of neurons was quite consistent, but it coexisted with some unpolarized cells (Figure 3.13 G).

In summary, in these experiments all of the constructs tested with the exception of RhoA N19 suppressed the multiple axons phenotype seen in neurons expressing miR-128. It is difficult to make conclusions about the signal transduction pathways that are disturbed by overexpression of miR-128 based on these experiments. In several cases (Cdc42 and Rac1), both constitutively active and dominant negative effectors rescued the multiple axons phenotype. This is unexpected if miR-128 is directly regulating the activity of these pathways. Another difficulty is that the effects of manipulating Cdc42, Rac1 and RhoA at DIV 5, when neurons have already established an axon and are elaborating their dendritic arbor, differ from their known effects earlier in polarization. For example, dominant negative RhoA does not lead to multiple axons when transfected at DIV 2, but to an overall increase in the length of minor neurites. We therefore cannot predict with confidence how miR-128 is interacting with signal transduction pathways that are not sufficiently characterized at this stage of neuronal maturation. One possible explanation for our findings is that miR-128 regulates the expression of one or more proteins that are involved in cytoskeletal rearrangement but that are far upstream of Cdc42, Rac1 or RhoA. In this scenario the downstream effectors we choose may be to far removed from the point of action of miR-128.

miR-128 Interaction with Par6b and Gsk3β

In a microarray assay done in P19 cells the protein Par6b was strongly downregulated in response to ectopic expression of miR-128 (unpublished observation). Par6b is also a high ranking predicted target for miR-128 as determined by TargetScan. We therefore performed a sensor assay on the Par6b 3'UTR to confirm its regulation by miR-128 (Figure 3.8). As discussed in the introduction (Section 1.2.4) Par6b is part of the polarization complex, a key player in directing neuronal outgrowth. One of the functions of the polarization complex is to inactivate Gsk3β by phosporylation in the future axon. Although we do not think that miR-128 is involved in the polarization process per se (see Section 3.3.1), we decided to test if the multiple axons phenotype could nonetheless be due to direct regulation of Par6b by miR-128. In N2A cells we expressed the microRNA and we tested the Par6b, Gsk3β and phosphorylated Gsk3β protein levels using Western blot. miR-128 overexpression reduced Par6b protein levels by half (Figure 3.14 A ad C). Phosphorylated Gsk3β levels, but not Gsk3β itself, were also reduced (Figure 3.14 B and D), probably because of the reduction in Par6b. A reduction in Gsk3β phosphorylation in Stage 3 (DIV 2) is associated with impaired axon formation and not multiple axons, the effects later in polarization (DIV 5) are not known. Alternatively, we hypothesized that Par6b could regulate additional proteins besides Gsk3β at later stages. We therefore tried to rescue the multiple axons phenotype by cotransfecting Par6b cDNA

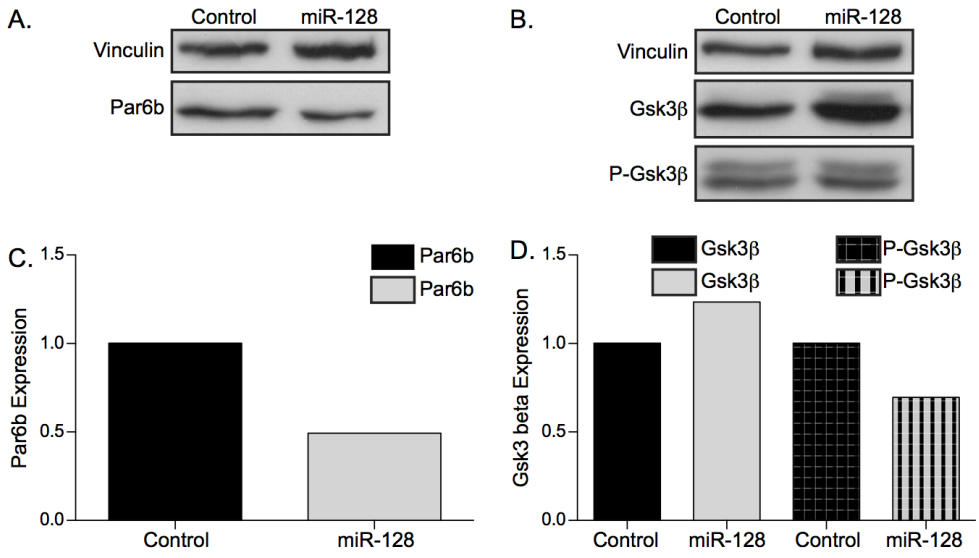

Figure 3.14: *miR-128 regulates the endogenous Par6b mRNA.* Western blot analysis showing Par6b down regulation after control or miR-128 transfection in N2A cells (Panel **A**). Protein levels of Gsk3β and phosphorylated Gsk3β after control or miR-128 transfection in N2A cells are shown in Panels **B**. Densitometric quantification of representative Western blots is shown in Panels **C** and **D**, as indicated. Protein expression is plotted relative to control transfection in arbitrary units.

together with overexpression and knockdown plasmids for miR-128. For this experiment we also compared the axon phenotype produced by both miR-128 precursor plasmids (pre-miR-128-2 and pre-miR-128-2). We observed, for the first time, that overexpression of pre-miR-128-1, like pre-miR-128-2, led to a significant increase in axon number (Figure 3.15 A and B). When Par6b was expressed in control or knockdown neurons, they had a slight increase in the axon number (Figure 3.15 A and B). Although consistent with the known regulation of Gskβ by Par6, the effect was not statistically significant when assayed at DIV 5. We noticed also that overexpression of Par6b together with pre-miR-128-1 but not with pre-miR-128-2 led to a non-significant reduction of axon number (Figure 3.15 B).

With these experiments we could show that miR-128 downregulated endogenous Par6b mRNA in N2A cells. We also showed that this regulation is not involved in the multiple axons phenotype we observed in miR-128 gain of function, because of the lack of efficient rescue.

miR-128 Interaction with Nrp2

Semaphorins and in particular Sema 3A are necessary for dendrite formation. miR-128 is predicted to target several semaphorins and their receptor Nrp2, that is mainly localizes in dendrites. We confirmed Nrp2 as a miR-128 target in a sensor assay (Figure 3.9). Downregulation of Nrp2 in neurons would reduce dendritic semaphorin signaling, thereby allowing their misspecification as axons. We tried to test this hypothesis by contransfecting an Nrp2 cDNA construct in a rescue experiment. When we cotransfected Nrp2 cDNA together with the overexpression of pre-miR-128-1 or pre-miR-128-2, we observed the usual multiple axons phenotype in miR-128 gain of function (Figure 3.16). Unfortunately, we could not rescue it

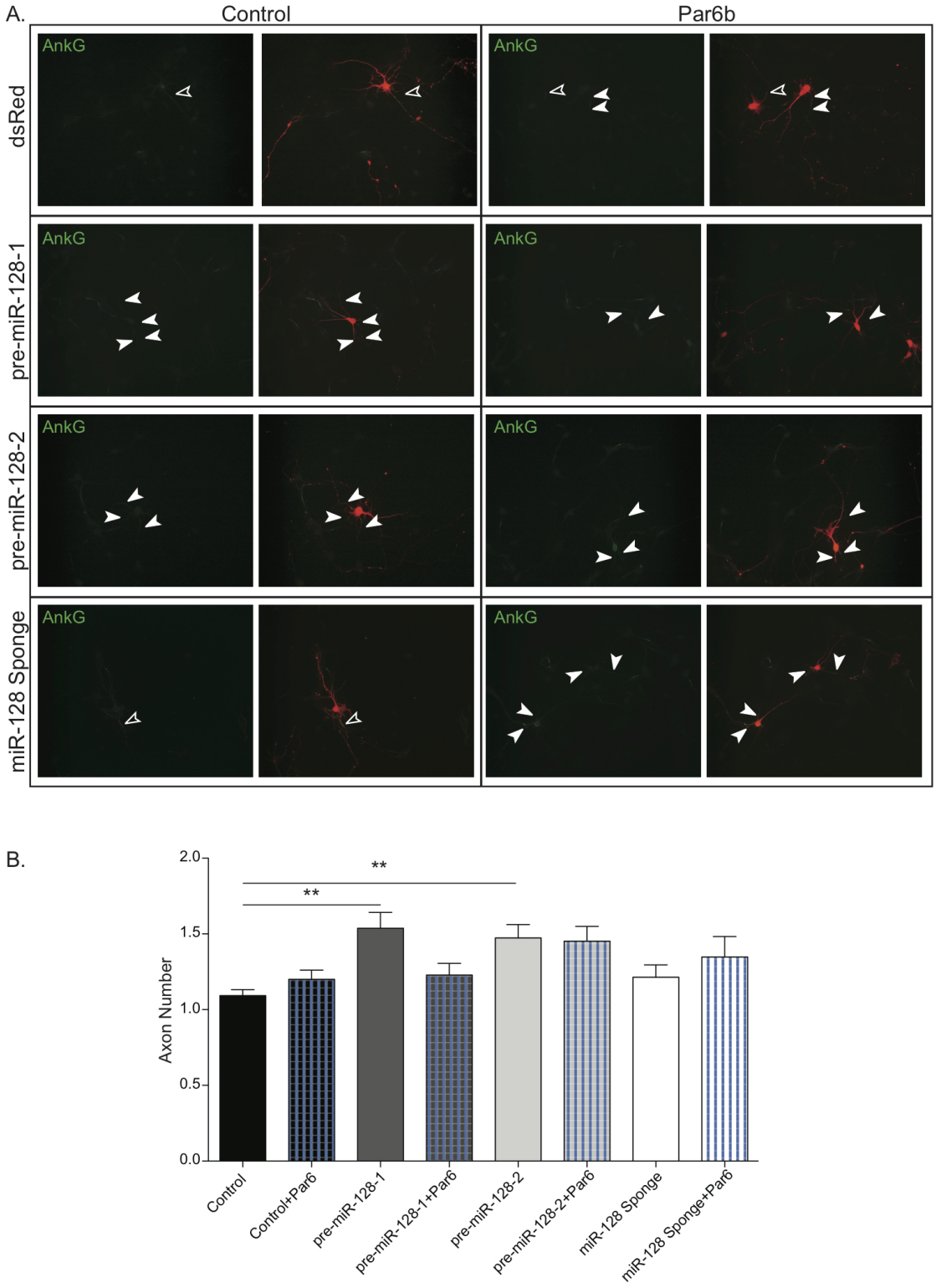

Figure 3.15: *Par6b cotransfection does not rescue the multiple axons phenotype.* The effect of Par6b co-transfection on axon number in miR-128 gain or loss of function conditions is shown. The co-transfected microRNA expression constructs used are indicated to the left, visualized by staining with anti-dsRed or anti-GFP antibody, as appropriate (red). Panel **A** shows the expression vector control (left two images) and Par6b co-transfections (right two images). Filled arrow heads indicate neurons with multiple axons, empty arrow heads indicate neurons with a single axon as identified with AnkyrinG counterstaining (AnkG, in green). Panel **B** shows the quantification of the axon number in the different conditions. The error bars represent the SEM (Standar Error of the Mean) of three independent experiments with $** \; p < 0.01$ and $*** \; p < 0.001$. The experiments are performed in primary hippocampal neurons.

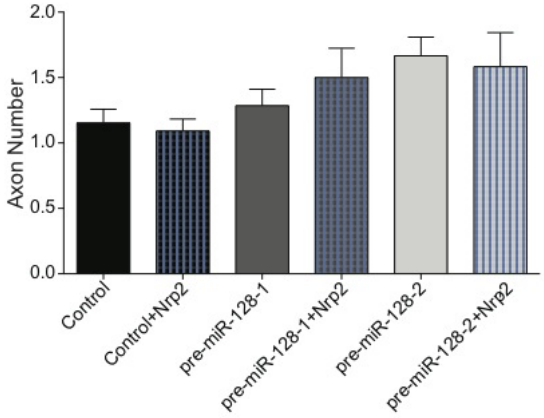

Figure 3.16: *Nrp2 contransfection does not rescue the multiple axons phenotype.* The effect of of Nrp2 coexpression on axon number in cells transfected with miR-128 gain of function constructs is quantified. The graph plots the axon number in the control transfection (vectors without inserts) or after transfection with indicated expression constructs. The error bars represent the SEM (Standar Error of the Mean)of three independent experiments. The experiments are performed in primary hippocampal neurons.

by coexpressing Nrp2 as there was not a significant decrease in axon number.

So far we could show that miR-128 gain of function in polarized neurons led to multiple axons. We tested several miR-128 targets involved either in neuronal polarization or in the maintenance of neuronal polarity, but as of now we have not identified the genes or pathways responsible for this phenotype.

3.3.3 miR-128 Gain of Function and Loss of Function *in vivo*

The spatial and temporal pattern we described for the onset of miR-128 expression coincides with the period of neuronal migration and cortical lamination during embryonic development. We wondered if miR-128 is important for neuronal migration during cortical development and whether the high level of expression in postmitotic neurons in the cortex implies a role in neuronal morphology. To address these questions we used the *in utero* electroporation technique (Section 2.2.15), expressing and knocking down the microRNA at different time points. We decided to target the population of progenitors for deeper layer neurons by electroporation at E12.5 and the population of progenitors for upper layer neurons at E14.5 and E15.5. To asses if miR-128 has a role in migration we analyzed the brains at E18.5 and P7 and to asses the roles in mature neurons we analyzed the brains at P15 and P21.

miR-128 Gain of Function Impairs Neuronal Migration

In the initial experiments to test if miR-128 has a role in migration we electroporated pre-miR-128-2 and the miR-128 sponge expression constructs at E12.5 and E14.5 and then analyzed right before birth at E18.5. At this stage the neurons are still migrating, so to minimize variability between control and test conditions we electroporated our overexpression or knockdown constructs in the same brain as the control. The electroporation was either sequential, with an interval of 10 minutes between the injection of the construct of interest and the control in the same hemisphere, or the injections were performed in contralateral hemispheres. Srini-

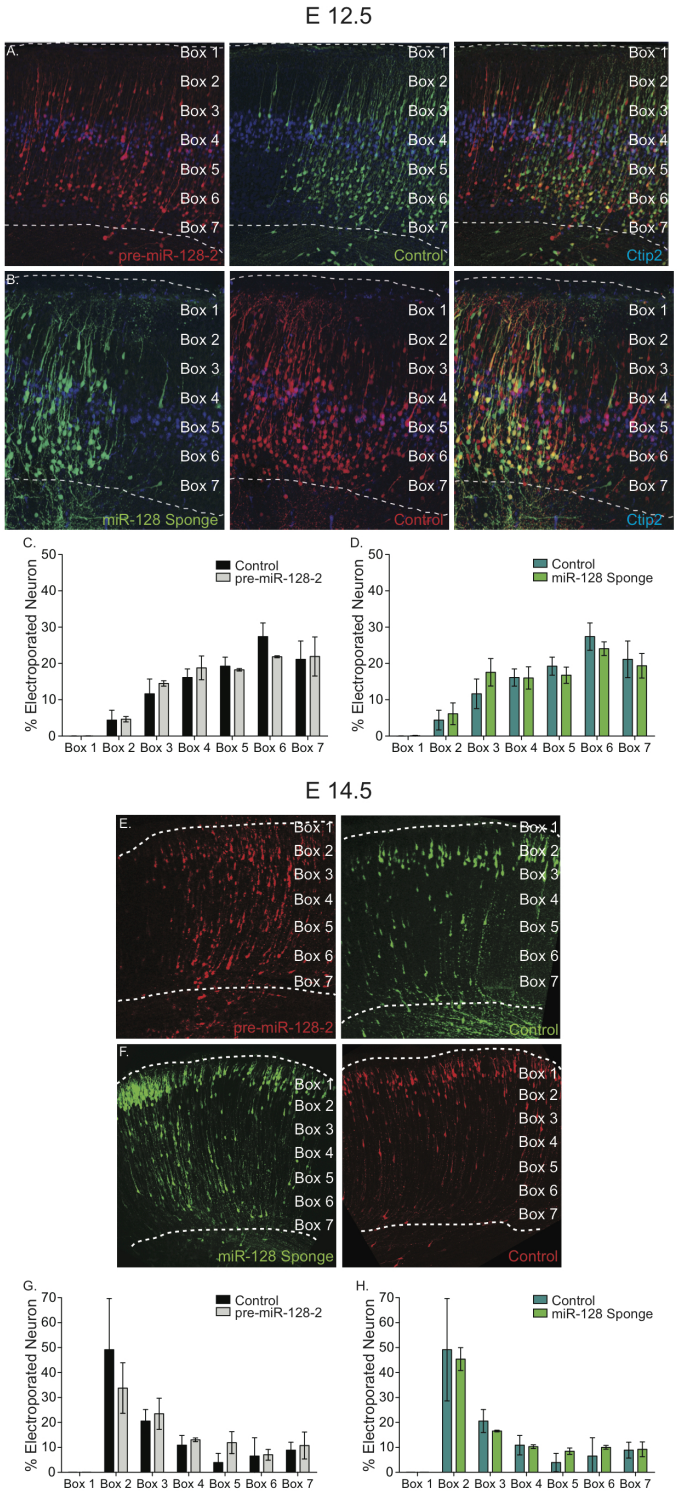

Figure 3.17: *miR-128 misexpression in migrating neurons.* miR-128 expression is manipulated in IUE experiments targeting the progenitor pool either for deeper layer (Panels **A, B, C** and **D**) or upper layer neurons (Panels **E, F, G** and **H**). The analysis is performed before birth at E18.5. In the experiments targeting the progenitor pool for deeper layer neurons miR-128 gain of function construct (Panel **A**) and miR-128 loss of function construct (Panel **B**) are electroporated in the same hemisphere as their respective control plasmids. In the experiments targeting the progenitor pool for upper layer neurons miR-128 gain of function construct (Panel **E**) and miR-128 loss of function construct (Panel **F**) are electroporated in the controlateral hemisphere compared to their respective control plasmids. Neuronal migration is quantified (Panels **C, D, G** and H) by dividing the electroporated region in boxes and counting the neurons in each box. Quantification is expressed for each box as a percent of total electroporated neurons. See Section 2.2.15. The electroporations for this cohort of experiments were perform by Srinivas Parthasarathy. The error bars represent the SD of at least three independent brains.

vas Parthasarathy performed all the electroporations in this cohort of experiments. To test migration we counted the neurons within the cortical plate, dividing it into 7 boxes. Box 1 corresponded to the marginal zone and Box 7 to the border of the cortical plate and the white matter. In the sequential electroporation we did not count double positive neurons.

Electroporation at E12.5 targets primarily neurons destined for layer VI (Section 1.2 and Figure 3.17 C and D). pre-miR-128-2 overexpression did not result in a strong and visible change in the distribution of targeted neurons (Figure 3.17 A and C), whereas knockdown neurons seemed to migrate a little further compared to control (Figure 3.17 B and D). In both cases, however, the differences were mild and overmigration seen with the sponge construct was not statistically significant.

At embryonic day 14.5 most of the targeted neurons are destined to become upper layer neurons (layer IV and II/III), as can be seen in the control curve (Figure 3.17 G and H). pre-miR-128-2 overexpression led to a stall or a delay in migration, with a shift in the position of the neurons towards the deeper layers compared to control (Figure 3.17 E and G). In the microRNA knockdown the mild migration discrepancy noticed at E12.5 was not present.

Using E18.5 as an endpoint for the migration analysis was not conclusive whether we targeted deeper layers or upper layer populations. We could, however, observe trends: neurons in which miR-128 was knockdown at E12.5 migrated a little further compared to control; and neurons in which miR-128 was overexpressed at E14.5 were delayed or stalled in deeper layers. In addition, we were not able to conclude if miR-128 overexpression was slowing down the migration process or bringing it to a premature stop. As mentioned, at E18.5 migration is not complete and the neurons are still reaching their final position.

We therefore decided to repeat the electroporations in which we targeted upper layer neurons, but one day later, at embryonic day 15.5. In this way we were sure of targeting only layer II/III populations. We then analyzed the brains when the migration process was completed (P7). We included also pre-miR-128-1 overexpression construct in this cohort of experiments, to check if the two microRNA precursors show the same behavior. In these experiments pre-miR-128-2 overexpression resulted in a strong phenotype (Figure 3.18 A and B). Targeted neurons were found scattered throughout all the six cortical layers and most of them did not reach the border with the marginal zone (Figure 3.18 A). Surprisingly, pre-miR-128-1 expressing neurons did not show a migration impairment, the brains were almost indistinguishable to the control ones. We also checked miR-128 knockdown and we noticed that the neurons were distributed more in the upper part of the cortex compared to control (Figure 3.18 C and D). Unfortunately, as previously at E12.5, this is only a trend and did not rise to the level of significance. It would be interesting to repeat the knockdown experiment at E12.5 but analyze the brains at P7 when the migration is completed to see if the overmigration phenotype would then be significant. As our next step we checked the fate of the ectopic neurons: do they have the identity of layer II/III or deeper layer neurons? We stained brains electroporated with either dsRed control or pre-miR-128-2 expression constructs for Cux1, an upper layer marker, and Ctip2, a layer V marker. We chose P0 for this analysis because at P7 the expression of layer markers is weaker and it is therefore more difficult to determine the cell fate. Both pre-miR-128-2 and control neurons were positive for Cux1 (Figure 3.18 E and

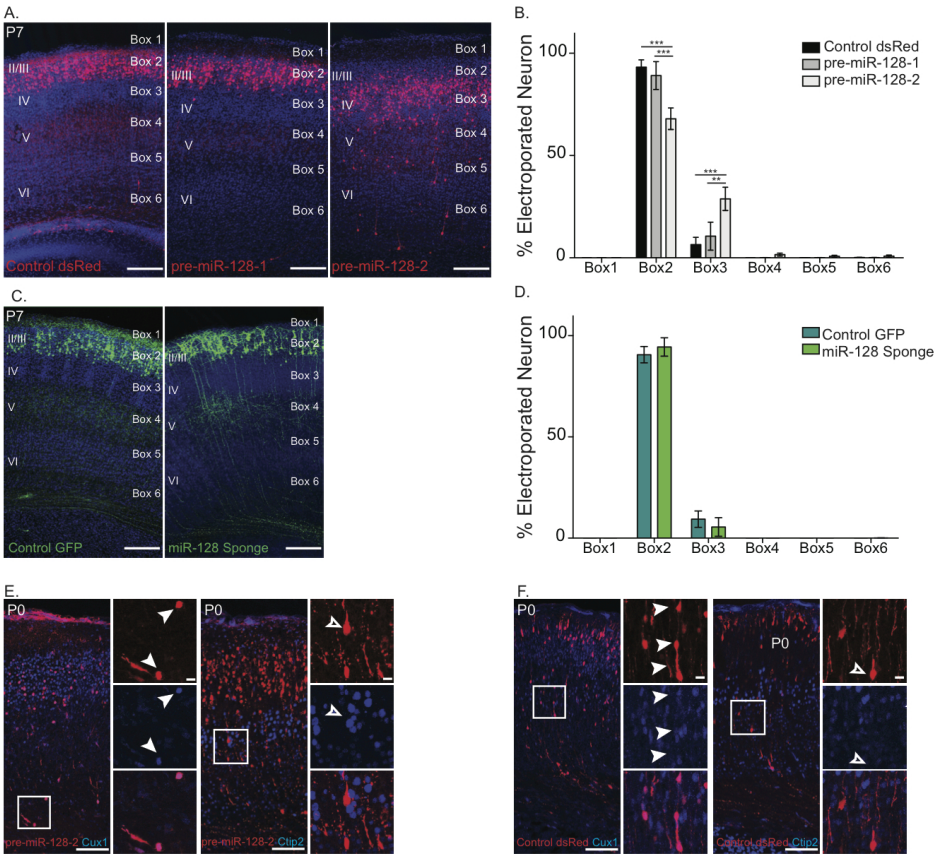

Figure 3.18: *miR-128 impairs neuronal migration.* miR-128 expression is manipulated in IUE experiments targeting the progenitor pool for upper layer neurons. The brains were analyzed at P7, when the migration is completed. Representative images of brains electroporated with miR-128 gain of function, or miR-128 loss of function constructs and their respective controls are shown in Panels **A** and **C**, as indicated. Neuronal migration is quantified by dividing the electroporated region in 6 boxes and counting the neurons in each of them. Quantification is expressed for each box as a percent of total electroporated neurons (Panels **B** and **D**). pre-miR-128-2 (Panel **E**) or dsRed (Panel **F**) P0 electroporated brains were stained with Cux1 (upper layer marker shown in blue) and Ctip2 (deeper layer marker shown in blue). For each costaining on the left there is the overview of a cortical section and on the right there is a magnification of a region of interest delineated by the white box in the overview. The magnified images are from top to bottom: electoporated neurons (red), antibody staining (blue) and the merged image. Arrow heads indicate that the layer marker is expressed in electroporated neurons and the empty arrow heads indicate that the layer marker is not expressed in electroporated neurons.The error bars represent the SD of at least three independent brains with $** \ p < 0.01$ and $*** \ p < 0.001$.

F arrow head), and negative for Ctip2 (Figure 3.18 E and F empty arrow head), regardless of their respective positions: whether they had reached their final place in the cortex or were still migrating.

We demonstrated that premature expression of pre-miR-128-2, but not pre-miR-128-1, in neuronal progenitors destined for layers II to III reduced their migration. This most likely is due to impairment and not simply a delay in migration, because the process is for the most part complete by P2. Furthermore, despite being scattered throughout the cortex the ectopic neurons had the appropriate layer II/III fate, as determined by their expression of layer-specific markers.

To better characterize the impairment in migration, we analyzed the effect of pre-miR128-2 on neuronal morphology at P0, when the neurons are predominantly in the cortical plate but have not reached their final position. Migrating neurons change morphology quickly, so

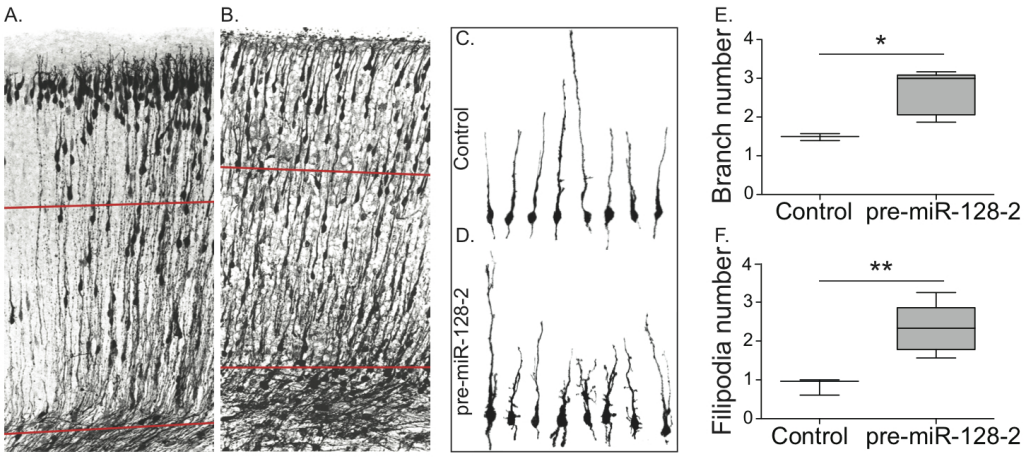

Figure 3.19: *miR-128 promotes premature branching of migrating neurons.* miR-128 expression is manipulated in IUE experiments targeting the progenitor pool for upper layer neurons. The brains were analyzed at P0, when some upper layer neurons are still migrating. Representative images of brain electroporated with dsRed control or pre-miR-128-2 constructs are shown in Panel **A** and **B**, respectively. Migrating upper layer neurons, localized in deeper layers (between the red lines in Panel **A** and **B**) were reconstructed. Panel **C** shows a sample of reconstructed neurons for dsRed control and Panel **D** shows a sample of reconstructed neurons for pre-miR-128-2. The number of branches (Panel **E**) and filopodia (Panel **F**) sprouting from the soma and the apical dendrite were counted (see Section 2.2.15). The error bars represent the maximum and minimum number of filopodia or branches observed with $* \; p < 0.05$ and $** \; p < 0.01$. At least three independent brains per condition, coming from the same litter were analyzed.

to avoid differences due to small variations in mating, electroporation or sacrifice time, we analyzed control and microRNA overexpression in the same litter. In controls the majority of the neurons were already at their correct place in layer II/III with long, radially oriented leading processes (Figure 3.19 A). In contrast, neurons expressing pre-miR-128-2 were still scattered throughout the cortical plate and the leading processes looked shorter and were not parallel to each other (Figure 3.19 B). To quantify this result, we reconstructed neurons located in deeper layers (in between the red lines in Figure 3.19 A and B), indicating that they were still in the process of active migration. The control neurons had a long and straight leading process, with occasional short filipodia (length inferior to 5 micrometers, Figure 3.19 C). pre-miR-128-2 expressing neurons, on the other hand, were consistently more branched and also had more filipodia (Figure 3.19 D, E and F). We used a length of 5 micrometers as a cutoff for distinguishing between branches and filipodia (see Section 2.2.15). With these experiments we confirmed that the migration defect was apparent during neuronal migration, before neurons reach their final position and that the defect is most likely related to abnormal morphology of the leading process.

Phf6 Rescues miR-128 Migration Impairment

To determine the molecular pathways responsible for the migration phenotype we tested two candidate genes known to be targeted by miR-128 with known functions in cortical lamination: the semaphorin receptor Nrp2 and Phf6 (Figure 3.9). We asked if co-electroporation of expression constructs for either protein could rescue the impairment seen upon premature expression of pre-miR-128-2. We again targeted progenitors for upper layer neurons by electroporation at E15.5, injecting either pre-miR-128-2 and GFP control or Nrp2 or Phf6 expression con-

structs (Figure 4). To our disappointment, cortical migration of cells co-expressing Nrp2 and

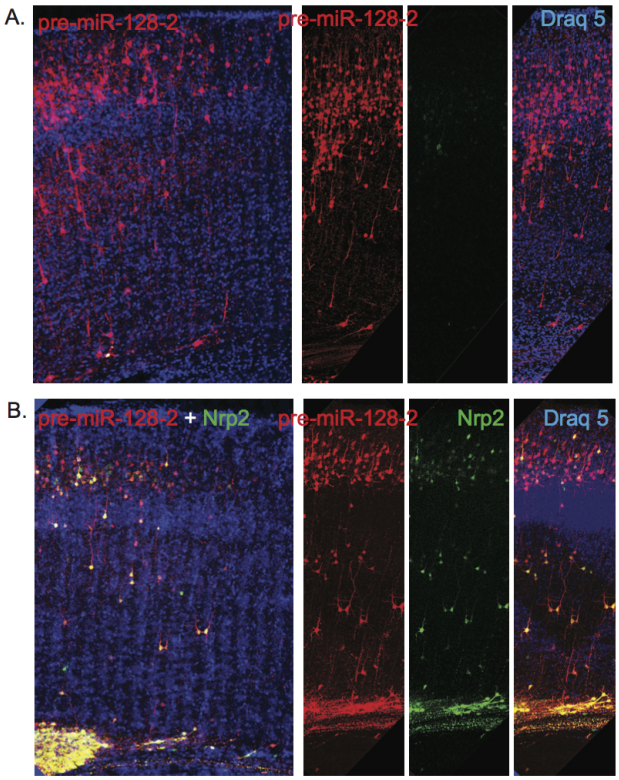

Figure 3.20: *Nrp2 does not rescue neuronal migration.* Coexpression of Nrp2 and pre-miR-128-2 in IUE (Panel **B**) does not rescue the migration impairment due to miR-128 expression in progenitors for upper layer neurons (Panel **A**). The neurons electroporated with pre-miR-128-2 are depicted in red, the neurons electroporated with Nrp2 expression construct are depicted in green, nuclear staining was achieved with Draq5 in blue. The exemplary images in Panel **A** and **B** were taken from littermates, therefore to recognize between the 2 conditions no GFP construct was injected pre-miR-128-2 brains.

pre-miR-128-2 did not differ substantially from cells expressing pre-miR-128-2 alone (Figure 3.20 B), and these brains were not analyzed further.

Phf6 is a nuclear/nucleolar protein recently shown to be important for migration (Section 1.2.6). We tried to rescue the migration phenotype by coelectroporation of pre-miR-128-2 and Phf6 cDNA (Figure 3.21 A and B). Compared to expression of pre-miR-128-2 alone, coexpression of Phf6 enabled the majority of the labeled neurons to reach their correct position in the cortex despite the presence of a few ectopic neurons. In particular, the neurons were able to reach the border between layer II and the marginal zone, something that was infrequent in the absence of Phf6 coexpression (Figure 3.21 A). Quantification of neuronal position at P7 showed that significantly more Phf6/miR-128 double-positive neurons reached the upper layer than those expressing miR-128 alone. We wanted then to be sure that miR-128 can down-regulate endogenous Phf6 and to compare their respective expression patterns in the brain and in neuronal cultures. To check if miR-128 is able to down-regulate endogenous Phf6 we expressed synthetic miR-128 in HEK 293T cells and analyzed the endogenous protein by Westen blot. HEK 293T cells were a good model in this case because they express Phf6 but not miR-128. In the presence of transfected miR-128 we detected a reduction in Phf6 protein of approximately half compared to cells transfected with a scrambled negative control (Figure

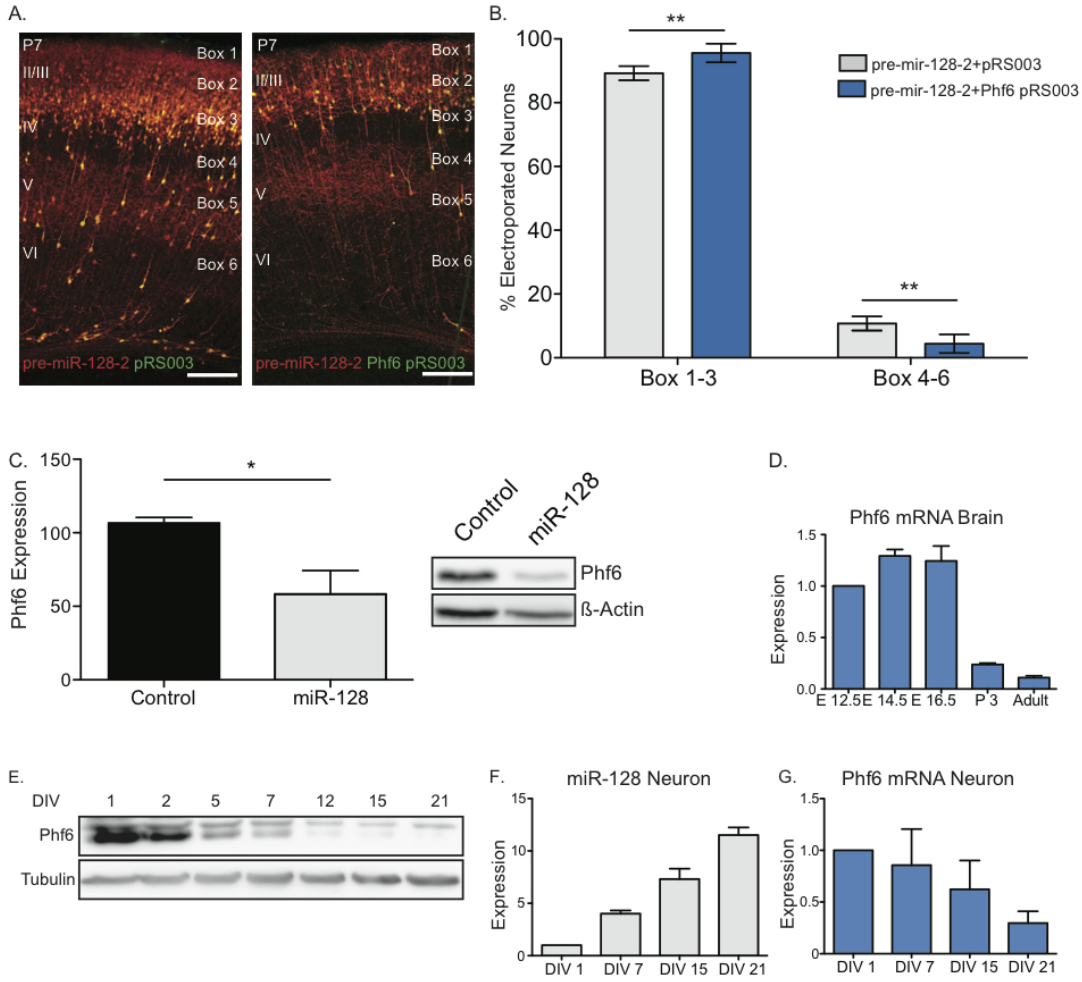

Figure 3.21: *Phf6 rescues miR-128 migration impairment.* Coexpression of Phf6 and pre-miR-128-2 (Panel **A** right side), *in vivo*, rescues the migration impairment due to pre-miR-128-2 expression in progenitors for upper layer neurons (Panel **A** left side). Migration rescue is quantified by dividing the electroporated area in boxes and counting the neurons in each of them. Boxes representing the upper layer (1-3) and the deeper layers (4-6) were grouped. Quantification is expressed as a percent of total electroporated neurons (Panels **B**). Panel **C** shows the regulation of endogenous Phf6 by expression of miR-128 in HEK 293T cells, on the right of Panel **C** there is a representative blot, on the left there is the quantification of Phf6 protein levels from 3 independent experiments. Panel **D** shows the quantification of Phf6 transcript in embryonic, early postnatal and adult mouse brains using qRT-PCR. Panels **E** and **G** show the protein levels and the quantified transcript on Phf6 in primary cortical neurons, respectively. Panel **F** shows the expression of mature miR-128 in primary cortical neurons, measured by TaqMan PCR. The error bars represent standard deviation of at least three independent experiments with $* \; p < 0.05$, $** \; p < 0.01$ and $*** \; p < 0.001$. The quantification of miR-128 in primary cortical neurons was performed by Frederick Rehfeld.

3.21 C). This result confirms the sensor assay using the Phf6 3'UTR (Figure 3.9) and extends it to show regulation of the endogenous mRNA by miR-128. As a next step we wanted to know if there are developmental stages in which expression of miR-128 and Phf6 overlap. We tested Phf6 mRNA levels by qRT-PCR using the same mRNA samples we hybridized in miR-128 Northern blots (Figure 3.1 and Figure 3.21 D). In the developmental series miR-128 increased and Phf6 mRNA decreased in an inverse manner. This pattern is consistent with regulation of Phf6 by miR-128 during brain development. Additional evidence for physiological relevance of the regulation was obtained by testing cultured neurons. We observed that Phf6 protein (Figure 3.21 E) and mRNA (Figure 3.21 G) levels smoothly decreased between DIV 1 and

DIV 21, with miR-128 again showing an inverse expression pattern (Figure 3.21 F, miR-128 TaqMan PCR performed by Frederick Rehfeld).

To summarize, we found that premature expression of pre-miR-128-2 by electroporation at E15.5 impaired the migration of upper layer neurons to their proper position in the cortex. miR-128 positive neurons were found inappropriately scattered throughout the whole cortical plate and also at eterotopic position in the white matter. We could rescue the phenotype (at least partially) by coexpressing Phf6 together with pre-miR-128-2. We cannot exclude that there are other genes regulated by miR-128 and involved in migration. However, these results illustrate the importance of correct temporal control of miR-128 expression to avoid interference with Phf6-mediated neuronal migration.

3.3.4 miR-128 Regulates Dendritic Arborization and Spines Density

Having studied the role of miR-128 during embryonic development, we wondered what the functions of miR-128 are in the postnatal and adult brain, in which high level miR-128 expression is maintained (introduction and Figure 3.1). Using *in utero* electroporation to target upper layer principal neurons, we looked at the effects of premature miR-128 expression and miR-128 knockdown on neuronal and dendritic spine morphology 21 days after birth. For these experiments we compared both miR-128 precursors and the miR-128 sponge knockdown construct, using either dsRed (pre-miR-128-1 and pre-miR-128-2) and GFP (miR-128 sponge) controls, as appropriate. After staining, we imaged layer II/III neurons, reconstructed the resulting Z-stack and ran Sholl analysis to quantify dendritic arbor complexity (Section 2.2.15).

Sholl analysis of miR-128 knockdown neurons revealed a slight increase in complexity compared to GFP electroporated neurons (Figure 3.22), but the difference was only a trend and not statistically significant (at least 10 neurons from at least three different brains). In contrast, expression of pre-miR-128-2 once again showed the strongest phenotype (Figure 3.23 C and D). Sholl analysis revealed a significant reduction in dendritic arbor complexity compared to both control (Figure 3.23 A) and pre-miR-128-1 (Figure 3.23 B). The reduced complexity, however, did not seem to affect the apical dendrite length (Figure 3.23 D).

Encouraged by these results we also performed electrophysiological recordings on neurons expressing pre-miR-128-2 15 days after birth, in collaboration with Sam Booker and Imre Vida (Charité, Berlin). The electrophysiological results will not be discussed in this thesis but the recorded neurons were filled with biocytin for the purpose of imaging and reconstruction. The recordings were performed in all cortical layers and in neighboring, non-electroporated neurons as controls. This allowed us to visualize the effect of premature miR-128 expression during development on the morphology of mature neurons not only in layer II/III but also in deeper layers. We could confirm the smaller dendritic arborization of pre-miR-128-2 electroporated neurons in layer II/III; and the layer II/III morphology of ectopic neurons in layer V and VI (Figure 3.24) after reconstruction and visual analysis.

With the morphological analysis of electroporated neurons at P21 and P15 we showed that miR-128 (in its pre-miR-128-2 form) was able to regulate genes important for correct dendritic arbor formation. One caveat of these experiments is that we were unable to show a

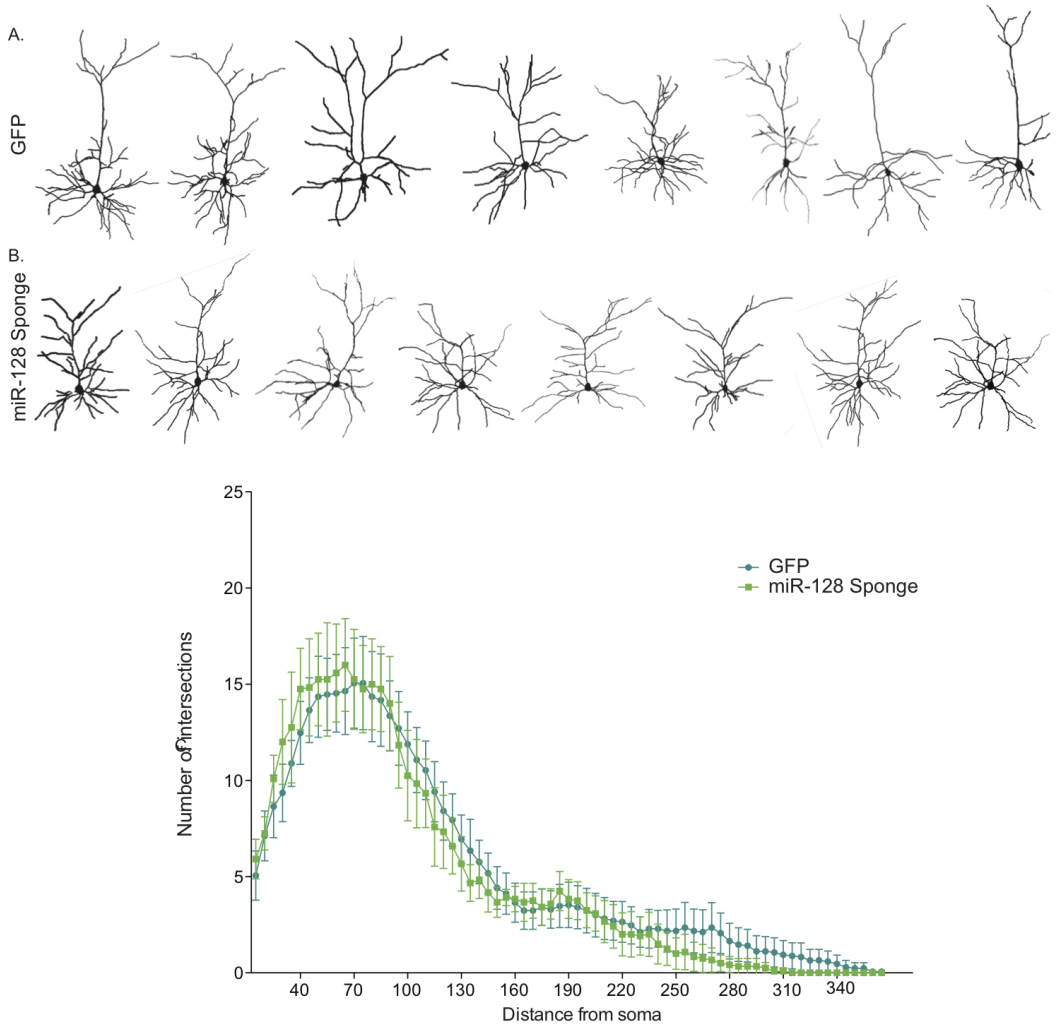

Figure 3.22: *Dendritic arborization in miR-128 knockdown neurons.* upper layer neurons electroporated either with GFP or miR-128 knockdown constructs were reconstructed (Panel **A** and **B**, respectively). Panel **C** shows Sholl analysis run on the reconstructed neurons of P21 animals. The X-axis represent the distance of the branches from the soma in μm and the Y-axis represents the number of intersection at a given distance from the soma. The error bars represent standard deviation of at least 10 neurons coming from 3 independent brains.

significant difference in the arborization of miR-128 knockdown neurons compared to control, although they appeared to be slightly more complex by visual inspection. At the moment, it is unclear if this reflects a temporal window for premature miR-128 expression that is unaltered by knockdown, the difficulty of achieving sufficient knockdown of a highly expressed miRNA like miR-128, or an upper limit on dendritic ramification imposed by the *in vivo* environment.

In parallel to the Sholl analysis we also checked for an influence of manipulating miR-128 on dendritic spines. In this case we analyzed littermates electroporated with either pre-miR-128-2 dsRed or, with GFP. This comparison is not the ideal, at least for morphological analysis. Although the two fluorophores are both cytoplasmatic, the results might be influenced by differing intracellular distributions or detection sensitivity. We measured in Z-stacks spine length, neck length, head width and spine density (spine number/ 100 micrometer) (Section 2.2.15). Neurons electroporated with pre-miR-128-2 showed a significant increase in total spine length as well as in neck length and in head width (Figure 3.25 C, D, E). The strongest effect was on spine density, which was drastically reduced (compare Figure 3.25 A and B and

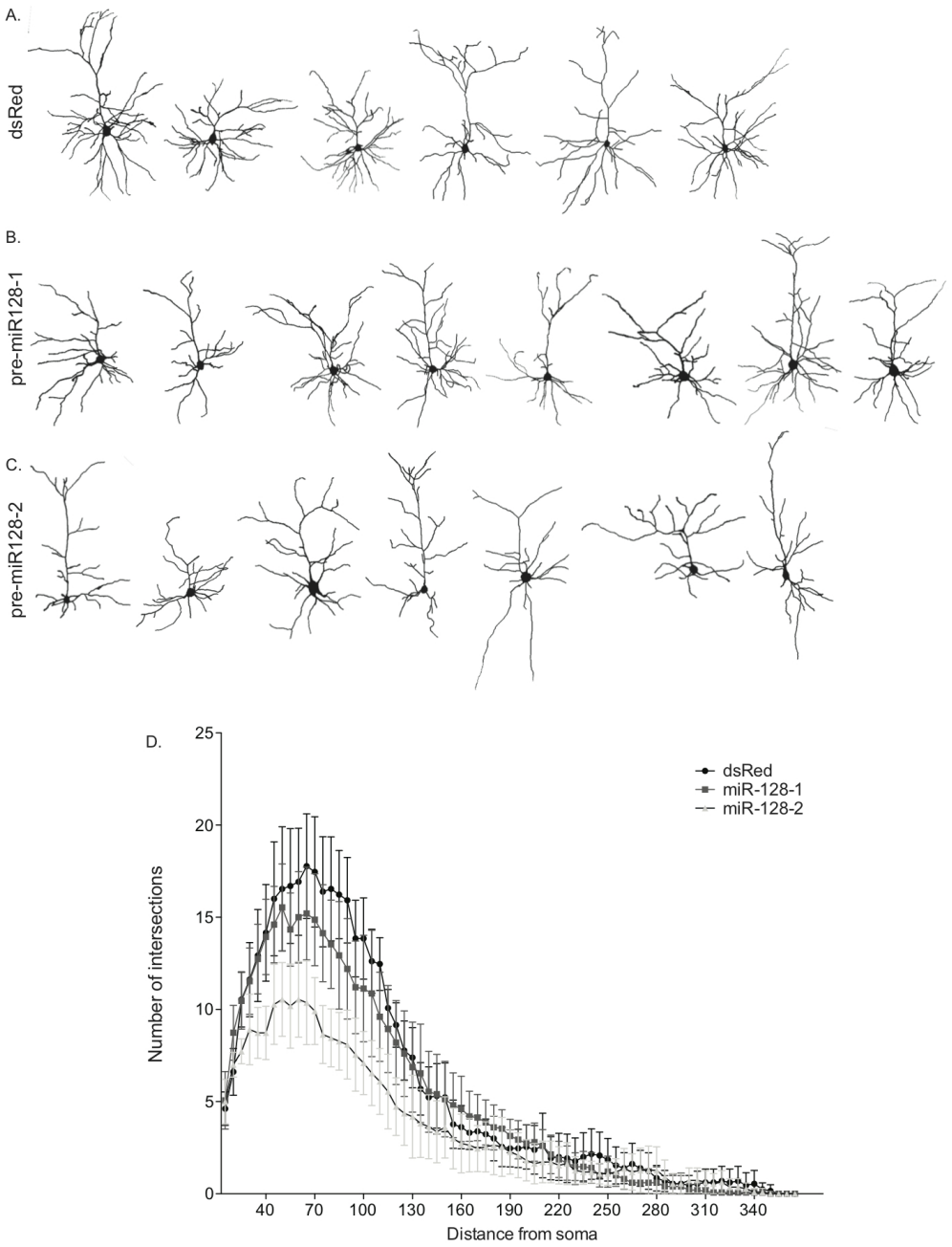

Figure 3.23: *miR-128 expression reduces dentritic arbor complexity.* upper layer neurons electroporated either with dsRed, pre-miR-128-1 or pre-miR-128-2 expression constructs were reconstructed (Panels **A, B** and **C**, respectively). Panel **D** shows the Sholl analysis run on the reconstructed neurons of P21 animals.The X-axis represent the distance of the branches from the soma in μm and the Y-axis represents the number of intersection at a given distance from the soma. The error bars represent the 95% confidence intervals of at least 10 neurons coming from 3 independent brains.

F). We believe that spine counts should be insensitive to the fluorophore used, and also note that an inverse effect on spine density has been reported in mice deficient for pre-miR-128-2 (see introduction). As candidate target genes for mediating the effect of miR-128 on spine morphology we identified (in addition to Phf6) Gria3 and Stargazin (Figure 3.10). Gria3 is one of the four subunits of the AMPA receptor (AMPAR) and Stargazin is the most influential of the Tarp proteins that are required for AMPAR membrane trafficking. A reduction of the spine number could be due to a reduction in the shuttling of the AMPAR to the synapse.

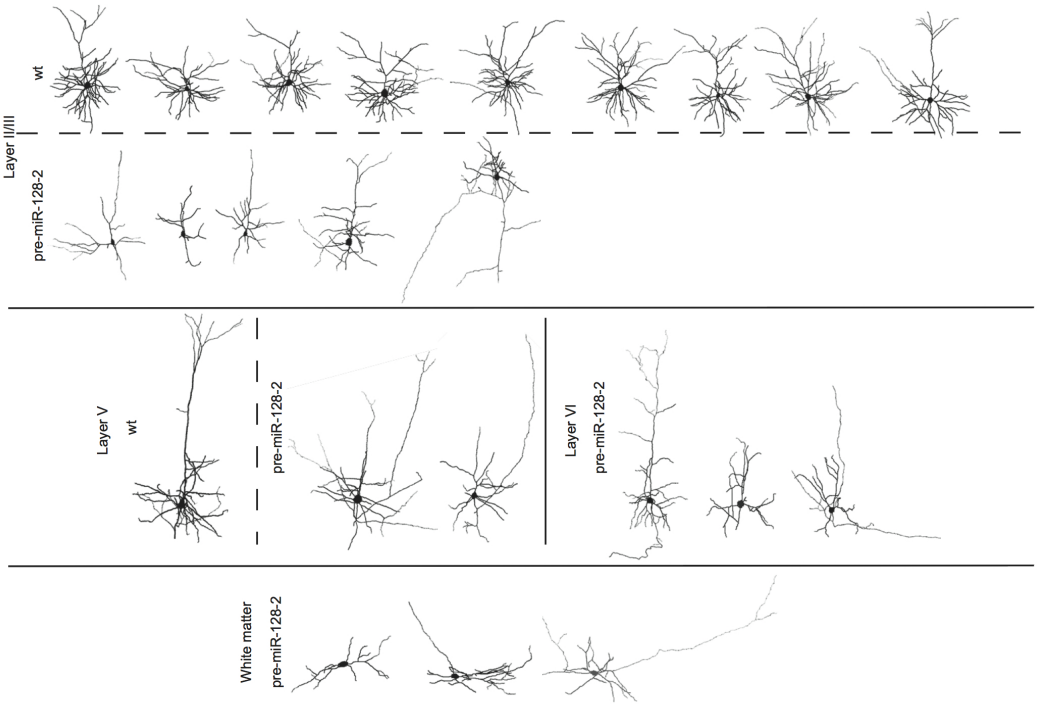

Figure 3.24: *miR-128 expression reduces dentritic arbor complexity 2.* Ectopic neurons expressing miR-128 were analyzed in electrophysiology experiments at P15 and filled with biocytin to allow subsequent visualization. The ectopic neurons analyzed were positioned in all cortical layers (II/III, V, VI) and in the white matter. Wild type neurons neighboring the electroporated ones were also analyzed and filled with biocytin. All the wild type and condition neurons were reconstructed and a sample is represent in the figure. The neurons are divided according to the cortical layer in which they are positioned and to their phenotype.

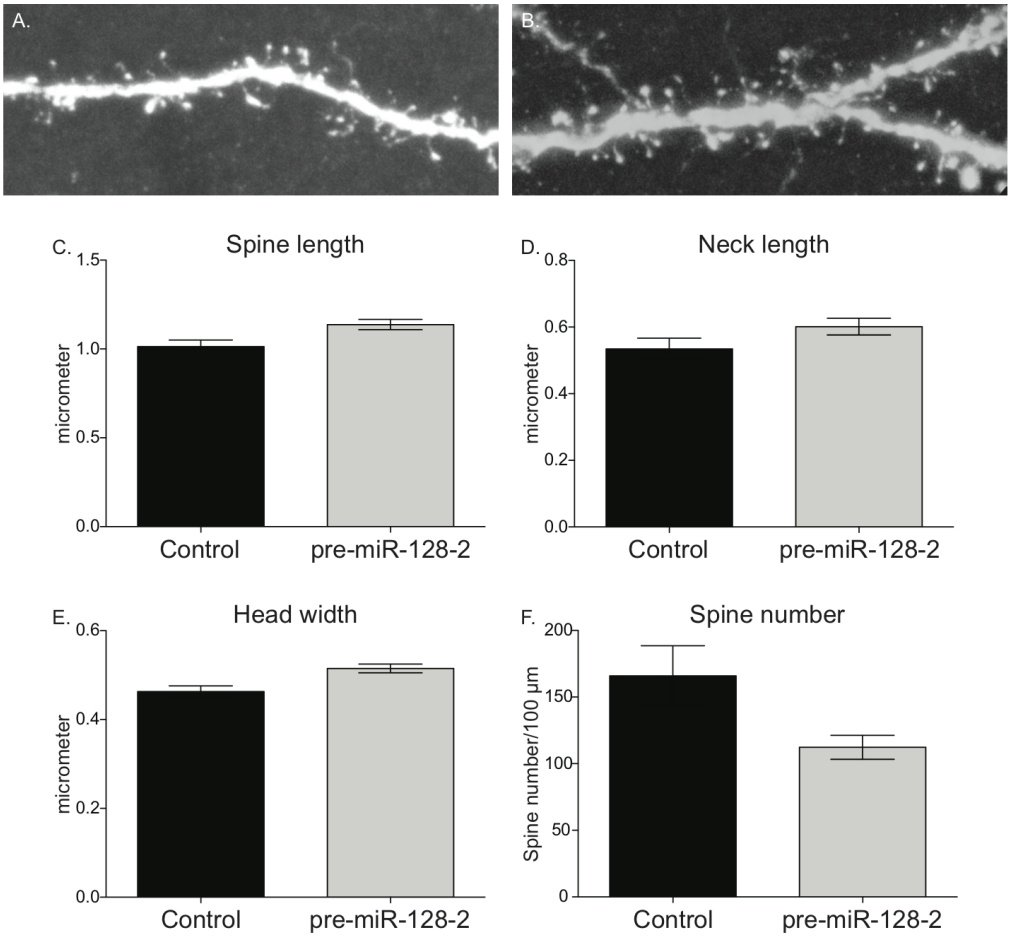

Figure 3.25: *miR-128 expressionreduces spine number.* Dendritic spines of P21 animals, electroporated with GFP (Panel **A**) or pre-miR-128-2 (Panel **B**), were analyzed. Panel **A** and **B** show a representative Z-projection of the z-stack images analyzed. Total spine length (Panel **C**), Neck length (Panel **D**), Head width (Panel **E**) and Number of spines in 100 μm were measured in z-stacks. The error bars represent the standard deviation of the at least 10 apical dendrites coming from 3 independent animals.

Chapter 4

Discussion

4.1 miR-128 and Axon Number

We manipulated miR-128 concentration in primary cortical and hippocampal culture because we thought it was a straightforward way to find the pathways in which miR-128 is involved. In the end, we were able to describe a new function for miR-128 in the control of axon and/or dendrite identity, but have not yet identified the pathway responsible.

We showed that miR-128 gain of function in polarized neurons (DIV 5) leads to multiple axons (Figure 3.11). The phenotype was dependent on the transfection day, not on the chosen gain of function methods. We used a plasmid based assay and a synthetic miR-128 mimic assay. The plasmids we used, pre-miR-128-1 and pre-miR-128-2, contain the individual precursors and flanking sequences required for nuclear microRNA processing. The synthetic mimic corresponds to the mature microRNA, that does not require cytoplasmic processing and are ready to be loaded into the miRISC complex. It surprising that miR-128 upregulation using the synthetic mimic at DIV 2 does not result in multiple axons. This might be because the RNA Binding Protein (RBP) involved in miR-128 regulation (see below) recognizes a sequence in the mature form, or because miR-128 is not regulating proteins necessary for neuronal polarization, but only for the maintenance of the polarized state.

We speculated that miR-128 could be involved in the regulation of the actin cytoskeleton, a key component in the establishment and in the maintenance of polarity. Therefore neurons were cotransfected with miR-128 gain/loss of function constructs and constitutively active or dominant negative constructs for several known factors involved in cytoskeleton remodeling (Figure 3.13). Both constitutively active and dominant negative Cdc42 and Rac1 rescued the axon number seen after miR-128 gain of function. We are still wondering about the meaning of this finding. It might be that the cytoskeleton regulators used for the rescue act independently and in parallel to the miR-128 target in the pathway and therefore mask the effect of miR-128. Another possibility is that miR-128 regulates the cytoskeleton but is upstream of the proteins we used for the rescue. Also in this circumstance the effect of miR-128 could be overcome by the constitutively active or dominant negative downstream proteins.

We also tested Par6b, part of the polarity complex and a target of miR-128 as determined by sensor assays and by knockdown of the endogenous protein by miR-128 overexpression in N2A cells. During polarization (Stage 3, Figure 1.3), knockdown of Par6b leads to a neuron

with no axons due to the inactivation of Gsk3β (reviewed in Hoogenraad and Bradke 2009). We hypothesized that after polarization is established (Stage 4, Figure 1.3), Par6b could govern additional processes necessary for axon dominance. We tried to rescue the multiple axon phenotype using a Par6b expression construct. We found that in neurons cotransfected with Par6b and either the control plasmid or the miR-128 loss of function construct, there is a slight increase in axon number. This novel effect of Par6b is compatible with continued regulation of Gsk3β phosphorylation during the axonal outgrowth phase subsequent to polarization. On the other hand, we did not observe a rescue in neurons cotransfected with Par6b and miR-128. We conclude that despite the ability of miR-128 to regulate Par6b in our heterologous assays, this interaction is unlikely to be involved in the multiple axon phenotype.

Lastly, we hypothesized that the multiple axon phenotype could be due not to the regulation of axon formation per se but to the impairment of dendritic development. It has been shown that Sema 3A governs dendritic fate (reviewed in Shelly and Poo 2011). One of the predicted targets for miR-128 is Nrp2, a receptor for semaphorin. Nrp2 is also important for neuronal migration *in vivo*. Nrp2 knockdown impairs neuronal migration in a similar way as miR-128 gain of function (Chen et al., 2008). We considered if the multiple axons phenotype *in vitro* and the migration impairment *in vivo* could be like the two faces of a single coin. We tried the rescue experiment with an Nrp2 expression construct both *in vitro* and *in vivo*. However, neither phenotype was alleviated by coexpression of Nrp2, suggesting that Nrp2 is not the predominant factor mediating the effect of miR-128 on axon number *in vitro* or migration *in vivo* (Figures 3.16 and 3.20).

As of now, we cannot explain why, when we express the miR-128 gain of function construct, we see multiple axons in neurons at DIV 5 but not at DIV 2. We tested several pathways in which miR-128 might have been involved and in all cases we could not prove that the regulatory interaction with the tested target genes is physiologically responsible for the phenotype. However, during the preparation of my thesis I developed two new hypotheses. In a recent publication it has been shown that miR-128 downregulates the HECT ubiquitin ligase Smurf2 in triple breast cancer (Liu et al., 2014a). Smurf2 is a critical determinant of polarity complex turnover in the neuronal polarization process (Schwamborn et al., 2007a). It remains to be determined if downregulation of Smurf2 mRNA could produce multiple axons in our assay. In addition, we showed that the microtubule-associated protein DCX is regulated by miR-128 in the sensor assay (Figure 3.7) and shows an inverse expression pattern to miR-128 in the RMS (Figure 3.6). DCX is required for microtubule stability during axonal outgrowth, and higher microtubule stability is a characteristic feature of axons compared to dendrites. By targeting DCX, miR-128 might play a role in the delicate balance of cytoskeletal dynamics required for maintaining proper neuronal morphology with outcomes that are difficult to predict.

4.2 miR-128 is Posttranscriptionally Regulated

microRNA posttranscriptional regulation is an emerging field in microRNA biology. Only a few studies have addressed posttranscriptional regulation of microRNAs. For example, the miR-138 precursor is expressed in several embryonic regions but the mature form is restricted to the brain (Obernosterer et al., 2006). The best-characterized posttranscriptional regulation

is for let-7, whose processing is repressed both at the primary and at the precursor level by Lin28A and Lin28B (Piskounova et al., 2011; Rybak et al., 2008; Heo et al., 2008). Here we have shown, for the first time, that miR-128 is posttranscriptionally regulated and that the regulation takes place during development and in particular regions of the adult brain.

miR-128 has two precursor forms, pre-miR-128-1 and pre-miR-128-2. We checked the temporal expression and the localization of mature and precursor forms by Northern blot analysis and *in situ* hybridization taking advantage of Locked nucleic acid (LNA) probes. LNA probes have a modified and stabilized ribose backbone, which facilitates pairing with the complementary sequence. LNA probes are a good tool to detect microRNAs, the LNA structure is highly intolerant of mismatches and allows probes to be as short as 20 nt, enabling detection of microRNAs with a high degree of confidence. For the characterization of miR-128, pre-miR-128-1 and pre-miR-128-2 we used probes able to specifically recognize each of them (Figures 2.1 and 2). We confirmed the specificity and functionality of all the probes in Northern Blot assays. We transfected HEK 293T cells with dsRed control, pre-miR-128-1 and pre-miR-128-2 expression constructs and then hybridized for each probe. Both precursor probes specifically recognized their respective precursor targets in cells transfected with their cognate expression construct. The probe for miR-128 recognized the mature form and both precursors in the lanes expressing the microRNA, but not in the dsRed transfected cells, as expected. Despite the specificity and stability of the probes we have not been able to detect the presence of pre-miR-128-1 either in Northern blot experiments or in *in situ* hybridization (Figures 3.1 and 3.4). These results are consistent with a very recent report on pre-miR-128-1 knockout mice, which show a reduction of less than 20% of the total miR-128 (Tan et al., 2013). However, the pre-miR-128-1 host gene, R3hdm1, is expressed in the adult brain (Allen Brain Atlas). Consistent with this, we showed in a sensor assay that pre-miR-128-1 repression of a miR-128 sensor construct (containing 4 perfectly complementary binding sites for miR-128) is weaker compared to the repression seen with pre-miR-128-2 (Figure 3). We think, therefore, that the regulation might happen either at the level of the primary transcript or at the early stages of processing. pre-miR-128-2, on the contrary, is expressed at high levels at embryonic stages (E12.5 Figure 3.1) or in certain brain regions, such as layer V or the Purkinje layer of the cerebellum, in which miR-128 is not detectable. Pre-miR-128-2 is hosted in an intron of the R3hdm3 gene (also known as Arpp21), and it has its own RNA Pol III promoter in human cells (Monteys et al., 2010). It has to be noted, however, that not all cell types express pre-miR-128-2 (Figure 3.2), which might be expected if the RNA pol III promoter makes an important contribution to transcription of the microRNA.

The two miR-128 precursors have only the mature sequence in common; we speculate that pre-miR-128-1 sequence might bind to RBPs that inhibit its processing and as a consequence pre-miR-128-1 might be degraded. In our group there is a line of investigation that aims to find the RNA binding proteins responsible for the processing of pre-miR-128-2 and pre-miR-128-1. It has been shown that miR-128 regulates the expression of Lin28A (Qian et al., 2012). Moreover, Lin28A is able to block pre-miR-128-2 processing in a negative feedback loop very similar to that described for let-7 (Rehfeld F. personal communication). Hence, Lin28A might be responsible for the regulation of pre-miR-128-2 processing *in vivo* at early stages

of embryogenesis. Lin28 is, in fact, an RNA binding protein expressed in pluripotent stem cells. We think that there might be several RNA binding proteins involved in the regulation of a single microRNA precursor. We showed that the expression of pre-miR-128-2 does not correlate perfectly with miR-128: for example neuronal progenitors (embryonic Figure 3.5 and adult Figure 3.6), and neurons of layer V (Figure 3.3) express the precursor but not the mature form. It seems unlikely that the same regulatory mechanism is acting in these very different stages and neuronal types. It will be of interest to further characterize the RNA binding proteins able to regulate pre-miR-128-2 processing during embryogenesis and in adult brain.

This is to our knowledge the first time that such a fine tuning of precursor processing in solely post mitotic neurons and only in specific brain regions has been shown. Other important brain microRNA such as miR-124, miR-125 or let-7 start to be active from neuronal progenitors and remain highly expressed in all neurons. Their expression pattern is more similar to the expression pattern of pre-miR-128-2 than of miR-128.

4.3 miR-128 is Postmitotically Expressed

As mentioned before miR-128 expression is restricted to postmitotic neurons in the embryonic (Figure 3.5) and adult brain (Figure 3.6). The precursor is more widely expressed and is present in the embryonic VZ, SVZ and IZ, and in the adult neurogenic niches of the RMS and dentate gyrus. Our findings do not completely agree with a previous report (Bruno et al., 2011) in which overexpression of miR-128 in P19 cells and NSCs promotes neuronal differentiation by regulating Mln51 (Casc3 or Barentz) and Upf1, two proteins required for NMD. To test the degree of neuronal differentiation in miR-128 transfected cells they used Tuj1 as an axonal marker. They measured the neurite length, finding that it was significantly increased in cells overexpressing miR-128. The discrepancy between our data and that of Bruno et al. relates to the timing of miR-128 activity. We believe it is only present in an active form in postmitotic neurons, they claim miR-128 is necessary for the progression from progenitors to postmitotic neurons. The difference is probably due to the chosen methods of analysis. We described an *in vivo* expression pattern, bruno et all manipulated miR-128 levels in an embryonic carcinoma cell line (P19) and in neuronal stem cells. Both cell types can be differentiated into neurons but they do not normally express the microRNA prior to differentiation. We do agree, however, on the fact that miR-128 is important for axonal outgrowth. So far little is known about the regulation of NMD *in vivo*, but it would be interesting to see if miR-128 is able to regulate Casc3 and Upf1 in mature neurons.

There are other studies in the cancer field that describe miR-128 as a negative regulator of proliferation. miR-128 is considered to be a tumor suppressor microRNA that represses genes involved in stem cell fate (Nanog and Lin28) or in the transduction of mitotic signals (Qian et al., 2012; Papagiannakopoulos et al., 2012). Furthermore, miR-128 expression is able to reduce the motility of carcinogenic neuroblastoma cells by downregulating DCX and Reelin (Evangelisti et al., 2009). This study is in line with our result in the sensor assay in which we showed that miR-128 is able to regulate these two 3' UTRs (Figure 3.7).

The expression of miR-128 in the cortical plate but not in the progenitor zones of the

VZ/SVZ/IZ during embryonic development and the absence of miR-128 in aNSC might imply that miR-128 is required for regulating processes fundamental for mature neurons. We showed that in the cortical plate miR-128 expression was not evenly distributed: at E16.5, for example, it was higher in the deep layer compared to the nascent upper layer (Figure 3.5 and 3.2). This pattern differed from the homogeneous expression of pre-miR-128-2 and miR-124 throughout the cortical plate. This suggests that miR-128 begins to influence gene regulation during the period in which neurons first assemble into networks.

4.4 miR-128 and Neuronal Migration

We showed that premature expression of miR-128 disrupted the essential and canonical polarized structure of the neurons *in vitro* and impaired neuronal migration *in vivo*. Neuronal migration is a complex process necessary for correct cortical lamination and the subsequent formation of functional neuronal networks. Several factors guide neuronal migration, some intrinsic such as cytoskeletal regulators (srGAP2), and some extrinsic such as Reelin or Sema 3A. Only two microRNAs, miR-9 and miR-132, have been shown to positively regulate neuronal migration (Clovis et al., 2012). We showed that miR-128 gain of function negatively regulates the correct lamination of the cortex through downregulation of Phf6 mRNA.

In our experiments we manipulated miR-128 expression either by gain or loss of function and we targeted the progenitor pool for the upper layer neurons. Early knockdown of miR-128 does not lead to a strong phenotype, however, the neurons seem to migrate a little farther compared to controls. We targeted upper layer neurons, that stop at the border with the marginal zone; a physical barrier for neuronal migration. We plan to repeat *in utero* electroporation experiments with miR-128 loss of function and to target lower layer neurons. It will then be easier to see if the overmigration trend is significantly different from the control situation.

Premature expression of pre-miR-128-2, but not pre-miR-128-1, leads to neurons that are scattered throughout the cortex (Figure 3.18) and to upper layer neurons that do not reach the border between layer II and the marginal zone. We observed, however, that all miR-128 gain of function cells, regardless of where they are located, have a layer II/III identity. This suggests that miR-128 does not affect specification but is the first microRNA shown to negatively regulate neuronal migration. miR-9 and miR-132, in fact, are considered positive regulators of neuronal migration because they are able to repress FoxP2 mRNA in migrating neuroblasts. Loss of miR-9 and miR-132 leads to a premature expression of FoxP2 and to an impairment of radial migration, probably due to inappropriate neurite outgrowth and branching (Clovis et al., 2012). It is unlikely that the migration impairment we observed overexpressing miR-128 is due to the regulation of FoxP2 (confirmed target, Heiko Fuchs). Regulation of FoxP2 has a positive effect on neuronal migration, whereas miR-128 gain of function has a negative role. We cannot exclude, however, that miR-128 and FoxP2 interact in other contexts in the brain where the two are coexpressed.

The correct timing of branching in a migrating neuron is one of the crucial steps for determining neuronal position in the cortex. srGAP2, for example, is a negative regulator of neuronal migration, helping the migrating neurons to sprout filipodia and lamellipodia when

they reach the right position in the cortical plate. Premature expression of srGAP2 impairs migration: the neurons branch more and have more filipodia. On the other hand, by preventing branching knockdown of srGAP2 leads to overmigration of cells that inappropriately maintain their bipolar conformation (Guerrier et al., 2009). In our experiments we found that premature expression of miR-128 disrupts the radial morphology of the migrating neurons, and increases the number of branches and filipodia (Figure 3.19). Regulation of srGAP2, a confirmed target in the sensor assay (Figure 3.8), by miR-128 is unlikely to account for the phenotype, because knockdown of srGAP2 has the opposite effect compared to what we observed.

Another potential target for miR-128 is DCX. RNAi knockdown of DCX by in utero electroporation resulted in failure of the affected neuroblasts to enter the cortical plate (Bai et al., 2003). In similar experiments miR-128 gain of function acts later in the process: the affected neurons are able to enter the cortical plate but not to reach their final position. Although this suggests that miR-128 is not acting via DCX prior to cortical plate entry, we cannot predict the effect of DCX downregulation once the neurons have reached the cortical plate.

4.4.1 Phf6 Rescues Neuronal Migration

We showed that miR-128 regulates Phf6 mRNA (Figure 3.21). Phf6 is a nuclear/nucleolar protein mutated in Börjeson-Foremann Lehmann syndrome and in some leukemia types. Phf6 is also necessary for neuronal migration thanks to the regulation of CALEB/NGC via the transcription elongation complex PAF1 (Zhang et al., 2013). Knockdown of Phf6 in migrating neurons, results in premature branching that is similar to what we observe in miR-128 gain of function experiments. We could rescue the miR-128 phenotype by coexpressing Phf6 (Figure 3.21). We also showed that miR-128 and Phf6 have a reciprocal expression pattern in brain and in cultured neurons (Figure 3.21), consistent with a functional role for their interaction *in vivo*. In some forms of AML and T-ALL leukemias the Phf6 gene is mutated and the protein is not functional (Van Vlierberghe et al., 2010, 2011). Moreover, miR-128 expression is increased in T-ALL (Fulci et al., 2009). Our results in the nervous system suggest that misregulation of Phf6 by miR-128 might be involved in the genesis of these leukemias.

4.5 miR-128 in Dendritic Branching and Neuronal Morphology

miR-128 is expressed at high levels throughout the postnatal and adult period of neuronal outgrowth and morphological maturation (Figure 3.1). We therefore tested if miR-128 gain and loss of function affects neuronal or dendritic spine morphology. We targeted, using *in utero* electroporation, the progenitors for the upper layers of the cortex and we analyzed dendritic branching and spine morphology at P21.

Spines were analyzed close to the most apical branch of the apical dendrite and we compared littermates expressing either pre-miR-128-2 dsRed or GFP. The analyzed conditions are not optimal because it has never been shown that cytoplasmic GFP and dsRed have the same intracellular distribution or detection sensitivity. It is evident, however, that the spine den-

sity in miR-128 gain of function is substantially lower compared to control. Our finding is in line with recently published data obtained with pre-miR-128-2 knockout mice: pre-miR-128-2 knockout neurons show an increase in spine number compared to control (Tan et al., 2013). We validated as miR-128 targets the Gria3 AMPAR subunit and Cacng2 (or Stargazin) in a sensor assay (Figure 3.10). The decrease in spine number might be the result of Stargazin downregulation. Stargazin is one of the TARPs, important auxiliary proteins for AMPAR trafficking to the synapse and between synaptic compartments. Reduction of AMPAR and Stargazin might lead to a situation similar to the silent synapse, a synapse in which NMDARs are the sole channels integrated into the membrane. In this situation strong stimulation is required for AMPAR incorporation at the postsynaptic site. Unfortunately to date no studies have described the overall morphology of silent synapses or their density in the dendritic shaft. There is, however, an extensive scientific literature on their electrophysiological behavior and their ultrastructure. In the near future we plan to validate the hypothesis that the decreased spine number is due to regulation of Cacng2 and Gria3. miR-128 knockout mice suffer from strong and lethal epileptic crisis (Tan et al., 2013), indicating that the microRNA is involved in neuronal excitability. We plan to check if the electrophysiological properties of the spines change upon miR-128 gain of function.

We analyzed the morphology of dendritic arbors using Sholl analysis. Unlike the spine analysis, in these experiments we could use the same fluorophore for control and test conditions: GFP for knockdown using our sponge construct and dsRed for overexpression. We showed that miR-128 knockdown neurons have a dendritic arbor slightly more complex than control (Figure 3.22). Furthermore, we showed that pre-miR-128-2, but not pre-miR-128-1 electroporated neurons have a simpler dendritic tree (Figure 3.23). Correct dendritic arborization is a prerequisite for the complexity of neuronal communication. A neuron with a less complex dendritic arbor is not able to establish all the connections needed for proper wiring. Despite the important function of dendrites little is known about the intrinsic mechanisms leading to dendritic branching. In upper layer neurons the transcription factors Cux1 and Cux2, as well as the Cdc42 pathway regulator NOMA-GAP, are key components of the process (Cubelos et al., 2010; Rosário et al., 2012). In addition, both mTOR complexes, mTORC1 and mTORC2, are able to stimulate dendritic branching. Of particular interest is the ability of mTORC2 to activate CALEB/NGC and promote dendritic branching and spine development (Brandt et al., 2007). Recently it has been shown that CALEB/NGC is under the transcriptional control of Phf6 and that the dowregulation of CALEB/NGC activity in Phf6 knockdown neurons is responsible for impaired migration (Zhang et al., 2013). We hypothesize that the simple dendritic tree observed after overexpression of pre-miR-128-2 can be attributed to this pathway. One consequence of Phf6 downregulation would be reduced levels of CALEB/NGC. We plan to rescue the phenotype coelectroporating pre-miR-128-2 and Phf6 in progenitors for upper layer neurons and checking the dendritic arbor at P21. As an independent test, it might also be possible to rescue the phenotype by manipulating mTORC2 activity.

In summary, our findings provide independent support for the recently described role of miR-128 in the regulation of dendritic spine formation. We show for the first time that

dendritic arborization is dependent on correct calibration of miR-128 levels during postnatal development.

Appendix

.1 LNA Probe Validation

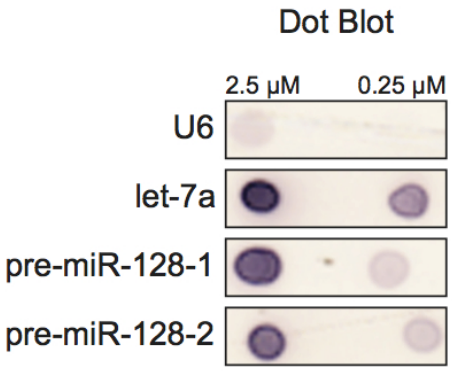

Figure 1: *LNA probes validation: dot blot.* To test the functionality of pre-miR-128-1 *in situ* hybridization probe, we performed a dot blot test. A dot blot test consists in pipetting on the Hybond-N^+ membrane the probes of interest, cross link the membrane and then detect the signal using the anti-DIG-AP antibody and the NBT/BCIP precipitate. pre-miR-128-1 probe resulted DIG labelled. Therefore it should give a positive signal if bound to the pre-miR-128-1 *in vivo*. As a positive control (from top to bottom) U6, let-7a, pre-miR-128-2 probes were used.

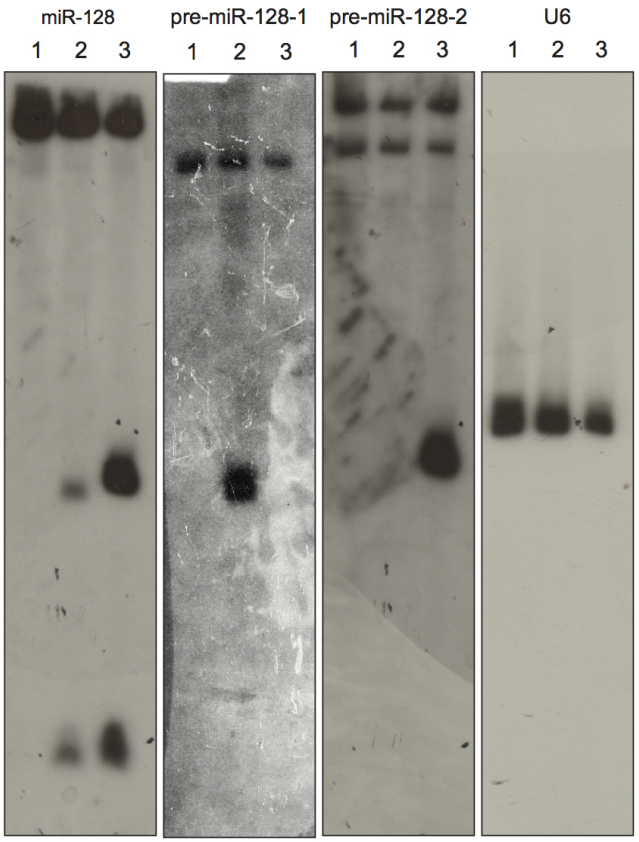

Figure 2: *Specificity of miR-128, pre-mir-128-1 and pre-miR-128-2 probes in Northern blot.* Northern blot analysis of HEK 293T transfected with dsRed control (lane 1), pre-miR-128-1 (lane 2) and pre-miR-128-2 (lane 3). The left panel shows the hybridization for miR-128 mature probe. In all the three lanes the upper band represent the primary transcript of miR-128. Only in lane 2 and 3, where the microRNA has been expressed, the precursor bands, in the middle, and the mature form band, at the bottom, are detected. When the same membrane is hybridized with a probe specific for pre-miR-128-1 (second blot from the left) only one band at precursor height is detected in lane 2. When the membrane is hybridized for pre-miR-128-2 (third blot from the left) only one band at precursor height is detected in lane 3. U6 is used as a loading control.
This experiment demonstrate that the miR-128 mature, pre-miR-128-1 and pre-miR-128-2 probes are specific.

.2 miR-128 Expression Constructs and miR-128 Sponge Construct Validation

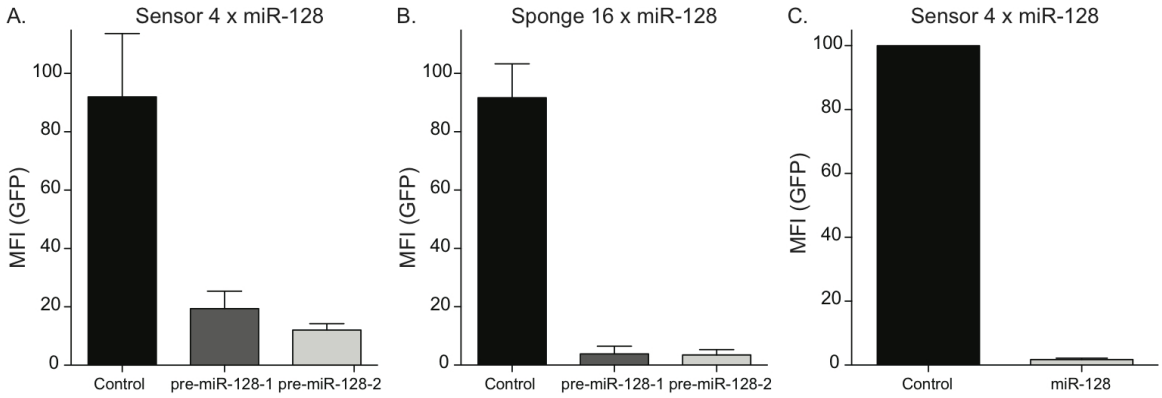

Figure 3: *miR-128 expression constructs and miR-128 sponge construct validation* .HEK 293T cells were cotransfected either with dsRed (control), pre-miR-128-1 or pre-miR-128-2 constructs and either miR-128 4xSensor (Panel **A**) or miR-128 16xSponge (Panel **B**) constructs. pre-miR-128-1 expression construct is processed and regulates both miR-128 4xSensor and miR-128 16xSponge, but to a lesser extent compared to pre-miR-128-2 (Panel **A** and **B**). HEK 293T cells were cotransfected with synthetic miR-128 and miR-128 4xSensor construct (Panel **C**). Synthetic miR-128 is able to regulate miR-128 4xSensor construct to an higher extent compared to miR-128 expression plasmids (compare Panel **A** and **C**).

.3 Phf6 and Nrp2 Expression Constructs Validation

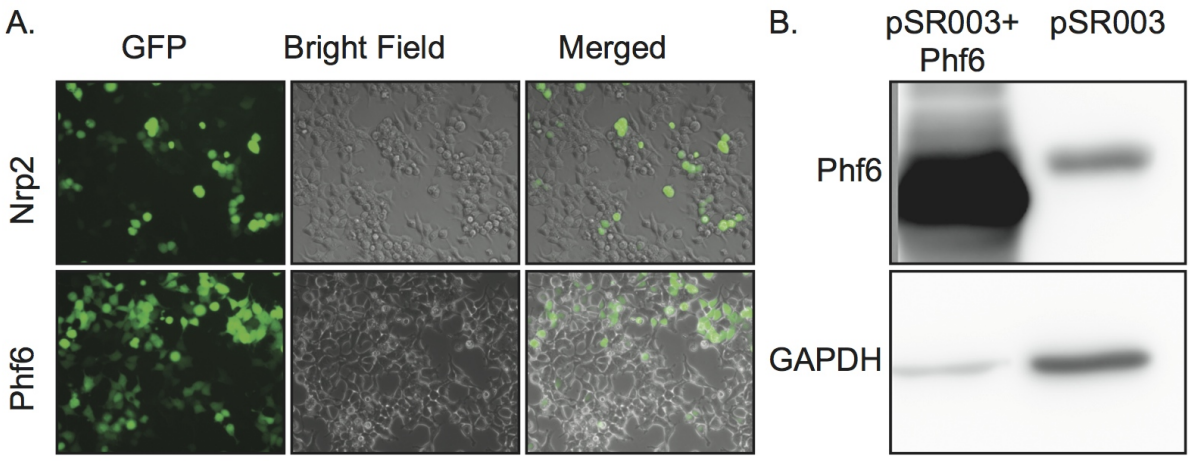

Figure 4: *Phf6 and Nrp2 expression constructs validation.* Phf6 and Nrp2 cDNA sequences were cloned into pSR003 expression plasmid. The insertion of the cDNA sequence was tested with enzymatic digestion and the sequence was validated by sequencing. HEK 293T cells were transfected with the Expression construct to test if they were working, producing GFP cells. Panel **A** shows Nrp2 expressing cells in the upper row of images and Phf6 expressing cells in the lower row of images. From left to right transfected cells (GFP), an overview of the HEK 293T cells (bright field) and the merged image are shown. Phf6 expression construct was validated also by Western blot analysis (Panel **B**).

.4 Transfected and Injected Constructs

The following tables show the cell lines and constructs used in transfections or the injected constructs used in IUE. The are also references of the experiments to which the conditions refers to.

Plate	Cell line	miR-128 gain of function	Sensor	DNA Carrier	
12-well	HEK 293T	Ambion 20 μM	75 ng and 200ng dsred	200 ng	3.7
12-well	N2A	Ambion 20 μM	75 ng 200ng dsred	200 ng	3.8
12-well	HEK 293T	Plasmid 100 ng	75 ng	800 ng	3.9, 3.10

Table 1: Constructs for Sensor Assay

Purpuse	Plate	Cell line	miR-128 gain of function	Figure
Par6 Downregulation	10 cm	N2A	Ambion 20 μM	3.14
Phf6 Downregulation	10 cm	HEK 293T	Ambion 20 μM	3.21

Table 2: Cosntructs for Downregulation of Endogenous Protein after miR-128 Expression

Plate	Cell line	Constructs	Figure
10 cm	HEK 293T	dsred construct 24μg	2
10 cm	HEK 293T	pre-miR-128-1 construct 24 μg	2
10 cm	HEK 293T	pre-miR-128-1 construct 24 μg	2

Table 3: Cosntructs for Test for miR-128, pre-miR-128-1 and pre-miR-128-2 probes used in Northern blot

Constructs 1	Constructs 2	Figure
dsred 150 ng	DNA carrier 350 ng	3.11
pre-miR-128-2 150 ng	DNA carrier 350 ng	3.11
Sponge 150 ng	DNA carrier 350 ng	3.11
Ambion control 20 μM	25 ng GFP	3.11
Ambion miR-128 mimic 20 μM	25 ng GFP	3.11
Eqicon miR-128 antisense	25 ng GFP	3.11

Table 4: Constructs for miR-128 and Axon Number

Purpuse	Condition	Rescue	DNA Carrier	Figure
Par6b rescue	dsred 150 ng	Par6b 150 ng	200 ng	3.15
Par6b rescue	pre-miR-128-1 150 ng	Par6b 150 ng	200 ng	3.15
Par6b rescue	pre-miR-128-2 150 ng	Par6b 150 ng	200 ng	3.15
Par6b rescue	miR-128 sponge 150 ng	Par6b 150 ng	200 ng	3.15
Nrp2 rescue	dsred 150 ng	Nrp2 150 ng	200 ng	3.16
Nrp2 rescue	pre-miR-128-1 150 ng	Nrp2 150 ng	200 ng	3.16
Nrp2 rescue	pre-miR-128-2 150 ng	Nrp2 150 ng	200 ng	3.16
Nrp2 rescue	miR-128 sponge 150 ng	Nrp2 150 ng	200 ng	3.16

Table 5: Constructs for miR-128 rescue of the Axon Number

Purpuse	Embryonic day	Constructs	Plasmid Concentration	Figure
Neuronal Migration	E12.5	pre-miR-128-2, dsRed, GFP, miR-128 Sponge	2 μg/μl	3.17
Neuronal Migration	E14.5	pre-miR-128-2, dsRed, GFP, miR-128 Sponge	2 μg/μl	3.17
Neuronal Migration	E15.5	pre-miR-128-1, pre-miR-128-2, dsRed, GFP, miR-128 Sponge	300 ng/μl	3.18
Neuronal Morphology P0	E15.5	pre-miR-128-2, dsRed	300 ng/μl	3.19
Neuronal Migration Rescue	E15.5	pre-miR-128-2, dsRed, Nrp2, Phf6	300 ng/μl each plasmid	3.20, 3.21
Neuronal Morphology P21	E15.5	pre-miR-128-1, pre-miR-128-2, dsRed, GFP, miR-128 Sponge	150 ng/μl	3.22, 3.23
Neuronal Morphology P15	E15.5	pre-miR-128-2	300 ng/μl	3.24

Table 6: Constructs for *In Utero* Electroporation Conditions.

Bibliography

Malin Åkerblom, Rohit Sachdeva, Isabelle Barde, Sonia Verp, Bernhard Gentner, Didier Trono, and Johan Jakobsson. MicroRNA-124 is a subventricular zone neuronal fate determinant. *Journal of Neuroscience*, 32(26):8879–8889, June 2012.

Victor Anggono and Richard L Huganir. Regulation of AMPA receptor trafficking and synaptic plasticity. *Current opinion in neurobiology*, 22(3):461–469, June 2012.

Nariko Arimura and Kozo Kaibuchi. Neuronal polarity: from extracellular signals to intracellular mechanisms. *Nature reviews Neuroscience*, 8(3):194–205, March 2007.

Joshua E Babiarz, Ruby Hsu, Collin Melton, Molly Thomas, Erik M Ullian, and Robert Blelloch. A role for noncanonical microRNAs in the mammalian brain revealed by phenotypic differences in Dgcr8 versus Dicer1 knockouts and small RNA sequencing. *RNA (New York, NY)*, 17(8):1489–1501, August 2011.

Jilin Bai, Raddy L Ramos, James B Ackman, Ankur M Thomas, Richard V Lee, and Joseph J LoTurco. RNAi reveals doublecortin is required for radial migration in rat neocortex. *Nature Neuroscience*, 6(12):1277–1283, December 2003.

Mahmud Bani-Yaghoub, Roger G Tremblay, Joy X Lei, Dongling Zhang, Bogdan Zurakowski, Jagdeep K Sandhu, Brandon Smith, Maria Ribecco-Lutkiewicz, Jessica Kennedy, P Roy Walker, and Marianna Sikorska. Role of Sox2 in the development of the mouse neocortex. *Developmental biology*, 295(1):52–66, July 2006.

Uwe Beffert, Gerardo Morfini, Hans H Bock, Huichuan Reyna, Scott T Brady, and Joachim Herz. Reelin-mediated signaling locally regulates protein kinase B/Akt and glycogen synthase kinase 3beta. *The Journal of biological chemistry*, 277(51):49958–49964, December 2002.

Isabelle Behm-Ansmant, Jan Rehwinkel, Tobias Doerks, Alexander Stark, Peer Bork, and Elisa Izaurralde. mRNA degradation by miRNAs and GW182 requires both CCR4:NOT deadenylase and DCP1:DCP2 decapping complexes. *Genes & development*, 20(14):1885–1898, July 2006.

Eugene Berezikov, Fritz Thuemmler, Linda W van Laake, Ivanela Kondova, Ronald Bontrop, Edwin Cuppen, and Ronald H A Plasterk. Diversity of microRNAs in human and chimpanzee brain. *Nature genetics*, 38(12):1375–1377, December 2006.

Emily Bernstein, Sang Yong Kim, Michelle A Carmell, Elizabeth P Murchison, Heather Alcorn, Mamie Z Li, Alea A Mills, Stephen J Elledge, Kathryn V Anderson, and Gregory J Hannon. Dicer is essential for mouse development. *Nature genetics*, 35(3):215–217, November 2003.

Shan Bian, Janet Hong, Qingsong Li, Laura Schebelle, Andrew Pollock, Jennifer L Knauss, Vidur Garg, and Tao Sun. MicroRNA cluster miR-17-92 regulates neural stem cell expansion and transition to intermediate progenitors in the developing mouse neocortex. *CellReports*, 3(5):1398–1406, May 2013.

Silvia Bicker, Sharof Khudayberdiev, Kerstin Weiß, Kathleen Zocher, Stefan Baumeister, and Gerhard Schratt. The DEAH-box helicase DHX36 mediates dendritic localization of the neuronal precursor-microRNA-134. *Genes & development*, 27(9):991–996, May 2013.

Parizad M Bilimoria, Luis de la Torre-Ubieta, Yoshiho Ikeuchi, Esther B E Becker, Orly Reiner, and Azad Bonni. A JIP3-regulated GSK3β/DCX signaling pathway restricts axon branching. *Journal of Neuroscience*, 30(50):16766–16776, December 2010.

Glen M Borchert, William Lanier, and Beverly L Davidson. RNA polymerase III transcribes human microRNAs. *Nature Publishing Group*, 13(12):1097–1101, December 2006.

F Bradke and C G Dotti. The role of local actin instability in axon formation. *Science*, 283 (5409):1931–1934, March 1999.

Nicola Brandt, Kristin Franke, Mladen-Roko Rasin, Jan Baumgart, Johannes Vogt, Sergey Khrulev, Burkhard Hassel, Elena E Pohl, Nenad Sestan, Robert Nitsch, and Stefan Schumacher. The neural EGF family member CALEB/NGC mediates dendritic tree and spine complexity. *The EMBO journal*, 26(9):2371–2386, May 2007.

Olga Britanova, Sergey Akopov, Sergey Lukyanov, Peter Gruss, and Victor Tarabykin. Novel transcription factor Satb2 interacts with matrix attachment region DNA elements in a tissue-specific manner and demonstrates cell-type-dependent expression in the developing mouse CNS. *The European journal of neuroscience*, 21(3):658–668, February 2005.

Olga Britanova, Camino de Juan Romero, Amanda Cheung, Kenneth Y Kwan, Manuela Schwark, Andrea Gyorgy, Tanja Vogel, Sergey Akopov, Miso Mitkovski, Denes Agoston, Nenad Sestan, Zoltán Molnár, and Victor Tarabykin. Satb2 is a postmitotic determinant for upper-layer neuron specification in the neocortex. *Neuron*, 57(3):378–392, February 2008.

Ivone G Bruno, Rachid Karam, Lulu Huang, Anjana Bhardwaj, Chih H Lou, Eleen Y Shum, Hye-Won Song, Mark A Corbett, Wesley D Gifford, Jozef Gécz, Samuel L Pfaff, and Miles F Wilkinson. Identification of a MicroRNA that Activates Gene Expression by Repressing Nonsense-Mediated RNA Decay. *Molecular Cell*, 42(4):500–510, May 2011.

Xuejun Chai, Eckart Förster, Shanting Zhao, Hans H Bock, and Michael Frotscher. Reelin stabilizes the actin cytoskeleton of neuronal processes by inducing n-cofilin phosphorylation at serine3. *The Journal of neuroscience : the official journal of the Society for Neuroscience*, 29(1):288–299, January 2009.

Mwe Mwe Chao, Matthew A Todd, Udo Kontny, Katherine Neas, Michael J Sullivan, Alasdair G Hunter, David J Picketts, and Christian P Kratz. T-cell acute lymphoblastic leukemia in association with Börjeson-Forssman-Lehmann syndrome due to a mutation in PHF6. *Pediatric blood & cancer*, 55(4):722–724, October 2010.

Gang Chen, Jian Sima, Ming Jin, Kai-Yu Wang, Xiao-Jing Xue, Wang Zheng, Yu-Qiang Ding, and Xiao-Bing Yuan. Semaphorin-3A guides radial migration of cortical neurons during development. *Nature Neuroscience*, 11(1):36–44, January 2008.

L Chen, D M Chetkovich, R S Petralia, N T Sweeney, Y Kawasaki, R J Wenthold, D S Bredt, and R A Nicoll. Stargazin regulates synaptic targeting of AMPA receptors by two distinct mechanisms. *Nature*, 408(6815):936–943, December 2000.

Li-Chun Cheng, Erika Pastrana, Masoud Tavazoie, and Fiona Doetsch. miR-124 regulates adult neurogenesis in the subventricular zone stem cell niche. *Nature Neuroscience*, 12(4): 399–408, April 2009.

Pei-lin Cheng, Hui Lu, Maya Shelly, Hongfeng Gao, and Mu-ming Poo. Phosphorylation of E3 ligase Smurf1 switches its substrate preference in support of axon development. *Neuron*, 69(2):231–243, January 2011.

Mette Christensen, Lars A Larsen, Sakari Kauppinen, and Gerhard Schratt. Recombinant Adeno-Associated Virus-Mediated microRNA Delivery into the Postnatal Mouse Brain Reveals a Role for miR-134 in Dendritogenesis in Vivo. *Frontiers in neural circuits*, 3:16, 2010.

S A Ciafrè, S Galardi, A Mangiola, M Ferracin, C-G Liu, G Sabatino, M Negrini, G Maira, C M Croce, and M G Farace. Extensive modulation of a set of microRNAs in primary glioblastoma. *Biochemical and biophysical research communications*, 334(4):1351–1358, September 2005.

Y M Clovis, W Enard, F Marinaro, W B Huttner, and D De Pietri Tonelli. Convergent repression of Foxp2 3'UTR by miR-9 and miR-132 in embryonic mouse neocortex: implications for radial migration of neurons. *Development (Cambridge, England)*, August 2012.

Jonathan A Cooper. Cell biology in neuroscience: mechanisms of cell migration in the nervous system. *The Journal of Cell Biology*, 202(5):725–734, September 2013.

Beatriz Cubelos, Alvaro Sebastián-Serrano, Leonardo Beccari, Maria Elisa Calcagnotto, Elsa Cisneros, Seonhee Kim, Ana Dopazo, Manuel Alvarez-Dolado, Juan Miguel Redondo, Paola Bovolenta, Christopher A Walsh, and Marta Nieto. Cux1 and Cux2 regulate dendritic branching, spine morphology, and synapses of the upper layer neurons of the cortex. *Neuron*, 66(4):523–535, May 2010.

Yi Cui, Zhifeng Xiao, Jin Han, Jie Sun, Wenyong Ding, Yannan Zhao, Bing Chen, Xiaoran Li, and Jianwu Dai. MiR-125b orchestrates cell proliferation, differentiation and migration in neural stem/progenitor cells by targeting Nestin. *BMC neuroscience*, 13:116, 2012.

G D'Arcangelo, G G Miao, S C Chen, H D Soares, J I Morgan, and T Curran. A protein related to extracellular matrix proteins deleted in the mouse mutant reeler. *Nature*, 374 (6524):719–723, April 1995.

Froylan Calderon de Anda, Giulia Pollarolo, Jorge Santos Da Silva, Paola G Camoletto, Fabian Feiguin, and Carlos G Dotti. Centrosome localization determines neuronal polarity. *Nature*, 436(7051):704–708, August 2005.

Colette Dehay and Henry Kennedy. Cell-cycle control and cortical development. *Nature reviews Neuroscience*, 8(6):438–450, June 2007.

A R Desai and S K McConnell. Progressive restriction in fate potential by neural progenitors during cerebral cortical development. *Development (Cambridge, England)*, 127(13):2863–2872, July 2000.

H Dill, B Linder, A Fehr, and U Fischer. Intronic miR-26b controls neuronal differentiation by repressing its host transcript, ctdsp2. *Genes & development*, 26(1):25–30, 2012.

L Dulabon, E C Olson, M G Taglienti, S Eisenhuth, B McGrath, C A Walsh, J A Kreidberg, and E S Anton. Reelin binds alpha3beta1 integrin and inhibits neuronal migration. *Neuron*, 27(1):33–44, July 2000.

Laura A B Elias, Doris D Wang, and Arnold R Kriegstein. Gap junction adhesion is necessary for radial migration in the neocortex. *Nature*, 448(7156):901–907, August 2007.

Ira Espuny-Camacho, Kimmo A Michelsen, David Gall, Daniele Linaro, Anja Hasche, Jerome Bonnefont, Camilia Bali, David Orduz, Angéline Bilheu, Adèle Herpoel, Nelle Lambert, Nicolas Gaspard, Sophie Péron, Serge N Schiffmann, Michele Giugliano, Afsaneh Gaillard, and Pierre Vanderhaeghen. Pyramidal Neurons Derived from Human Pluripotent Stem Cells Integrate Efficiently into Mouse Brain Circuits In Vivo. *Neuron*, 77(3):440–456, February 2013.

Ana Eulalio, Jan Rehwinkel, Mona Stricker, Eric Huntzinger, Schu-Fee Yang, Tobias Doerks, Silke Dorner, Peer Bork, Michael Boutros, and Elisa Izaurralde. Target-specific requirements for enhancers of decapping in miRNA-mediated gene silencing. *Genes & development*, 21(20):2558–2570, October 2007.

C Evangelisti, M Florian, I Massimi, C Dominici, G Giannini, S Galardi, M Buè, S Massalini, H McDowell, E Messi, A Gulino, M Farace, and S Ciafrè. MiR-128 up-regulation inhibits Reelin and DCX expression and reduces neuroblastoma cell motility and invasiveness. *The FASEB journal : official publication of the Federation of American Societies for Experimental Biology*, August 2009.

Witold Filipowicz, Suvendra N Bhattacharyya, and Nahum Sonenberg. Mechanisms of post-transcriptional regulation by microRNAs: are the answers in sight? *Nature reviews Genetics*, 9(2):102–114, February 2008.

Roberto Fiore, Sharof Khudayberdiev, Mette Christensen, Gabriele Siegel, Steven W Flavell, Tae-Kyung Kim, Michael E Greenberg, and Gerhard Schratt. Mef2-mediated transcription of the miR379-410 cluster regulates activity-dependent dendritogenesis by fine-tuning Pumilio2 protein levels. *The EMBO journal*, 28(6):697–710, March 2009.

Gord Fishell and Carina Hanashima. Pyramidal neurons grow up and change their mind. *Neuron*, 57(3):333–338, February 2008.

Santos J Franco and Ulrich Müller. Shaping our minds: stem and progenitor cell diversity in the mammalian neocortex. *Neuron*, 77(1):19–34, January 2013.

Kristin Franke, Wolfgang Otto, Sascha Johannes, Jan Baumgart, Robert Nitsch, and Stefan Schumacher. miR-124-regulated RhoG reduces neuronal process complexity via ELMO/Dock180/Rac1 and Cdc42 signalling. *The EMBO journal*, 31(13):2908–2921, June 2012.

G D Frantz and S K McConnell. Restriction of late cerebral cortical progenitors to an upper-layer fate. *Neuron*, 17(1):55–61, July 1996.

Valerio Fulci, Teresa Colombo, Sabina Chiaretti, Monica Messina, Franca Citarella, Simona Tavolaro, Anna Guarini, Robin Foà, and Giuseppe Macino. Characterization of B- and T-lineage acute lymphoblastic leukemia by integrated analysis of MicroRNA and mRNA expression profiles. *Genes, chromosomes & cancer*, 48(12):1069–1082, December 2009.

Nicolas Gaspard, Tristan Bouschet, Raphael Hourez, Jordane Dimidschstein, Gilles Naeije, Jelle van den Ameele, Ira Espuny-Camacho, Adèle Herpoel, Lara Passante, Serge N Schiffmann, Afsaneh Gaillard, and Pierre Vanderhaeghen. An intrinsic mechanism of corticogenesis from embryonic stem cells. *Nature*, 455(7211):351–357, September 2008.

David Gatfield, Gwendal Le Martelot, Charles E Vejnar, Daniel Gerlach, Olivier Schaad, Fabienne Fleury-Olela, Anna-Liisa Ruskeepää, Matej Oresic, Christine C Esau, Evgeny M Zdobnov, and Ueli Schibler. Integration of microRNA miR-122 in hepatic circadian gene expression. *Genes & development*, 23(11):1313–1326, June 2009.

Philip Gaughwin, Maciej Ciesla, Henry Yang, Bing Lim, and Patrik Brundin. Stage-specific modulation of cortical neuronal development by Mmu-miR-134. *Cerebral Cortex*, 21(8): 1857–1869, August 2011.

Jozef Gécz, Gillian Turner, John Nelson, and Michael Partington. The Börjeson-Forssman-Lehman syndrome (BFLS, MIM #301900). *European journal of human genetics : EJHG*, 14(12):1233–1237, December 2006.

Magdalena Götz and Wieland B Huttner. The cell biology of neurogenesis. *Nature reviews Molecular cell biology*, 6(10):777–788, October 2005.

Ruth Grosskortenhaus, Bret J Pearson, Amanda Marusich, and Chris Q Doe. Regulation of temporal identity transitions in Drosophila neuroblasts. *Developmental cell*, 8(2):193–202, February 2005.

Sabrice Guerrier, Jaeda Coutinho-Budd, Takayuki Sassa, Aurélie Gresset, Nicole Vincent Jordan, Keng Chen, Wei-Lin Jin, Adam Frost, and Franck Polleux. The F-BAR Domain of srGAP2 Induces Membrane Protrusions Required for Neuronal Migration and Morphogenesis. *Cell*, 138(5):990–1004, September 2009.

Amitabh Gupta, Kamon Sanada, David T Miyamoto, Susan Rovelstad, Bagirathy Nadarajah, Alan L Pearlman, Jan Brunstrom, and Li-Huei Tsai. Layering defect in p35 deficiency is linked to improper neuronal-glial interaction in radial migration. *Nature Neuroscience*, 6 (12):1284–1291, December 2003.

S M Hammond, S Boettcher, A A Caudy, R Kobayashi, and G J Hannon. Argonaute2, a link between genetic and biochemical analyses of RNAi. *Science*, 293(5532):1146–1150, August 2001.

Yasunori Hayashi and Ania K Majewska. Dendritic spine geometry: functional implication and regulation. *Neuron*, 46(4):529–532, May 2005.

Miao He, Yu Liu, Xiaowo Wang, Michael Q Zhang, Gregory J Hannon, and Z Josh Huang. Cell-Type-Based Analysis of MicroRNA Profiles in the Mouse Brain. *Neuron*, 73(1):35–48, January 2012.

Julian Ik-Tsen Heng, Alain Chariot, and Laurent Nguyen. Molecular layers underlying cytoskeletal remodelling during cortical development. *Trends in neurosciences*, 33(1):38–47, 2010.

Inha Heo, Chirlmin Joo, Jun Cho, Minju Ha, Jinju Han, and V Narry Kim. Lin28 mediates the terminal uridylation of let-7 precursor MicroRNA. *Molecular Cell*, 32(2):276–284, October 2008.

Casper C Hoogenraad and Anna Akhmanova. Dendritic spine plasticity: new regulatory roles of dynamic microtubules. *The Neuroscientist : a review journal bringing neurobiology, neurology and psychiatry*, 16(6):650–661, December 2010.

Casper C Hoogenraad and Frank Bradke. Control of neuronal polarity and plasticity–a renaissance for microtubules? *Trends in cell biology*, 19(12):669–676, December 2009.

Hai Yang Hu, Liu He, Kseniya Fominykh, Zheng Yan, Song Guo, Xiaoyu Zhang, Martin S Taylor, Lin Tang, Jie Li, Jianmei Liu, Wen Wang, Haijing Yu, and Philipp Khaitovich. Evolution of the human-specific microRNA miR-941. *Nature Communications*, 3:1145, 2012.

Shu-Hong Huang, Shan Duan, Tao Sun, Jue Wang, Ling Zhao, Zhao Geng, Jing Yan, Hai-Ji Sun, and Zhe-Yu Chen. JIP3 mediates TrkB axonal anterograde transport and enhances BDNF signaling by directly bridging TrkB with kinesin-1. *Journal of Neuroscience*, 31(29): 10602–10614, July 2011.

Richard L Huganir and Roger A Nicoll. AMPARs and synaptic plasticity: the last 25 years. *Neuron*, 80(3):704–717, October 2013.

Eric Huntzinger and Elisa Izaurralde. Gene silencing by microRNAs: contributions of translational repression and mRNA decay. *Nature reviews Genetics*, 12(2):99–110, February 2011.

Eric Huntzinger, Joerg E Braun, Susanne Heimstädt, Latifa Zekri, and Elisa Izaurralde. Two PABPC1-binding sites in GW182 proteins promote miRNA-mediated gene silencing. *The EMBO journal*, 29(24):4146–4160, December 2010.

Carolina Ibáñez-Ventoso, Mehul Vora, and Monica Driscoll. Sequence relationships among C. elegans, D. melanogaster and human microRNAs highlight the extensive conservation of microRNAs in biology. *PLoS ONE*, 3(7):e2818, 2008.

Hui Jiang, Wei Guo, Xinhua Liang, and Yi Rao. Both the establishment and the maintenance of neuronal polarity require active mechanisms: critical roles of GSK-3beta and its upstream regulators. *Cell*, 120(1):123–135, January 2005.

Yves Jossin and André M Goffinet. Reelin signals through phosphatidylinositol 3-kinase and Akt to control cortical development and through mTor to regulate dendritic growth. *Molecular and cellular biology*, 27(20):7113–7124, October 2007.

Yves Jossin, Nina Ignatova, Thomas Hiesberger, Joachim Herz, Catherine Lambert de Rouvroit, and André M Goffinet. The central fragment of Reelin, generated by proteolytic processing in vivo, is critical to its function during cortical plate development. *Journal of Neuroscience*, 24(2):514–521, January 2004.

Hosung Jung, Byung C Yoon, and Christine E Holt. Axonal mRNA localization and local protein synthesis in nervous system assembly, maintenance and repair. *Nature reviews Neuroscience*, 13(5):308–324, May 2012.

Patrick O Kanold and Heiko J Luhmann. The subplate and early cortical circuits. *Annual review of neuroscience*, 33:23–48, 2010.

Geoffrey A Kerchner and Roger A Nicoll. Silent synapses and the emergence of a postsynaptic mechanism for LTP. *Nature reviews Neuroscience*, 9(11):813–825, November 2008.

Sharof A Khudayberdiev, Federico Zampa, Marek Rajman, and Gerhard Schratt. A comprehensive characterization of the nuclear microRNA repertoire of post-mitotic neurons. *Frontiers in molecular neuroscience*, 6:43, 2013.

V Narry Kim, Jinju Han, and Mikiko C Siomi. Biogenesis of small RNAs in animals. *Nature reviews Molecular cell biology*, 10(2):126–139, February 2009a.

Woo-Yang Kim, Xinshuo Wang, Yaohong Wu, Bradley W Doble, Satish Patel, James R Woodgett, and William D Snider. GSK-3 is a master regulator of neural progenitor homeostasis. *Nature Neuroscience*, 12(11):1390–1397, November 2009b.

Yun Tai Kim, Eun-Mi Hur, William D Snider, and Feng-Quan Zhou. Role of GSK3 Signaling in Neuronal Morphogenesis. *Frontiers in molecular neuroscience*, 4:48, 2011.

Jacek Krol, Volker Busskamp, Ilona Markiewicz, Michael B Stadler, Sebastian Ribi, Jens Richter, Jens Duebel, Silvia Bicker, Hans Jörg Fehling, Dirk Schübeler, Thomas G Oertner, Gerhard Schratt, Miriam Bibel, Botond Roska, and Witold Filipowicz. Characterizing light-regulated retinal microRNAs reveals rapid turnover as a common property of neuronal microRNAs. *Cell*, 141(4):618–631, May 2010a.

Jacek Krol, Inga Loedige, and Witold Filipowicz. The widespread regulation of microRNA biogenesis, function and decay. *Nature reviews Genetics*, 11(9):597–610, September 2010b.

Vaishali A Kulkarni and Bonnie L Firestein. The dendritic tree and brain disorders. *Molecular and cellular neurosciences*, 50(1):10–20, May 2012.

Min Jeong Kye, Pierre Neveu, Yong-Seok Lee, Miou Zhou, Judith A Steen, Mustafa Sahin, Kenneth S Kosik, and Alcino J Silva. NMDA Mediated Contextual Conditioning Changes miRNA Expression. *PLoS ONE*, 6(9):e24682, September 2011.

M Lagos-Quintana, R Rauhut, W Lendeckel, and T Tuschl. Identification of novel genes coding for small expressed RNAs. *Science*, 294(5543):853–858, October 2001.

Bridget E LaMonica, Jan H Lui, Xiaoqun Wang, and Arnold R Kriegstein. OSVZ progenitors in the human cortex: an updated perspective on neurodevelopmental disease. *Current opinion in neurobiology*, 22(5):747–753, October 2012.

N C Lau, L P Lim, E G Weinstein, and D P Bartel. An abundant class of tiny RNAs with probable regulatory roles in Caenorhabditis elegans. *Science*, 294(5543):858–862, October 2001.

Kihwan Lee, Joung-Hun Kim, Oh-Bin Kwon, Kyongman An, Junghwa Ryu, Kwangwook Cho, Yoo-Hun Suh, and Hye-Sun Kim. An activity-regulated microRNA, miR-188, controls dendritic plasticity and synaptic transmission by downregulating neuropilin-2. *Journal of Neuroscience*, 32(16):5678–5687, April 2012.

R C Lee and V Ambros. An extensive class of small RNAs in Caenorhabditis elegans. *Science*, 294(5543):862–864, October 2001.

R C Lee, R L Feinbaum, and V Ambros. The C. elegans heterochronic gene lin-4 encodes small RNAs with antisense complementarity to lin-14. *Cell*, 75(5):843–854, December 1993.

Yoontae Lee, Minju Kim, Jinju Han, Kyu-Hyun Yeom, Sanghyuk Lee, Sung Hee Baek, and V Narry Kim. MicroRNA genes are transcribed by RNA polymerase II. *The EMBO journal*, 23(20):4051–4060, October 2004.

Jost Leemhuis and Hans H Bock. Reelin modulates cytoskeletal organization by regulating Rho GTPases. *Communicative & integrative biology*, 4(3):254–257, May 2011.

Jost Leemhuis, Elisabeth Bouché, Michael Frotscher, Frank Henle, Lutz Hein, Joachim Herz, Dieter K Meyer, Marina Pichler, Günter Roth, Carsten Schwan, and Hans H Bock. Reelin Signals through Apolipoprotein E Receptor 2 and Cdc42 to Increase Growth Cone Motility

and Filopodia Formation. *The Journal of neuroscience : the official journal of the Society for Neuroscience*, 30(44):14759–14772, November 2010.

Molin Li, Weiming Fu, Lulu Wo, Xiaohong Shu, Fang Liu, and Chuangang Li. miR-128 and its target genes in tumorigenesis and metastasis. *Experimental cell research*, 319(20): 3059–3064, December 2013.

Quan Lin, Wei Wei, Carlos M Coelho, Xiang Li, Danay Baker-Andresen, Kevin Dudley, Vikram S Ratnu, Zoran Boskovic, Michael S Kobor, Yi E Sun, and Timothy W Bredy. The brain-specific microRNA miR-128b regulates the formation of fear-extinction memory. *Nature Neuroscience*, 14(9):1115–1117, September 2011.

Changmei Liu, Zhao-Qian Teng, Nicholas J Santistevan, Keith E Szulwach, Weixiang Guo, Peng Jin, and Xinyu Zhao. Epigenetic regulation of miR-184 by MBD1 governs neural stem cell proliferation and differentiation. *Cell stem cell*, 6(5):433–444, May 2010.

Changmei Liu, Zhao-Qian Teng, Andrea L McQuate, Emily M Jobe, Christa C Christ, Sergei J von Hoyningen-Huene, Marie D Reyes, Eric D Polich, Yina Xing, Yue Li, Weixiang Guo, and Xinyu Zhao. An epigenetic feedback regulatory loop involving microRNA-195 and MBD1 governs neural stem cell differentiation. *PLoS ONE*, 8(1):e51436, 2013.

Jidong Liu, Michelle A Carmell, Fabiola V Rivas, Carolyn G Marsden, J Michael Thomson, Ji-Joon Song, Scott M Hammond, Leemor Joshua-Tor, and Gregory J Hannon. Argonaute2 is the catalytic engine of mammalian RNAi. *Science*, 305(5689):1437–1441, September 2004.

Xianpeng Liu, Xin Gu, Limin Sun, Ashley B Flowers, Alfred W Rademaker, Yiran Zhou, and Hiroaki Kiyokawa. Downregulation of Smurf2, a tumor-suppressive ubiquitin ligase, in triple-negative breast cancers: involvement of the RB-microRNA axis. *BMC cancer*, 14:57, 2014a.

Zhonghua Liu, Fudong Li, Ke Ruan, Jiahai Zhang, Yide Mei, Jihui Wu, and Yunyu Shi. Structural and Functional Insights into the Human Borjeson-Forssman-Lehmann Syndrome Associated Protein PHF6. *Journal of Biological Chemistry*, February 2014b.

Joseph J LoTurco and Jilin Bai. The multipolar stage and disruptions in neuronal migration. *Trends in neurosciences*, 29(7):407–413, July 2006.

Karen M Lower, Gillian Turner, Bronwyn A Kerr, Katherine D Mathews, Marie A Shaw, Ági K Gedeon, Susan Schelley, H Eugene Hoyme, Susan M White, Martin B Delatycki, Anne K Lampe, Jill Clayton-Smith, Helen Stewart, Conny M A van Ravenswaay, Bert B A de Vries, Barbara Cox, Markus Grompe, Shelley Ross, Paul Thomas, John C Mulley, and Jozef Gécz. Mutations in PHF6 are associated with Börjeson–Forssman–Lehmann syndrome. *Nature genetics*, 32(4):661–665, November 2002.

Laura Anne Lowery and David Van Vactor. The trip of the tip: understanding the growth cone machinery. *Nature reviews Molecular cell biology*, 10(5):332–343, May 2009.

Giovanni Lugli, Vetle I Torvik, John Larson, and Neil R Smalheiser. Expression of microRNAs and their precursors in synaptic fractions of adult mouse forebrain. *Journal of neurochemistry*, 106(2):650–661, July 2008.

Susan Magdaleno, Lakhu Keshvara, and Tom Curran. Rescue of ataxia and preplate splitting by ectopic expression of Reelin in reeler mice. *Neuron*, 33(4):573–586, February 2002.

Eugene V Makeyev, Jiangwen Zhang, Monica A Carrasco, and Tom Maniatis. The MicroRNA miR-124 promotes neuronal differentiation by triggering brain-specific alternative pre-mRNA splicing. *Molecular Cell*, 27(3):435–448, August 2007.

Oscar Marín, Manuel Valiente, Xuecai Ge, and Li-Huei Tsai. Guiding neuronal cell migrations. *Cold Spring Harbor perspectives in biology*, 2(2):a001834, February 2010.

Katharine J Marler, Philipp Suetterlin, Asha Dopplapudi, Aine Rubikaite, Jihad Adnan, Nicola A Maiorano, Andrew S Lowe, Ian D Thompson, Manav Pathania, Angélique Bordey, Tudor Fulga, David L Van Vactor, Robert Hindges, and Uwe Drescher. BDNF Promotes Axon Branching of Retinal Ganglion Cells via miRNA-132 and p250GAP. *Journal of Neuroscience*, 34(3):969–979, January 2014.

S K McConnell and C E Kaznowski. Cell cycle dependence of laminar determination in developing neocortex. *Science*, 254(5029):282–285, October 1991.

H S McLoughlin, S K Fineberg, L L Ghosh, L Tecedor, and B L Davidson. Dicer is required for proliferation, viability, migration and differentiation in corticoneurogenesis. *Neuroscience*, 223:285–295, October 2012.

Elizabeth McNeill and David Van Vactor. MicroRNAs Shape the Neuronal Landscape. *Neuron*, 75(3):363–379, August 2012.

Aaron D Milstein and Roger A Nicoll. Regulation of AMPA receptor gating and pharmacology by TARP auxiliary subunits. *Trends in pharmacological sciences*, 29(7):333–339, July 2008.

Alex Mas Monteys, Ryan M Spengler, Ji Wan, Luis Tecedor, Kimberly A Lennox, Yi Xing, and Beverly L Davidson. Structure and activity of putative intronic miRNA promoters. *RNA (New York, NY)*, 16(3):495–505, March 2010.

Makoto Nishiyama, Kazunobu Togashi, Melanie J von Schimmelmann, Chae-Seok Lim, Shinichi Maeda, Naoya Yamashita, Yoshio Goshima, Shin Ishii, and Kyonsoo Hong. Semaphorin 3A induces CaV2.3 channel-dependent conversion of axons to dendrites. *Nature cell biology*, 13(6):676–685, June 2011.

Stephen C Noctor, Verónica Martínez-Cerdeño, Lidija Ivic, and Arnold R Kriegstein. Cortical neurons arise in symmetric and asymmetric division zones and migrate through specific phases. *Nature Neuroscience*, 7(2):136–144, February 2004.

Gregor Obernosterer, Philipp J F Leuschner, Mattias Alenius, and Javier Martinez. Post-transcriptional regulation of microRNA expression. *RNA (New York, NY)*, 12(7):1161–1167, July 2006.

Patricia Paez-Gonzalez, Khadar Abdi, Dominic Luciano, Yan Liu, Mario Soriano-Navarro, Emma Rawlins, Vann Bennett, Jose Manuel Garcia-Verdugo, and Chay T Kuo. Ank3-dependent SVZ niche assembly is required for the continued production of new neurons. *Neuron*, 71(1):61–75, July 2011.

T Papagiannakopoulos, D Friedmann-Morvinski, P Neveu, J C Dugas, R M Gill, E Huillard, C Liu, H Zong, D H Rowitch, B A Barres, I M Verma, and K S Kosik. Pro-neural miR-128 is a glioma tumor suppressor that targets mitogenic kinases. *Oncogene*, 31(15):1884–1895, April 2012.

Manavendra Pathania, Juan Torres-Reveron, Lily Yan, Tomoki Kimura, Tiffany V Lin, Valerie Gordon, Zhao-Qian Teng, Xinyu Zhao, Tudor A Fulga, David Van Vactor, and Angélique Bordey. miR-132 enhances dendritic morphogenesis, spine density, synaptic integration, and survival of newborn olfactory bulb neurons. *PLoS ONE*, 7(5):e38174, 2012.

Bret J Pearson and Chris Q Doe. Regulation of neuroblast competence in Drosophila. *Nature*, 425(6958):624–628, October 2003.

John T G Pena, Cherin Sohn-Lee, Sara H Rouhanifard, Janos Ludwig, Markus Hafner, Aleksandra Mihailovic, Cindy Lim, Daniel Holoch, Philipp Berninger, Mihaela Zavolan, and Thomas Tuschl. miRNA in situ hybridization in formaldehyde and EDC–fixed tissues. *Nature Methods*, 6(2):139–141, January 2009.

Israel Pichardo-Casas, Loyal A Goff, Mavis R Swerdel, Alejandro Athie, Jonathan Davila, Mariana Ramos-Brossier, Martha Lapid-Volosin, Wilma J Friedman, Ronald P Hart, and Luis Vaca. Expression profiling of synaptic microRNAs from the adult rat brain identifies regional differences and seizure-induced dynamic modulation. *Brain research*, 1436:20–33, February 2012.

Luisa Pinto and Magdalena Götz. Radial glial cell heterogeneity–the source of diverse progeny in the CNS. *Progress in neurobiology*, 83(1):2–23, September 2007.

Elena Piskounova, Christos Polytarchou, James E Thornton, Robert J LaPierre, Charalabos Pothoulakis, John P Hagan, Dimitrios Iliopoulos, and Richard I Gregory. Lin28A and Lin28B inhibit let-7 microRNA biogenesis by distinct mechanisms. *Cell*, 147(5):1066–1079, November 2011.

F Polleux and William Snider. Initiating and growing an axon. *Cold Spring Harbor perspectives in biology*, 2(4):a001925, April 2010.

F Polleux, T Morrow, and A Ghosh. Semaphorin 3A is a chemoattractant for cortical apical dendrites. *Nature*, 404(6778):567–573, April 2000.

S V Puram and A Bonni. Cell-intrinsic drivers of dendrite morphogenesis. *Development (Cambridge, England)*, 140(23):4657–4671, November 2013.

Peng-Xu Qian, Arindam Banerjee, Zheng Sheng Wu, Xiao Zhang, Hong Wang, Vijay Pandey, Weijie Zhang, Xue-Fei Lv, Sheng Tan, Peter E Lobie, and Tao Zhu. Loss of SNAIL regulated

miR-128-2 on chromosome 3p22.3 targets multiple stem cell factors to promote transformation of mammary epithelial cells. *Cancer research*, September 2012.

Priyamvada Rajasethupathy, Ferdinando Fiumara, Robert Sheridan, Doron Betel, Sathyanarayanan V Puthanveettil, James J Russo, Chris Sander, Thomas Tuschl, and Eric Kandel. Characterization of small RNAs in aplysia reveals a role for miR-124 in constraining synaptic plasticity through CREB. *Neuron*, 63(6):803–817, September 2009.

S V Rakhilin. A Network of Control Mediated by Regulator of Calcium/Calmodulin-Dependent Signaling. *Science*, 306(5696):698–701, October 2004.

Carmen Ramírez-Castillejo, Francisco Sánchez-Sánchez, Celia Andreu-Agullo, Sacri R Ferrón, J Daniel Aroca-Aguilar, Pilar Sánchez, Helena Mira, Julio Escribano, and Isabel Fariñas. Pigment epithelium-derived factor is a niche signal for neural stem cell renewal. *Nature Neuroscience*, 9(3):331–339, March 2006.

Marta Rosário, Steffen Schuster, René Jüttner, Srinivas Parthasarathy, Victor Tarabykin, and Walter Birchmeier. Neocortical dendritic complexity is controlled during development by NOMA-GAP-dependent inhibition of Cdc42 and activation of cofilin. *Genes & development*, 26(15):1743–1757, August 2012.

Agnieszka Rybak, Heiko Fuchs, Lena Smirnova, Christine Brandt, Elena E Pohl, Robert Nitsch, and F Gregory Wulczyn. A feedback loop comprising lin-28 and let-7 controls pre-let-7 maturation during neural stem-cell commitment. *Nature cell biology*, 10(8):987–993, July 2008.

Reuben Saba, Peter H Störchel, Ayla Aksoy-Aksel, Frauke Kepura, Giordano Lippi, Tim D Plant, and Gerhard M Schratt. Dopamine-regulated microRNA MiR-181a controls GluA2 surface expression in hippocampal neurons. *Molecular and cellular biology*, 32(3):619–632, February 2012.

Tetsuichiro Saito. In vivo electroporation in the embryonic mouse central nervous system. *Nature protocols*, 1(3):1552–1558, November 2006.

Akira Sakakibara, Ryota Ando, Tamar Sapir, and Teruyuki Tanaka. Microtubule dynamics in neuronal morphogenesis. *Open biology*, 3(7):130061, July 2013a.

Akira Sakakibara, Toshiyuki Sato, Ryota Ando, Namiko Noguchi, Makoto Masaoka, and Takaki Miyata. Dynamics of Centrosome Translocation and Microtubule Organization in Neocortical Neurons during Distinct Modes of Polarization. *Cerebral Cortex*, January 2013b.

Kazunobu Sawamoto, Hynek Wichterle, Oscar Gonzalez-Perez, Jeremy A Cholfin, Masayuki Yamada, Nathalie Spassky, Noel S Murcia, Jose Manuel Garcia-Verdugo, Oscar Marín, John L R Rubenstein, Marc Tessier-Lavigne, Hideyuki Okano, and Arturo Alvarez-Buylla. New neurons follow the flow of cerebrospinal fluid in the adult brain. *Science*, 311(5761): 629–632, February 2006.

Gerhard M Schratt, Fabian Tuebing, Elizabeth A Nigh, Christina G Kane, Mary E Sabatini, Michael Kiebler, and Michael E Greenberg. A brain-specific microRNA regulates dendritic spine development. *Nature*, 439(7074):283–289, January 2006.

J C Schwamborn, M R Khazaei, and A W Puschel. The Interaction of mPar3 with the Ubiquitin Ligase Smurf2 Is Required for the Establishment of Neuronal Polarity. *Journal of Biological Chemistry*, 282(48):35259–35268, September 2007a.

Jens C Schwamborn and Andreas W Püschel. The sequential activity of the GTPases Rap1B and Cdc42 determines neuronal polarity. *Nature Neuroscience*, 7(9):923–929, September 2004.

Jens C Schwamborn, Myriam Müller, Annemarie Hm Becker, and Andreas W Püschel. Ubiquitination of the GTPase Rap1B by the ubiquitin ligase Smurf2 is required for the establishment of neuronal polarity. *The EMBO journal*, 26(5):1410–1422, March 2007b.

Jens C Schwamborn, Eugene Berezikov, and Juergen A Knoblich. The TRIM-NHL protein TRIM32 activates microRNAs and prevents self-renewal in mouse neural progenitors. *Cell*, 136(5):913–925, March 2009.

Menahem Segal. Dendritic spines, synaptic plasticity and neuronal survival: activity shapes dendritic spines to enhance neuronal viability. *The European journal of neuroscience*, 31 (12):2178–2184, June 2010.

Ning-Yi Shao, Hai Yang Hu, Zheng Yan, Ying Xu, Hao Hu, Corinna Menzel, Na Li, Wei Chen, and Philipp Khaitovich. Comprehensive survey of human brain microRNA by deep sequencing. *BMC genomics*, 11:409, 2010.

Maya Shelly and Mu-ming Poo. Role of LKB1-SAD/MARK pathway in neuronal polarization. *Developmental Neurobiology*, 71(6):508–527, June 2011.

Maya Shelly, Laura Cancedda, Sarah Heilshorn, Germán Sumbre, and Mu-ming Poo. LKB1/STRAD promotes axon initiation during neuronal polarization. *Cell*, 129(3):565–577, May 2007.

Maya Shelly, Byung Kook Lim, Laura Cancedda, Sarah C Heilshorn, Hongfeng Gao, and Mu-ming Poo. Local and long-range reciprocal regulation of cAMP and cGMP in axon/dendrite formation. *Science*, 327(5965):547–552, January 2010.

Maya Shelly, Laura Cancedda, Byung Kook Lim, Andrei T Popescu, Pei-lin Cheng, Hongfeng Gao, and Mu-ming Poo. Semaphorin3A Regulates Neuronal Polarization by Suppressing Axon Formation and Promoting Dendrite Growth. *Neuron*, 71(3):433–446, August 2011.

Qin Shen, Yue Wang, John T Dimos, Christopher A Fasano, Timothy N Phoenix, Ihor R Lemischka, Natalia B Ivanova, Stefano Stifani, Edward E Morrisey, and Sally Temple. The timing of cortical neurogenesis is encoded within lineages of individual progenitor cells. *Nature Neuroscience*, 9(6):743–751, June 2006.

Mikihito Shibata, Hiromi Nakao, Hiroshi Kiyonari, Takaya Abe, and Shinichi Aizawa. MicroRNA-9 regulates neurogenesis in mouse telencephalon by targeting multiple transcription factors. *Journal of Neuroscience*, 31(9):3407–3422, March 2011.

Asli N Silahtaroglu, Dorrit Nolting, Lars Dyrskjøt, Eugene Berezikov, Morten Møller, Niels Tommerup, and Sakari Kauppinen. Detection of microRNAs in frozen tissue sections by fluorescence in situ hybridization using locked nucleic acid probes and tyramide signal amplification. *Nature protocols*, 2(10):2520–2528, 2007.

Sergi Simó and Jonathan A Cooper. Regulation of dendritic branching by Cdc42 GAPs. *Genes & development*, 26(15):1653–1658, August 2012.

Haruhiko Siomi and Mikiko C Siomi. Posttranscriptional regulation of microRNA biogenesis in animals. *Molecular Cell*, 38(3):323–332, May 2010.

Lena Smirnova, Anja Gräfe, Andrea Seiler, Stefan Schumacher, Robert Nitsch, and F Gregory Wulczyn. Regulation of miRNA expression during neural cell specification. *The European journal of neuroscience*, 21(6):1469–1477, March 2005.

David J Solecki. Sticky situations: recent advances in control of cell adhesion during neuronal migration. *Current opinion in neurobiology*, 22(5):791–798, October 2012.

Mehmet Somel, Xiling Liu, Lin Tang, Zheng Yan, Haiyang Hu, Song Guo, Xi Jiang, Xiaoyu Zhang, Guohua Xu, Gangcai Xie, Na Li, Yuhui Hu, Wei Chen, Svante Pääbo, and Philipp Khaitovich. MicroRNA-driven developmental remodeling in the brain distinguishes humans from other primates. *PLoS Biology*, 9(12):e1001214, December 2011.

Kimberly L Stark, Bin Xu, Anindya Bagchi, Wen-Sung Lai, Hui Liu, Ruby Hsu, Xiang Wan, Paul Pavlidis, Alea A Mills, Maria Karayiorgou, and Joseph A Gogos. Altered brain microRNA biogenesis contributes to phenotypic deficits in a 22q11-deletion mouse model. *Nature genetics*, 40(6):751–760, June 2008.

Michael Stiess and Frank Bradke. Neuronal polarization: the cytoskeleton leads the way. *Developmental Neurobiology*, 71(6):430–444, June 2011.

Alfred X Sun, Gerald R Crabtree, and Andrew S Yoo. MicroRNAs: regulators of neuronal fate. *Current opinion in cell biology*, 25(2):215–221, April 2013.

Tomoko Tada and Morgan Sheng. Molecular mechanisms of dendritic spine morphogenesis. *Current opinion in neurobiology*, 16(1):95–101, February 2006.

Chan Lek Tan, Joshua L Plotkin, Morten T Venø, Melanie von Schimmelmann, Philip Feinberg, Silas Mann, Annie Handler, Jørgen Kjems, D James Surmeier, Dónal O'Carroll, Paul Greengard, and Anne Schaefer. MicroRNA-128 governs neuronal excitability and motor behavior in mice. *Science*, 342(6163):1254–1258, December 2013.

V Tarabykin, A Stoykova, N Usman, and P Gruss. Cortical upper layer neurons derive from the subventricular zone as indicated by Svet1 gene expression. *Development (Cambridge, England)*, 128(11):1983–1993, June 2001.

Roberto Tiribuzi, Lucia Crispoltoni, Serena Porcellati, Martina Di Lullo, Fulvio Florenzano, Matteo Pirro, Francesco Bagaglia, Toshitaka Kawarai, Mauro Zampolini, Aldo Orlacchio, and Antonio Orlacchio. miR128 up-regulation correlates with impaired amyloid β(1-42) degradation in monocytes from patients with sporadic Alzheimer's disease. *Neurobiology of aging*, 35(2):345–356, February 2014.

Fadel Tissir and André M Goffinet. Reelin and brain development. *Nature reviews Neuroscience*, 4(6):496–505, June 2003.

Matthew A M Todd and David J Picketts. PHF6 Interacts with the Nucleosome Remodeling and Deacetylation (NuRD) Complex. *Journal of Proteome Research*, 11(8):4326–4337, August 2012.

Malgorzata Urbanska, Agata Gozdz, Lukasz J Swiech, and Jacek Jaworski. Mammalian target of rapamycin complex 1 (mTORC1) and 2 (mTORC2) control the dendritic arbor morphology of hippocampal neurons. *Journal of Biological Chemistry*, 287(36):30240–30256, August 2012.

Eva van Rooij, Lillian B Sutherland, Xiaoxia Qi, James A Richardson, Joseph Hill, and Eric N Olson. Control of stress-dependent cardiac growth and gene expression by a microRNA. *Science*, 316(5824):575–579, April 2007.

P Van Vlierberghe, J Patel, O Abdel-Wahab, C Lobry, C V Hedvat, M Balbin, C Nicolas, A R Payer, H F Fernandez, M S Tallman, E Paietta, A Melnick, P Vandenberghe, F Speleman, I Aifantis, J Cools, R Levine, and A Ferrando. PHF6 mutations in adult acute myeloid leukemia. *Leukemia*, 25(1):130–134, January 2011.

Pieter Van Vlierberghe, Teresa Palomero, Hossein Khiabanian, Joni Van Der Meulen, Mireia Castillo, Nadine Van Roy, Barbara De Moerloose, Jan Philippé, Sara González-García, María L Toribio, Tom Taghon, Linda Zuurbier, Barbara Cauwelier, Christine J Harrison, Claire Schwab, Markus Pisecker, Sabine Strehl, Anton W Langerak, Jozef Gécz, Edwin Sonneveld, Rob Pieters, Elisabeth Paietta, Jacob M Rowe, Peter H Wiernik, Yves Benoit, Jean Soulier, Bruce Poppe, Xiaopan Yao, Carlos Cordon-Cardo, Jules Meijerink, Raul Rabadan, Frank Speleman, and Adolfo Ferrando. PHF6 mutations in T-cell acute lymphoblastic leukemia. *Nature genetics*, 42(4):338–342, April 2010.

Jaya Visvanathan, Seunghee Lee, Bora Lee, Jae W Lee, and Soo-Kyung Lee. The microRNA miR-124 antagonizes the anti-neural REST/SCP1 pathway during embryonic CNS development. *Genes & development*, 21(7):744–749, April 2007.

Ngan Vo, Matthew E Klein, Olga Varlamova, David M Keller, Tadashi Yamamoto, Richard H Goodman, and Soren Impey. A cAMP-response element binding protein-induced microRNA regulates neuronal morphogenesis. *Proceedings of the National Academy of Sciences of the United States of America*, 102(45):16426–16431, November 2005.

Anne K Voss, Robin Gamble, Caitlin Collin, Cheryl Shoubridge, Mark Corbett, Jozef Gécz, and Tim Thomas. Protein and gene expression analysis of Phf6, the gene mutated in

the Börjeson–Forssman–Lehmann Syndrome of intellectual disability and obesity. *Gene Expression Patterns*, 7(8):858–871, October 2007.

J Wang, J W c Leung, Z Gong, L Feng, X Shi, and J Chen. PHF6 Regulates Cell Cycle Progression by Suppressing Ribosomal RNA Synthesis. *Journal of Biological Chemistry*, 288(5):3174–3183, February 2013.

Yangming Wang, Rostislav Medvid, Collin Melton, Rudolf Jaenisch, and Robert Blelloch. DGCR8 is essential for microRNA biogenesis and silencing of embryonic stem cell self-renewal. *Nature genetics*, 39(3):380–385, March 2007.

Ligang Wu, Jihua Fan, and Joel G Belasco. MicroRNAs direct rapid deadenylation of mRNA. *Proceedings of the National Academy of Sciences of the United States of America*, 103(11): 4034–4039, March 2006.

F G Wulczyn, L Smirnova, A Rybak, C Brandt, E Kwidzinski, O Ninnemann, M Strehle, A Seiler, S Schumacher, and R Nitsch. Post-transcriptional regulation of the let-7 microRNA during neural cell specification. *The FASEB journal : official publication of the Federation of American Societies for Experimental Biology*, 21(2):415–426, February 2007.

Yuanchao Xue, Kunfu Ouyang, Jie Huang, Yu Zhou, Hong Ouyang, Hairi Li, Gang Wang, Qijia Wu, Chaoliang Wei, Yanzhen Bi, Li Jiang, Zhiqiang Cai, Hui Sun, Kang Zhang, Yi Zhang, Ju Chen, and Xiang-Dong Fu. Direct Conversion of Fibroblasts to Neurons by Reprogramming PTB-Regulated MicroRNA Circuits. *Cell*, 152(1-2):82–96, January 2013.

Jun Yao, Yangling Mu, and Fred H Gage. Neural stem cells: mechanisms and modeling. *Protein & cell*, 3(4):251–261, April 2012.

Norihiko Yokoi, Masaki Fukata, and Yuko Fukata. Synaptic plasticity regulated by protein-protein interactions and posttranslational modifications. *International review of cell and molecular biology*, 297:1–43, 2012.

Andrew S Yoo, Brett T Staahl, Lei Chen, and Gerald R Crabtree. MicroRNA-mediated switching of chromatin-remodelling complexes in neural development. *Nature*, 460(7255): 642–646, July 2009.

Andrew S Yoo, Alfred X Sun, Li Li, Aleksandr Shcheglovitov, Thomas Portmann, Yulong Li, Chris Lee-Messer, Ricardo E Dolmetsch, Richard W Tsien, and Gerald R Crabtree. MicroRNA-mediated conversion of human fibroblasts to neurons. *Nature*, 476(7359):228–231, August 2011.

Yoshihiro Yoshihara, Mathias De Roo, and Dominique Muller. Dendritic spine formation and stabilization. *Current opinion in neurobiology*, 19(2):146–153, April 2009.

Takeshi Yoshimura, Yoji Kawano, Nariko Arimura, Saeko Kawabata, Akira Kikuchi, and Kozo Kaibuchi. GSK-3beta regulates phosphorylation of CRMP-2 and neuronal polarity. *Cell*, 120(1):137–149, January 2005.

Chi Zhang, Luis A Mejia, Ju Huang, Pamela Valnegri, Eric J Bennett, Julius Anckar, Arezu Jahani-Asl, Gilbert Gallardo, Yoshiho Ikeuchi, Tomoko Yamada, Michael Rudnicki, J Wade Harper, and Azad Bonni. The X-Linked Intellectual Disability Protein PHF6 Associates with the PAF1 Complex and Regulates Neuronal Migration in the Mammalian Brain. *Neuron*, 78(6):986–993, June 2013.

Chunmei Zhao, Wei Deng, and Fred H Gage. Mechanisms and functional implications of adult neurogenesis. *Cell*, 132(4):645–660, February 2008.

Chunnian Zhao, GuoQiang Sun, Shengxiu Li, and Yanhong Shi. A feedback regulatory loop involving microRNA-9 and nuclear receptor TLX in neural stem cell fate determination. *Nature structural & molecular biology*, 16(4):365–371, April 2009.

Shanting Zhao and Michael Frotscher. Go or stop? Divergent roles of Reelin in radial neuronal migration. *The Neuroscientist : a review journal bringing neurobiology, neurology and psychiatry*, 16(4):421–434, August 2010.

Yeping Zhou, Rou-Afza F Gunput, and R Jeroen Pasterkamp. Semaphorin signaling: progress made and promises ahead. *Trends in biochemical sciences*, 33(4):161–170, April 2008.

Yuan-Dong Zhu, Li Wang, Chao Sun, Lei Fan, Dan-Xia Zhu, Cheng Fang, Yin-Hua Wang, Zhi-Jian Zou, Su-Jiang Zhang, Jian-Yong Li, and Wei Xu. Distinctive microRNA signature is associated with the diagnosis and prognosis of acute leukemia. *Medical oncology (Northwood, London, England)*, 29(4):2323–2331, December 2012.

Céline Zimmer, Marie-Catherine Tiveron, Rolf Bodmer, and Harold Cremer. Dynamics of Cux2 expression suggests that an early pool of SVZ precursors is fated to become upper cortical layer neurons. *Cerebral cortex (New York, N.Y. : 1991)*, 14(12):1408–1420, December 2004.